CERTIFICATO DI FIRMA DIGITALE

Si certifica che questo documento informatico

Phd_unisi_086779.pdf

composto da n°132 pagine

È stato firmato digitalmente in data odierna con Firma Elettronica Qualificata (FEQ), avente l'efficacia e gli effetti giuridici equivalenti a quelli di una firma autografa, ai sensi dell'art. 2702 del Codice Civile e dell'art. 25 del Regolamento UE n. 910/2014 eIDAS (electronic IDentification Authentication and Signature).

PROCESSI INFORMATICI COMPLETATI

- **Apposizione di Firma Elettronica Qualificata Remota** emessa da Intesi Group S.p.A. in qualità di prestatore di servizi fiduciari qualificati autorizzato da AgID, per garantire con certezza l'autenticità, l'integrità, il non ripudio e l'immodificabilità del documento informatico e la sua riconducibilità in maniera manifesta e inequivoca all'autore, ai sensi dell'art. 20 comma 2 del CAD - D.lgs 82/2005.
- **Apposizione di Marca Temporale Qualificata** emessa da Intesi Group S.p.A. in qualità di prestatore di servizi fiduciari qualificati autorizzato da AgID, per attribuire una data e un orario opponibile a terzi, ai sensi dell'art. 20 comma 3 del CAD - D.lgs 82/2005 e per far sì che la Firma Elettronica Qualificata apposta su questo documento informatico, risulti comunque valida per i prossimi 20 anni a partire dalla data odierna, anche nel caso in cui il relativo certificato risultasse scaduto, sospeso o revocato.
- **Apposizione di Contrassegno Elettronico**, l'unica soluzione tecnologica che permette di prorogare la validità giuridica di un documento informatico sottoscritto con firma digitale e/o marcato temporalmente, rendendolo inalterabile, certo e non falsificabile, una volta stampato su supporto cartaceo, ai sensi dell'art. 23 del CAD - D.lgs 82/2005.

  Per risalire all'originale informatico è necessario scansionare il Contrassegno Elettronico, utilizzando l'applicazione HONOS, disponibile per dispositivi Android e iOS.

cheFirma!® - powered by LetteraSenzaBusta.com

UNIVERSITÀ DI SIENA
1240

DIPARTIMENTO DI BIOTECNOLOGIE, CHIMICA E FARMACIA

UNIVERSITÀ DEGLI STUDI DI SIENA

DIPARTIMENTO DI BIOTECNOLOGIE, CHIMICA E FARMACIA

DOTTORATO DI RICERCA IN

CHEMICAL AND PHARMACEUTICAL SCIENCES

CICLO XXXIV

Coordinatore del corso: Prof. Maurizio Taddei
Settore scientifico-disciplinare: CHIM/08

IMPACT OF THE MULTIVALENT DISPLAY OF MINIMAL CARBOHYDRATE EPITOPES ON THE IMMUNOGENICITY OF GLYCOCONJUGATE VACCINE

DOTTORANDA

Francesca Nonne

TUTOR

Prof. Maurizio Taddei

Firmato digitalmente da
FRANCESCA NONNE
24/04/2022 19:43:00 +0200
powered by cheFirma!

GSK TUTOR

Dott.ssa Maria R. Romano

ANNO ACCADEMICO 2021/2022

TABLE OF CONTENTS

ABSTRACT

The development and use of antibacterial glycoconjugate vaccines have significantly reduced the occurrence of potentially fatal childhood and adult diseases such as bacteremia, bacterial meningitis, and pneumonia. These vaccines are composed of a weak saccharide antigen, usually represented by microbial polysaccharides and oligosaccharides, which is covalently bound to a carrier protein to increase its immunogenicity and trigger a T-dependent immune response, allowing thus the generation of high affinity antibodies and an immunological memory.

The identification and characterization of saccharide epitopes essential for the recognition by protective antibodies are crucial for the new glycoconjugate vaccines design. The aim of my thesis was to study and identify the antigenic determinants of *Haemophilus influenzae* type b (Hib) and *Staphylococcus aureus* serotypes 5 (CP5) and 8 (CP8) polysaccharides (PSs).

Regarding the Hib project, after identifying the minimal saccharide length required for antibody recognition through competitive SPR experiments, the binding between antigen and a protective anti-Hib PS monoclonal antibody was characterized at the atomic level by a synergistic combination of STD-NMR and x-ray crystallography techniques, which identify DP2 as the ideal length for antibody binding. Next, an *in vivo* study confirmed that two repeating units represent the minimal immunogenic epitope of Hib PS.

Studies on *S. aureus* have instead focused on evaluating how different variables can influence the immunogenicity of a glycoconjugate vaccine. Since variables such as saccharide chain length and degree of glycosylation showed a minor impact on immunogenicity, we focused on the role of O-acetyl (OAc), a functional group present in CP5 and CP8 PSs and demonstrated as essential for the generation of functional antibodies. Competitive SPR experiments with anti-CP5 and anti-CP8 polyclonal sera highlighted a greater importance of OAc for the recognition of CP8, while for CP5 it does not seem to have a critical impact. This different behavior could in part be explained by the different conformation of the two PSs observed in Molecular Dynamics experiments. Subsequently, the same SPR experiments performed with monoclonal antibodies (mAbs) allowed the identification of both CP5 and CP8 antibodies preferentially recognizing the O-acetylated epitope over the fully de-O-acetylated and vice versa. Functional studies on these mAbs revealed a possible correlation between functionality and O-acetylation, as the mAbs most closely related to the acetylated epitopes show greater functionality than those preferentially recognizing the de-O-acetylated epitopes.

The study and characterization of different glycoconjugates variables represent a key step in the development of effective next-generation glycoconjugate vaccines.

RIASSUNTO

Lo sviluppo e l'uso di vaccini glicoconiugati batterici hanno ridotto significativamente l'insorgenza di malattie potenzialmente fatali in bambini e adulti come batteriemia, meningite batterica e polmonite. Tali vaccini sono composti da un antigene saccaridico scarsamente immunogenico, solitamente rappresentato da polisaccaridi e oligosaccaridi microbici, che viene covalentemente legato ad una proteina trasportatrice (carrier) per aumentarne l'immunogenicità e convertire la risposta immunitaria da T-indipendent a T-dipendent, permettendo così la generazione di anticorpi ad alta affinità e la creazione di una memoria immunologica.

L'identificazione e la caratterizzazione degli epitopi saccaridici essenziali per il riconoscimento di anticorpi protettivi sono di fondamentale importanza nella progettazione di nuovi ed efficaci vaccini glicoconiugati. Lo scopo della mia tesi è stato quello di studiare e identificare i determinanti antigenici dei polisaccaridi (PSs) di *Haemophilus influenzae* di tibo b (Hib) e *Staphylococcus aureus* CP5 e CP8.

Per quanto riguarda il progetto di Hib, dopo aver identificato la lunghezza minima di saccaride necessaria per il riconoscimento anticorpale attraverso studi di competitive SPR, il legame tra antigene e un anticorpo monoclonale protettivo anti Hib PS è stato caratterizzato a livello atomico da una combinazione sinergica di tecniche che comprendono STD-NMR e cristallografia a raggi x, identificando nel DP2 la lunghezza ideale per il legame con l'anticorpo. Attraverso uno studio *in vivo* è stato poi possibile confermare che due unità ripetenti rappresentino l'epitopo minimo immunogenico.

Gli studi su *S. aureus* si sono invece incentrati sulla valutazione di come diverse variabili possano influenzare l'immunogenicità di un vaccino glicoconiugato. Dopo aver inizialmente constatato tramite uno studio *in vivo* che variabili come lunghezza della catena saccaridica e grado di glicosilazione avevano un impatto minore sull'immunogenicità, ci siamo focalizzati sul ruolo dell'O-acetile, gruppo funzionale presente nel polisaccaride di CP5 e CP8 e dimostrato essere essenziale per la generazione di anticorpi funzionali. Esperimenti di competitive SPR con sieri policlonali anti-CP5 e anti-CP8 hanno evidenziato una maggiore importanza dell'OAc per il riconoscimento del CP8, mentre per il CP5 non sembra avere un impatto determinante. Questo diverso comportamento potrebbe in parte essere spiegato dalla diversa conformazione dei due PSs osservata in esperimenti di Dinamica Molecolare. Successivamente, gli stessi studi SPR fatti utilizzando anticorpi monoclonali hanno permesso di identificare sia per CP5 che per

CP8 anticorpi riconoscenti preferenzialmente l'epitopo acetilato rispetto a quello de-O-acetilato e viceversa. Studi funzionali su questi mAbs hanno rivelato una possibile correlazione tra funzionalità e O-acetilazione, in quanto i monoclonali maggiormente affini all'epitopo acetilato hanno mostrano una funzionalità maggiore rispetto a quelli riconoscenti preferenzialmente l'epitopo de-O-acetilato.

Lo studio e la caratterizzazione delle diverse variabili impattanti l'immunogenicità di un glicoconiugato rappresentano uno step chiave nello sviluppo di efficaci vaccini glicoconiugati di nuova generazione.

LIST OF ABBREVIATIONS

Ab	Antibody
avDP	Average Degree of Polymerization
ClfA	Clumping factor A
CPS	Capsular Polysaccharide
CP5	Capsular Polysaccharide type 5
CP8	Capsular Polysaccharide type 8
DEA	Diethanolamine
DeOAc	De-O-acetylation/acetylated
DMSO	Dimethlyl sulfoxide
DP	Degree of Polymerization
ELISA	Enzyme-linked immunosorbent assay
EtOAc	Ethyl acetate
Fab	Fragment antigen binding
H-chain	Heavy chain
Hib	Haemophilus influenzae type b
Hla	Alpha-hemolysin
hmAb	Human monoclonal antibody
HPAEC-PAD	High-performance anion-exchange chromatography with pulsed amperometric detection
HPLC	High Performance Liquid Chromatography
K_D	Dissociation kinetics
L-chain	Light chain
mAb	Monoclonal antibody
MD	Molecular Dynamic
MFI	Mean Fluorescence Intensity
OAc	O-acetyl/acetylation/acetylated
OPKA	Opsono Phagocytic Killing Assay
OS	Oligosaccharide
pAb	Polyclonal antibody
PBS	Phosphate Buffer Saline

PS	Polysaccharide
RLU	Relative Luminex Units
RU	Repeating Unit
SA	Streptavidin
SIDEA	Di-(N-succinimidyl) adipate
SPR	Surface Plasmon Resonance
STD-NMR	Saturation Transfer Difference – Nuclear Magnetic Resonance
TNBSA	2,4,6-trinitrobenzene sulfonic acid
TT	Tetanus Toxoid

CHAPTER 1: INTRODUCTION

1.1 Bacteria

Bacteria represent a class of microorganisms responsible for a wide variety of infectious diseases. Bacteria are unicellular prokaryotic microorganisms composed of a plasma membrane, a semipermeable barrier consisting of phospholipids and proteins surrounding the cytoplasm. The plasma membrane is in turn enclosed by the cell wall, which mainly provides structural support and protection and acts as a filtering mechanism. Bacteria are different from all other cells, because of the presence of a dense coating of external carbohydrates generally referred to as *glycocalyx*. This coating makes bacteria resistant to phagocytes and delays the protective action of specific immunological systems. The cell surface polysaccharides (PSs) are polymers that can be formed from a single monosaccharide unit or more complex repetitions of oligosaccharides. These can be charged or neutral and can covalently bind proteins or lipids, forming *glycoproteins* and *glycolipids* respectively [1].

Based on the ability to react or not to the staining method developed by Christian Gram in 1884, the bacteria are divided into two classes: *Gram-positive* and *Gram-negative*. Gram-positive and Gram-negative bacteria are characterized by a different structure of the cell wall (**Figure 1**) [2] and for this reason they respond differently to Gram staining [3]. Gram-positive cells are characterized by a thick membrane layer (200-800 Å) of peptidoglycan whereas Gram-negative ones have a thinner layer (50-100 Å). Gram-negative cell wall presents an outer membrane (OM), an intermediate compartment called *periplasm* containing the peptidoglycan and an internal membrane (IM). The cell wall of Gram-positive, on the other hand, does not have an external membrane and is made up of a larger layer of peptidoglycan responsible for the rigidity of the wall itself. Peptidoglycan is a polymer consisting of alternate units of *N*-acetyl-glucosamine and *N*-acetylmuramic acid. The latter sugar can be linked to a peptide consisting of three to five amino acids. Furthermore, the peptide sequence creates cross-links forming a 3D mesh-like layer.

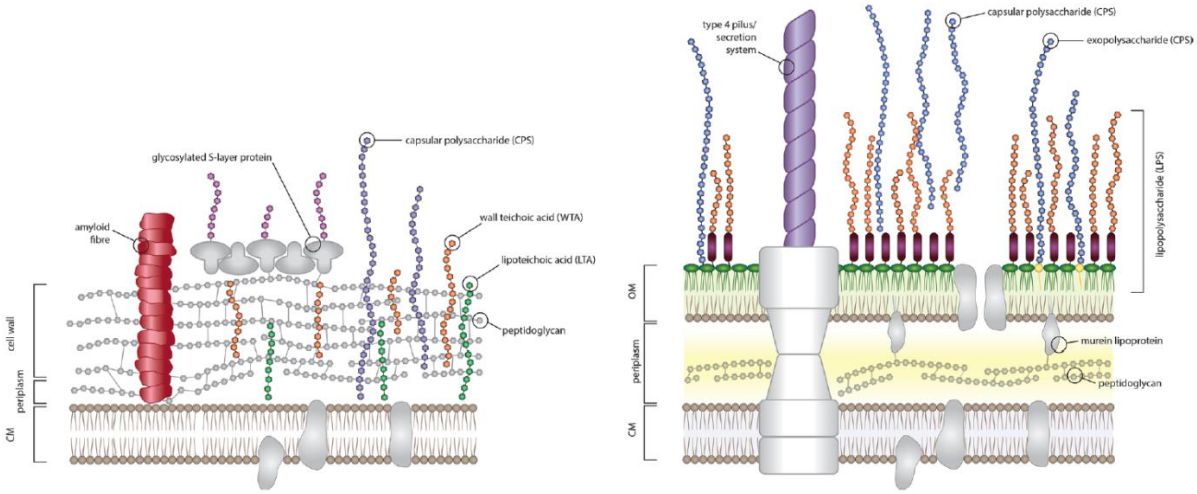

Figure 1. Schematic representation of the cell envelope of Gram+ (left) and Gram- (right) bacteria [2].

.

1.2 Immune system and principle of vaccination

The immune system is an important defense mechanism for our organism capable of recognizing and destroying invading microorganisms. Our immune system is able to recognize healthy cells *(self)* from the foreign and infected cells *(non-self)* and trigger an immune response against the latter as a defense mechanism. A foreign substance recognized as dangerous and capable of triggering an immune response is known as antigen. The immune response can be divided into innate immunity and adaptive immunity. The innate immunity is a rapid and non-specific response that is considered as first defensive line. The adaptive immunity is directed specifically against an antigen and involves many different types of cells called lymphocytes, belonging to the class of leukocytes. The adaptive response differs from the innate for:

- *Specificity*: the antigens recognition through the production of specialized lymphocytes and specific antibodies;
- *Diversity*: the capacity of the immune system to respond specifically to millions of different antigens thanks to the presence of many lymphocyte cells, each of which is specific to a particular immunologic agent;
- *Recognition of self from non-self*: the ability to distinguish own-body molecules from antigens;
- *Memory:* remember the antigen already encountered to recognize it when subsequent exposure to the same antigen occurs. As a result, the action will be faster and more effective.

Vaccination practice is based on the potential of adaptive immunity. In fact, the principle of vaccination is that exposure to a small sample of a disease-causing microorganism - or to a part or portion of it - teaches the immune system to rapidly recognize the menace and to create memory that enables the body to fight the real pathogen efficiently during a later encounter. Vaccination basically mimics a natural infection without causing disease. Lymphocytes are the main responsible for the immune response and are distinct in *B* and *T* lymphocytes. Both have a plasma membrane surrounded by receptors that recognize specific antigens. When cell-antigen interaction occurs, lymphocyte splits in many effector cells. B lymphocytes generate plasma cells and secrete antibodies specific to antigen. Moreover, they are responsible of the humoral response. T lymphocytes produce T cytotoxic and T helper cells, which are involved in both humoral and cell-mediated immunity. These two types of lymphocytes can also cooperate in a process that leads to the formation of the memory B cells, whose peculiarity is the ability to generate specific immunoglobulins when a second exposure to the same antigen takes place. Antibodies are a class of proteins called *Immunoglobulins (Ig)* which are able to bind complementary structural particles, called *antigens*. Usually, they are not able to recognize the whole molecule, but only a small specific superficial portion, called *epitope*. Carbohydrates have been widely applied as antigens in the development of vaccines which have been hugely successful in preventing bacterial infections. The long polysaccharide chains found on bacterial capsule are T-independent (TI) antigens as they do not require T-cell activation for the induction of specific B-cell (antibody) response. Polysaccharide antigens directly activate polysaccharide-specific B cells which differentiate then into plasma cells to produce antibodies, but memory B cells are not formed. In general, the antibody response to bacterial polysaccharides is poorly affected by adjuvants. IgM represents the major class of antibodies induced and since their immune response does not induce memory, it is not boosted by subsequent immunizations. Moreover a pre-existing memory B-cell pool can be depleted by immunization with unconjugated polysaccharide, with risk of hypo-responsiveness on subsequent immunizations [4]. The activation of a B cell to create memory B cells requires the participation of macrophages or T-helper cells and this can only be stimulated by T-dependent (TD) antigens, like proteins. Upon interaction with antigen presenting cells (APCs) - such as dendritic cells, macrophages and B cells - the protein antigens are internalized and processed into small peptides which are then re-exposed and presented to T lymphocytes in association with the Major Histocompatibility Complex (MHC) class II molecules. Interaction with T-cells induces B cells to differentiate into plasma cells and memory B cells, thus initiating downstream adaptive immune responses. Unlike TI antigens, TD antigens are immunogenic early in infancy

and the immune response induced can be boosted, enhanced by adjuvants and is characterized by antibody class switch with production of antigen-specific IgG. However, the polysaccharides can be covalently linked to carrier proteins used as source of T-cell epitopes. When this happens, the resulting conjugates bind the B-cell receptor specific to the polysaccharide and are brought into the endosomes. Once inside the cell, the protein portion is digested by proteases to release peptide epitopes, which are exposed on the surface in association with MHCII and presented to the αβ receptor of CD4+ T-cells. Peptide/MHCII-activated T-cells release cytokines to stimulate B-cell maturation into memory cells and induce immunoglobulin class switching from IgM to polysaccharide-specific IgG, so that upon exposure to the same carbohydrate antigen large amounts of high-affinity IgG antibodies can be produced. Consequently, immunization with glycoconjugates induces long-lasting protection against encapsulated bacteria, even among infants and people in high-risk groups [4]. Furthermore, the immune response against glycoconjugates is boosted by subsequent vaccinations.

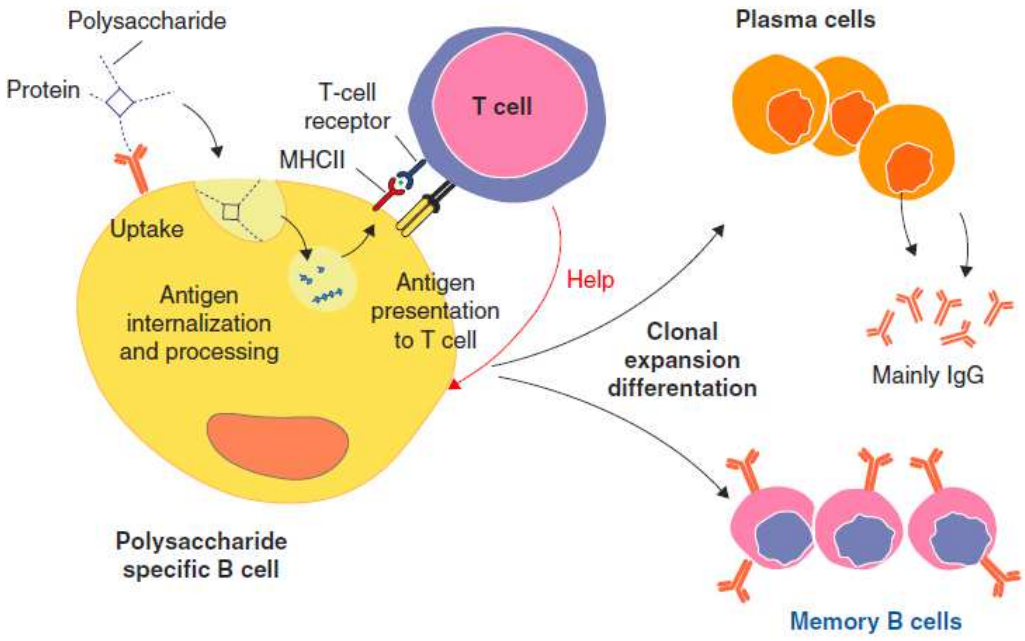

Figure 2. Mechanism of action of glycoconjugates vaccines [4].

1.3 Polysaccharide-based and glycoconjugate vaccines

Bacterial polysaccharides are important virulence factors. Around the 1930s the protective role of antibodies (Abs) induced by pneumococcal polysaccharides started to be investigated and in 1945 the first vaccine composed of purified polysaccharides from selected pneumococcal serotypes was tested in humans [5]. The research on vaccines development was subsequently slowed down by the introduction of antibiotics. However, with the emergence of drug resistant strains, the development of polysaccharide vaccines started again and several of them have been studied in large clinical studies. Polysaccharide vaccines against *Neisseria meningitidis* serogroups ACWY, *Streptococcus pneumoniae* and *Haemophilus influenzae* type b were licensed between the seventies and the eighties [6, 7]. These bacteria possess polysaccharides which are either polymers formed by one monosaccharide unit (homopolymers) or more complex oligosaccharide repeats (heteropolymers), that can be charged or neutral.

Polysaccharide vaccines however did not completely solve the problem of bacterial diseases caused by encapsulated microorganisms. Although their efficacy in adults, they fail to evoke immunological memory or long-lived antibody production being T-cell independent antigens. For their scarce immunogenicity in children less than two years of age, polysaccharide vaccines can be used in adults, but not in infancy and elderly which are the most sensitive target populations [8-10]. Conjugation of bacterial polysaccharides to carrier proteins have allowed to overcome limitations of unconjugated polysaccharide vaccines. The T-cell helper provided by protein epitopes present in glycoconjugates imparts the capacity to induce a long lasting and boostable IgG antibody production to the appended carbohydrates also in children below the age of two [8, 9]. Also, vaccination with glycoconjugates has been proven more effective than the one with polysaccharides in adult population [11, 12]. Finally, conjugate vaccines have been shown to reduce carriage or impact on transmission of meningococci, while there is some evidence that plain polysaccharide vaccines cannot [13].

Avery and Goebel in 1931 were the first to demonstrate that protein conjugates of oligosaccharides instead of polysaccharides alone could also elicit protective antibodies: in their first trial, rabbits immunized with a disaccharide fragment of Type III *Pneumococcus* capsular polysaccharide covalently linked to a carrier protein were protected against challenge by the homologous organism [14]. Nevertheless, the first application of this concept to a vaccine for human use started in 1980 with the development of the first glycoconjugate vaccine against *Haemophilus influenzae* type b (Hib) [15]. Since then, glycoconjugates have been proven

efficacious and cost effective to combat many life-threatening bacteria, such as *Streptococcus pneumoniae* (23 serotypes) [16], *Neisseria meningitidis* (A, C, W and Y) [17] and *Salmonella Typhi* [18-20]. A summary list of all bacterial glycoconjugate vaccines licensed or in development has been recently reported (Table 1) [21].

Table 1. Examples of glycoconjugate vaccines in the market or in development. *Adapted from [21]*

Type of glycan	Organism	Manufacturer	Saccharide	Approach[a]	Carrier
Capsular poly-saccharide	Hib	GSK	PS	SS	TT
		Sanofi	PS	SS	TT
		GSK	Oligo	SS	CRM_{197}
		Merck	Size reduced PS	SS	OMPC
		Pfizer	Oligo	SS	CRM_{197}
		SIIL	PS	SS	TT
		CIGB	Oligo	ST	TT
		Hilleman Lab	Size reduced PS	SS	TT
		Bionet-Asia			
	Hia	NRC Canada	Size reduced PS	SS	CRM_{197} and Protein D
	Meningococcus	GSK	Oligo MenC	SS	CRM_{197}
		Pfizer (Nuron)	MenC size reduced PS	SS	CRM_{197}
		Baxter	MenC PS De-OAc Size reduced	SS	TT
		Hilleman Lab	MenX	ST	TT
		SIIL	MenA Size reduced PS	SS	TT

Type of glycan	Organism	Manufacturer	Saccharide	Approach[a]	Carrier
		GSK	MenX Ps size reduced	SS	CRM_{197}
		GSK	MenACWY Oligos	SS	CRM_{197}
		Pfizer formerly GSK	MenACWY size reduced PS	SS	TT
		Sanofi	MenACWY size reduced PS	SS	DT
		Sanofi	MenACWY	SS	TT
		SIIL	MenACWYX PS	SS	TT, CRM_{197}
	Pneumococcus	Pfizer	4, 6B, 9V, 14, 18C, 19F, 23F, PS except 18C size reduced	SS	CRM_{197}
		Pfizer	1, 3, 4, 5, 6A, 6B, 7F, 9V, 14, 18C, 19A, 19F, 23F PS except 18C size reduced	SS	CRM_{197}
		GSK	1, 4, 5, 6B, 7F, 9V, 14, 18C, 19F, 23F PS except 23F size reduced	SS	Protein D, TT(18C), DT(19F)
		Limmatech Biologics	Multivalent	B	rEPA
		Merck	15 valent	SS	CRM_{197}
		CIGB	1, 5, 6B, 14, 18C, 19F, 23F	NA	TT
	GBS	GSK	Ia, Ib, III PS	SS	CRM_{197}
		GSK	Ia, Ib, II, III, V PS	SS	CRM_{197}

Type of glycan	Organism	Manufacturer	Saccharide	Approach[a]	Carrier
		Various	Ia, Ib, II, III, IV, V, VI, VII and VIII Ps	SS	TT and CRM_{197}
		Pfizer	Multivalent	Platform developed for pneumo conjugates	CRM_{197}
	Staphylococcus aureus	GSK	Type 5 and 8 PS	SS	TT
		Pfizer	Type 5 and 8 PS	SS	CRM_{197}
		GlycoVaxyn (now Limmatech Biologics)	Type 5 and 8 PS	B	rEPA
	Salmonella Typhi	NIH, GVGH/ Biological E, Biomed, Barath Biotech	Vi PS and Fragments	SS	CRM_{197}, TT, DT, rEPA
	Burkholderia pseudomallei	DSTL	Oligo	ST	TetHc
	Klebsiella pneumoniae	Max Plank Institute	CPS repeating unit	ST	CRM_{197}
	Shigella	Limmatech Biologics	*Sh. dysenteriae* type 1 PS	B	rEPA
			Sh. flexneri 2a PS		
		NICHHD	*S. sonnei* and *Sh. flexneri* 2a PS	SS	rEPA
		Institute Pasteur	*Sh. flexneri* 2a oligo	ST	TT
O-Antigen	*Escherichia coli*	Limmatech Biologics/J&J	O1, O2, O6, O25 Expec	B	rEPA
	Salmonella Para typhi A and	NVGH, NIH, IVI	O2 *S. Para-thyphi* A, O9 *S. Enteritidis*,	SS	TT, CRM_{197}, DT

Type of glycan	Organism	Manufacturer	Saccharide	Approach[a]	Carrier
	Non-typhoidal *Salmonella*		O4, 5 *S.Typhimurium*		
	Pseudomonas aeruginosa	SSVI/WRAIR program stopped	O1,2,3,4,5,6,11,12	SS	EPA
	Klebsiella pneumoniae	University Maryland	O1, O2a, O2a,c, O3, O4, O5, O7, O8, O12	SS	PA flagellin
	Vibrio cholerae	NIH, Institut Pasteur	O1 (Inaba and Ogawa), O139	SS; ST	BSA, rEPA, TThc
	Francisella tularensis	CCRC-NRCC and DSTL	O-Ag	ST; B	KLH; rEPA
	Burkholderia pseudomallei	Academic	OPSII	B; ST	AcrA;
	Moraxella catarrhalis	NRC Canada	Truncated LPS	SS	CRM_{197}
		NDCD/NIH	Detox LPS serotype A, B and C	SS	TT, NTHi HMP, UspA, CD, CRM_{197}
Teichoic acids	*Enterococcus faecalis*	UML/Leiden University	LTA	ST	BSA
PNAG	*Acinetobacter baumannii* and other pathogens	Harvard Medical School, Alopexx	β-(1→6)-oligo glucosamine	ST	TT
ExoPS	*Pseudomonas aeruginosa*	Harvard Medical School	Poly-mannuronic acid; alginate	ST	ExoA, Flagellin; TT, KLH, OMV, synthetic peptides
	Clostridium difficile	Guelph University, Max Planck Institute	PS-I	ST	CRM_{197}
		GSK, Guelph University, Max Planck Institute	PS-II	ST; SS	CRM_{197}, *C.difficile* rToxins

Type of glycan	Organism	Manufacturer	Saccharide	Approach[a]	Carrier
		Max Planck Institute	PS-III	ST	CRM_{197}
Cell Wall PS	Group A *Streptococcus* (GAS)	GSK	GAC fragments	ST	CRM_{197}
		Rockefeller University	PS	ST	TT
		Various Academic Institutions	GlcNAc deficient PS	ST	Sp0435
	Aspergillus fumigatus	Zelinsky Inst. Org. Chem./Institute Pasteur	α-(1→3)-glucans	ST	BSA
	Candida albicans	GSK, CCRC	β-(1→3)/β-(1→6)-glucans	SS; ST	CRM_{197}
Fungal glycans		Alberta University/ Theracarb/ Novadigm	β-(1→2)-mannotriose	ST	TT, *Candida* peptides
	Cryptococcus neoformans	Dublin University/J. Hopkins Bloomberg SPH	GXM PS and oligosaccharides	SS; ST	HSA
Myco-bacterial glycans	*Mycobacterium tubercolosis*	Uppsala University/Eurocine AB	AM	SS	Ag85B, TT

a Semisynthetic conjugates from natural carbohydrates: SS; Conjugates synthetic carbohydrates: ST; Bioconjugates: B; not available: na

1.4 Glycoconjugate vaccines preparation

In glycoconjugate vaccines, a covalent linkage between the carbohydrate moiety and the carrier protein has to be installed (**Figure 3**) [4]. Two main approaches based on different chemistry of conjugation have been used so far for glycoconjugate vaccines preparation.

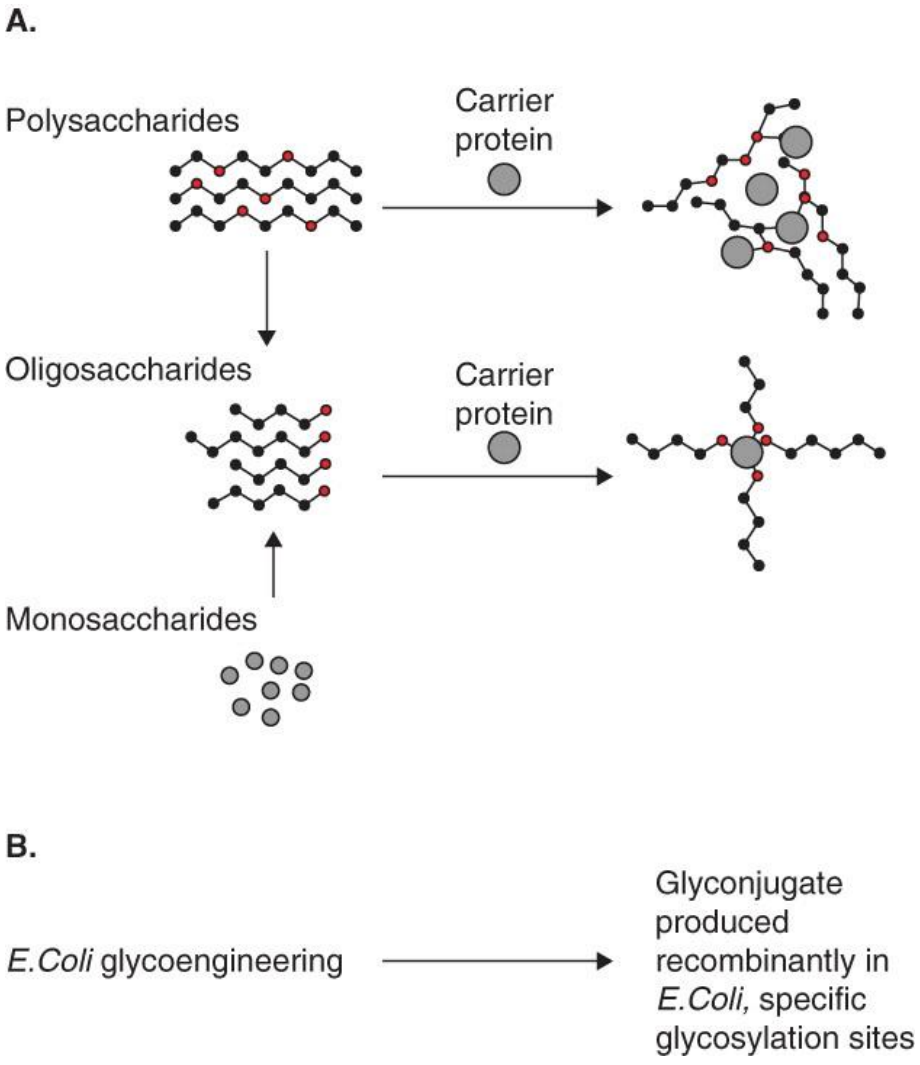

Figure 3. Schematic representation of A) different poly- and oligosaccharide–protein chemical couplings and B) Different way to make glycoconjugate vaccines [4].

One is based on the random chemical activation of the saccharide chain followed by covalent binding with the protein carrier, obtaining a cross-linked structure between the polysaccharide and the protein. A second approach is based on the generation, by controlled fragmentation of

the native polysaccharide, of appropriately sized oligosaccharides which are then activated at their terminal groups, usually with a linker molecule, and subsequently conjugated to the carrier protein obtaining a radial structure (Figure 3)[4]. Six proteins are used as carriers in licensed vaccines: Tetanus toxoid (TT), Diphtheria toxoid (DT), CRM_{197}, the Outer Membrane Protein Complex of meningococcus B (OMPC), Protein D from *H. influenzae* and recombinant Exotoxin A of *P. aeruginosa* [4, 22-25].

Glycan-protein conjugation can take place using the carbohydrate functional moieties (e.g. hydroxyl, carboxyl groups) or alternatively derivatizing the polysaccharide with linkers to allow insertion of specific functionalities (e.g. thiols, bromide) and reduce the steric hindrance between protein and saccharide. One of the most employed transformations for conjugation entails the use of a $NaIO_4$ oxidation which generates aldehydes from cis-diols. These chemical groups can be directly linked to the ε-amine of the protein lysine residues by reductive amination, or further derivatized before linkage to the protein [26-29]. CDAP strategy (1-Cyano-4-dimethylaminopyridinium tetrafluoroborate) is also randomly applied to commonly use hydroxyl groups of polysaccharides for condensation with the amines of the protein [30]. Recently, pneumococcal polysaccharides, pre-activated with sodium periodate, have been conjugated to CRM_{197} carrier protein by an in vacuo glycation method, and capped using sodium borohydride to prepare a 13-valent vaccine which was shown to give an immune response comparable to Prevnar13 for 10 out of 13 serotypes [31]. Dry-glycation (or in vacuo glycation) is a water free conjugation method consisting of co-lyophilization of the protein with the activated sugar, and then subjecting the lyophilized mixture to a vacuum at high temperature.

On a manufacture standpoint, use of shorter oligosaccharides facilitates consistency of production, sterile filtration, purification of the resulting conjugate, particularly from unreacted polysaccharide, and its characterization. Oligosaccharides can be linked to the protein through the reducing end of the sugar directly, or via a spacer. Production of well-defined and uniform lower molecular weight polysaccharide populations is typically achieved by chemical or mechanical polysaccharide fragmentation followed by size fractionation [32-34]. Depending on the polysaccharide structure, $NaIO_4$ oxidation results in simultaneous fragmentation and generation of terminal aldehyde groups available for conjugation (e.g. *H. influenzae* type b CPS). Alternatively, the polysaccharides can be fragmented by treatment with hydrogen peroxide [35] or via acid hydrolysis, and sized by chromatography or ultrafiltration techniques to isolate populations more defined in length for conjugation [34, 36]. Individual bacterial strains may also express a wide range of saccharide sizes, as it is usually the case of O-

polysaccharides, that, in some instances, may not include the desired target size for vaccine development. Also, in this case, isolation of the sugar with desired length is required, impacting on overall yield and complexity of the process.

Although isolation of polysaccharides from bacterial growth is the primary approach used for manufacturing licensed vaccines, approaches avoiding large scale pathogen fermentation have emerged over the last decades [37]. Organic synthesis has shown it can meet the demand of bacterial related oligosaccharides, with the advantages of a more defined structure, ease of characterization, lack of bacterial contaminants, higher batch-to-batch reproducibility, and more robust correlation of the elicited immune response with the oligosaccharide chemical structure [38].

The first synthetic carbohydrate vaccine developed was Quimi-Hib vaccine[39], which was produced by a polymerization approach based on H-phosphonate chemistry. However, chemical synthesis of oligosaccharides remains challenging and time consuming, especially compared to the synthesis of other biopolymers such as peptides and oligonucleotides. Finally, on other more recent approach called bioconjugation and based on glyco-engineering N-glycosylation pathway in bacteria such as *Escherichia coli* is also emerging. The polysaccharide, encoded by the inserted genes, is produced on a polyisoprenoid carrier and then is transferred to an asparagine residue of the carrier protein which has to contain at least one (native or engineered) N-glycosylation site [40, 41].

1.5 The influence of glycoconjugate variables on the immunogenicity

Different variables play an important role on the immunogenicity of glycoconjugates vaccines: size of the saccharide chain, glycosylation degree (or saccharide:protein ratio), conjugation chemistry, the nature of the spacer between saccharide and protein and the kind of carrier proteins. Immunogenic epitopes involved in the interaction with specific antibodies usually comprise precise glycan structures [42]. An early study by Seppälä and Mäkelä investigating the effect of saccharide size and saccharide:protein ratio on the immunogenicity of dextrans-protein conjugates, found that dextrans of low molecular weight conjugated to chicken serum albumin induced strong anti-dextran responses in mice, while increasing the dextrans size resulted in reduced immunogenicity [43]. Laferriere et al. found little influence of the carbohydrate chain length on the immunogenicity of pneumococcal conjugate vaccines in mice

[44]. Pozsgay et al. studied the immunogenicity in mice of synthetic *Shigella dysenteriae* type 1 LPS oligosaccharides conjugated to human serum albumin (HSA). The authors found that octa-, dodeca-, and hexadecasaccharide fragments induced high levels of lipopolysaccharide binding IgG antibodies in mice after three injections and were superior to a tetrasaccharide conjugate. The influence of the carbohydrate:protein ratio was different for the three conjugates. The octasaccharide-HSA conjugate with the highest density evoked a good immune response, while in the case of dodeca- and hexadecasaccharide conjugates, the median density was optimal [45]. Clinical studies of Hib glycoconjugates in 1-year-old infants showed that oligosaccharides with an average degree of saccharide polymerization (avDP) of 7 were equally highly immunogenic as those produced with avDP20, but the shorter one had an higher saccharide:protein ratio [46]. These studies suggest that oligosaccharide chain length and number of saccharide chains loaded on the protein are interconnected in determining the immunogenicity of glycoconjugate vaccines. Once the minimal structure containing protective epitopes has been identified, the optimal value for both variables must be evaluated for each type of conjugate vaccine.

The spacer used for the conjugation could also have an impact on the immunogenicity. It is a short linear molecule that is generally linked to the polysaccharide chain or to the protein or to both moieties, depending on the chemistry, used to facilitate the coupling between the protein and sugar. There is evidence in the literature which suggest that rigid, constrained spacers, like cyclohexyl maleimide, elicit a significant amount of undesirable antibodies, with the risk of driving the immune response away from the targeted epitope on the hapten [47, 48]. The use of a flexible alkyl type maleimide spacer has been reported as a way to overcome the previous observed immunogenicity of cyclic maleimide linkers [49].

Several protein carriers have been used so far in preclinical and clinical evaluation of conjugate vaccines. Proteins such as diphtheria and tetanus toxoids, which derive from the respective toxins after chemical detoxification with formaldehyde, were initially selected as carriers because of the safety track record accumulated with tetanus and diphtheria vaccination. CRM_{197}, a non-toxic mutant of diphtheria toxin [50] which instead does not need chemical detoxification, has been extensively used as carrier for licensed Hib, pneumococcal, meningococcal conjugate vaccines and for other vaccines being developed. An outer membrane protein complex of serogroup B meningococcus has been used by Merck as carrier for their Hib conjugate vaccine [51]. GSK in their multivalent pneumococcal conjugate vaccine introduced the use of the Hib-related protein D as carrier for most of the polysaccharides included into the

vaccine [52, 53]. The team of John Robbins made extensive use of the recombinant non-toxic form of *Pseudomonas aeruginosa* exo-toxin as carrier for *Staphylococcus aureus* type 5 and 8 as well as for *Salmonella typhi* Vi conjugates [54, 55]. A number of clinical trials have been conducted to compare the immunogenicity of different conjugate vaccines with different carrier proteins [56-60]. It is however very difficult a direct comparison of the effect of different protein carriers, due to the coexistence of other variables as conjugation chemistry, saccharide chain length, adjuvant, formulation technology, and previous or concomitant vaccination with other antigens.

1.6 Role of O-acetylation on the immunogenicity

Bacterial capsular polysaccharide (CPS) are composed of monosaccharide structures that can exhibit different substituent groups in their backbone, such as O-acetyl and phosphate moieties. These decorative groups could be part of the epitope and have a key role on the development of an immune response. PS repeating units can contain O-acetyl groups both inside or outside the monosaccharides ring and the presence or its different positions could represent the only difference between the bacteria serotypes. O-acetylation patterns have been determined for several polysaccharide antigens (**Table 2**) [61].

The role of O-acetylation in immunogenicity and pathogenicity cannot be generalized for all microorganisms. Several published papers concerning the impact of bacterial polysaccharide O-acetylation on immunogenicity have been summarized in a recent review [61].

Capsular polysaccharide of *Neisseria Meningitidis* serogroup A (MenA) is largely O-acetylated at position C-3 (>90%) and slightly at position C-4. The importance of O-acetyl groups of MenA PS on the immunogenicity was evaluated in vivo through immunization in mouse [62]. De-O-acetylation of polysaccharides drastically reduced the ability to induce functional antibodies. Native PS alone and conjugated to TT protein induced much higher levels of functional antibody than either conjugated or unconjugated de-O-Ac PS. Anyway, mice immunized with de-O-acetylated conjugate developed functional antibodies, suggesting that epitopes not composed of O-acetyl groups may still contribute to the formation of a protective immune response [62].

Table 2. Structures of the repeating units containing O-acetyl groups of bacterial PS antigens of vaccines licensed or tested in clinical trials [61]

Polysaccharide	Repeat Unit
Neisseria meningitidis	
Group A	→6)-α-D-Man*p*NAc(3/4OAc)-(1→OPO_3→
Group C	→9)-α-D-Neu5Ac(7/8OAc)-(2→
Group W	→6)-α-D-Gal*p*-(1→4)-α-D-Neu5Ac(7/9OAc)-(2→
Group Y	→6)-α-D-Glc*p*-(1→4)-α-D-Neu5Ac(7/9OAc)-(2→
Group B *Streptococcus*	
Type Ia	→4)-[α-D-Neu5Ac(7/8/9OAc)-(2→3)-β-D-Gal*p*-(1→4)-β-D-Glc*p*NAc-(1→3)]-β-D-Gal*p*-(1→4)-β-D-Glc*p*-(1→
Type Ib	→4)-[α-D-Neu5Ac(7/8/9OAc)-(2→3)-β-D-Gal*p*-(1→3)-β-D-Glc*p*NAc-(1→3)]-β-D-Gal*p*-(1→4)-β-D-Glc*p*-(1→
Type II	→3)-β-D-Glc*p*-(1→2)-[α-D-Neu5Ac(7/8/9OAc)-(2→3)]-β-D-Gal*p*-(1→4)-β-D-Glc*p*NAc-(1→3)-[β-D-Gal*p*-(1→6)]-β-D-Gal*p*-(1→4)-β-D-Glc*p*-(1→
Type III	→6)-[α-D-Neu5Ac(7/8/9OAc)-(2→3)-β-D-Gal*p*-(1→4)]-β-D-Glc*p*NAc-(1→3)]-β-D-Gal*p*-(1→4)-β-D-Glc*p*-(1→
Type V	→4)-[α-D-Neu5Ac(7/8/9OAc)-(2→3)-β-D-Gal*p*-(1→4)-β-D-Glc*p*NAc-(1→6)]-α-D-Glc*p*-(1→4)-[β-D-Glc*p*-(1→3)]-β-D-Gal*p*-(1→4)-β-D-Glc*p*-(1→
Type VI	→6)-[α-D-Neu5Ac(7/8/9OAc)-(2→3)-β-D-Gal*p*-(1→3)]-β-D-Glc*p*-(1→3)-β-D-Gal*p*-(1→4)-β-D-Glc*p*-(1→
Streptococcus pneumoniae	
Type 1	→3)-D-AAT-α-Gal*p*-(1→4)-α-D-Gal*p*A(2/3OAc)-(1→3)-α-D-Gal*p*A-(1→
Type 7F	→6)-[β-D-Gal*p*-(1→2)]-α-D-Gal*p*-(1→3)-β-L-Rha*p*(2OAc)-(1→4)-β-D-Glc*p*-(1→3)-[α-D-Glc*p*NAc-(1→2)-α-L-Rha*p*-(1→4)]-β-D-Gal*p*NAc-(1→
Type 9V	→4)-α-D-Glc*p*(2/3OAc)-(1→4)-α-D-Glc*p*A-(1→3)-α-D-Gal*p*-(1→3)-β-D-Man*p*NAc(4/6OAc)-(1→4)-β-D-Glc*p*-(1→
Type 15B	→6)-[α-D-Gal*p*(2/3/4/6OAc)-(1→2)-[Gro-(2→P→3)]-β-D-Gal*p*-(1→2)]-β-D-Glc*p*NAc-(1→3)-β-D-Gal*p*-(1→4)-β-D-Glc*p*-(1→
Type 17F	→3)-β-L-Rha*p*-(1→4)-β-D-Glc*p*-(1→3)-α-D-Gal*p*-(1→3)-β-L-Rha*p*(2OAc)-(1→4)-α-L-Rha*p*-(1→2)-D-Ara-ol-(1→P→
Type 18C	→4)-β-D-Glc*p*-(1→4)-[α-D-Glc*p*(6OAc)-(1→2)][Gro-(1→P→3)]-β-D-Gal*p*-(1→4)-α-D-Glc*p*-(1→3)-β-L-Rha*p*-(1→
Type 22F	→4)-β-D-Glc*p*A-(1→4)-[α-D-Glc*p*-(1→3)]-β-L-Rha*p*(2OAc)-(1→4)-α-D-Glc*p*-(1→3)-α-D-Gal*f*-(1→2)-α-L-Rha*p*-(1→
Type 33F	→3)-β-D-Gal*p*-(1→3)-[α-D-Gal*p*-(1→2)]-α-D-Gal*p*-(1→3)-β-D-Gal*f*-(1→3)-β-D-Glc*p*-(1→5)-β-D-Gal*f*(2OAc)-(1→
Salmonella enterica	
typhi Vi	→)-α-D-Gal*p*NAcA(3OAc)-(1→
Staphylococcus aureus	
Type 5	→4)-β-D-Man*p*NAcA-(1→4)-α-L-Fuc*p*NAc(3OAc)-(1→3)-β-D-Fuc*p*NAc-(1→
Type 8	→3)-β-D-Man*p*NAcA(4OAc)-(1→3)-α-L-Fuc*p*NAc-(1→3)-α-D-Fuc*p*NAc-(1→

Abbreviations: Glc, Glucose; Gal, Galactose; Neu5Ac, *N*-acetyl neuraminic acid (sialic acid); Rha, Rhamnose; GlcNAc, *N*-acetyl Glucosamine; GalNAc, *N*-acetyl Galactosamine; FucNAc, *N*-acetyl Fucosamine; ManNAcA, *N*-acetyl Mannuronic Acid; AAT, 2-acetamido-4-amino-2,4,6-trideoxygalactose; Gro, glycerol, Pne, 2-acetamido-2,6-dideoxytalose; Sug, 2-acetamido-2,6-deoxyhexose-4-ulose; P, phosphate in a phosphodiester linkage.

The high relevance of the O-acetyl moieties for MenA could also be related to the presence of this decorative group within the saccharide ring, probably influencing and specifying the epitope in a unique arrangement that could not be easily mimicked in its absence[61]. In contrast, clinical data from *N.Meningitidis* serogroup C (MenC) vaccination confirmed that both O-acetylated and de-O-acetylated conjugates were very immunogenic and efficacious in humans [63, 64]. MenC CPS is highly O-acetylated at the C-7 and C-8 positions of the sialic acid glycerol chain. The fact that O-acetyl group position is outside of the saccharide ring could explain its low influence on the immunogenicity [61].

Group B Streptococcus (GBS) present a O-acetyl group in the terminal sialic acid residue [65]. Since GBS glycoconjugate vaccines were composed of de-O-acetylated polysaccharide due to

acetyl loss during vaccine preparation, the discovery of acetylated sialic acid made it necessary to evaluate the impact of acetylation on immunogenicity. Thus, human sera coming from immunization with de-O-Ac PS-TT glycoconjugate vaccines of GBS Ia, Ib, II, III, or V strains were analyzed by opsonophagocytosis assay. The study revealed that the vaccine-induced antibodies were effectively functional against all strains of GBS, including Ib, III and V strains despite their high level of acetylation [66].

Regarding *Streptococcus Pneumoniae* CPS, the impact of O-acetyl has been studied only for the 9V and 18C serotypes. In both cases the presence of O-acetyl groups does not seem essential to elicit a functional antibody response [67, 68].

The capsular polysaccharide (Vi) of *Salmonella Typhi* is the most virulent factor and represents the major vaccines target [69]. Vi PS is variably O-acetylated at the C-3 of the repeating monosaccharide [70]. Degree of O-acetylation represent one of the most important factors that influence the Vi immunogenicity and it varies in different Vi preparations [69]. O-acetyl group is the dominant epitope of Vi [71] and though partial PS de-O-acetylation may slightly increase immunogenicity, the complete de-O-acetylation results in reduced antigenicity and immunogenicity [69, 71]. Therefore, for Vi and Vi-protein conjugate vaccines, the level of O-acetylation is regarded as a measure of vaccine potency and is required to be at least 52% [70].

Staphylococcus aureus serotype 5 (CP5) and serotype 8 (CP8) repeating units share similar trisaccharide structural that is identical in monosaccharide composition differing only in the glycosidic linkages between the sugars and the sites of O-acetylation [72]. The native and fully de-O-Ac polysaccharides of CP5 and CP8 were conjugated to the CRM protein and the impact of O-acetylation was evaluated through an immunization study in mice. Analysis of the opsonophagocytic activity of the sera (**Figure 4**) revealed that the antibody response requires the presence of O-acetyl modifications on the CPS, therefore variations in O-Acetyl level should be minimized to ensure consistent functional immune responses and efficacy [73].

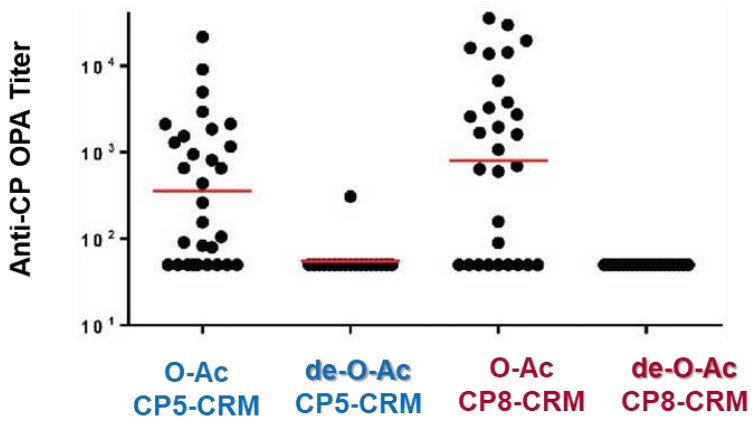

Figure 4. O-acetylation is necessary for capsular polysaccharide conjugates to induce effective opsonophagocytic killing responses [73].

O-acetyl groups have been shown to influence the immunogenicity or antigenicity of various bacterial PSs and therefore is an important parameter to monitor during conjugation. It appears to play a more important role for those antigens composed of few repeating units of saccharides and when it is located in the ring positions. In any case, it is clear how each bacterial polysaccharide antigen should be considered and analyzed independently as there is no general rule for all [61].

1.7 Glycans epitope mapping

Epitope identification allows design of immunogenic antigens important for vaccine development, diagnostics and therapeutics [74]. "Epitope" is the specific region of the antigen recognized by the antibodies of the immune system, whereas, the part of an antibody that binds the epitope is called "paratope". B cell epitopes are usual classified as sequential or linear (continuous) and conformational (discontinuous). A linear epitope is recognized as the primary structure of an antigen while a conformational epitope consists of residues that may be distantly separated in the primary structure and are recognized due to the close proximity within the folded 3D structure [75]. Conformational epitopes are associated with a distinct secondary structure of the glycan, a feat that may only be achieved in longer sequences comprising multiple repeating units [76]. Epitope mapping is the determination of the antigen-antibody binding site through structural studies and it is usually used for protein-antibody complexes but can also be suitable to carbohydrates. However, the heterogeneous composition of bacterial

polysaccharides makes it difficult to identify the structural features necessary for immune protection. Instead, shorter and well-defined oligosaccharide structures are more suitable for characterization of the antigen epitope. Design of an effective vaccine needs elucidation of the right antigenic epitope that confers the production of antibodies that can protect the host from a pathogen (so-called protective epitopes) [76]. The identification of the epitope recognized by the immune system could provide the basis for the development of a new immunogenic glycoconjugate vaccine.

Antibodies recognize their target with high affinity and specificity. There are many techniques used to study antigen-antibody interaction and characterize the structural epitope involved in binding. Some of these techniques are represented by *Surface Plasmon Resonance* (SPR), *enzyme-linked immunosorbent assay* (ELISA), Mass *Spectrometry*, *Isothermal titration calorimetry* (ITC), *Nuclear Magnetic Resonance* (NMR), *X-Ray Crystallography* and *Molecular Dynamic* (MD) simulations. A synergistic approach involving multiple techniques is usually used.

Seeberger and coworkers reported a combination of synthetic glycan microarray, SPR, and saturation transfer difference (STD) NMR used to analyze the antibody-antigen binding of *Bacillus anthracis*. The RU is composed of three rhamnose residues and a terminal anthrose. Synthetic tetrasaccharide was selected for STD-NMR analysis unveiling a preferential binding of the disaccharide moiety anthrose-(β1→3)-rhamnose substructure [77]. In a subsequent work they demonstrated the potential of multivalent display of *Clostridium Difficile* disaccharides to obtain the antigenicity characteristic of larger glycans [78, 79]. Besides, disaccharide structure of *Candida albicans* PS has been identified as a possible target epitope of glycoconjugate vaccine development [80]. A conformational epitope was described for *Shigella flexneri* serotype 2a by X-ray crystallography. The epitope is contained within two consecutive RUs but only six discontinuous sugar rings of a decasaccharide make direct contacts with the antibody [81]. In our group, structural studies aimed to map polysaccharide antigenic determinants and epitope conformations have been applied to different bacteria. A combined technique strategy involving STD-NMR and X-ray crystallography was used to study at atomic level the minimal epitope of *Group B Streptococcus* type III revealing a sialylated hexasaccharide epitope within two adjacent repeating units [82]. The same approach applied to *Neisseria Meningitidis* Serogroup A identified a O-Acetylated trisaccharide as the minimal antigenic epitope [83].

Structure-based rational design promises improvements in vaccine efficacy. Recently, structure-based studies have also been apply to identify accessible epitopes of the Spike (S) protein exposed on the surface of the SARS-CoV-2 virus, the cause of the ongoing COVID-19 global pandemic [84]. Glycan shields allow viruses to hide from their host's immune system. It seems that glycans of Protein S may also play a critical role in gaining access to the cell, without which the virus would be rendered harmless. [85]

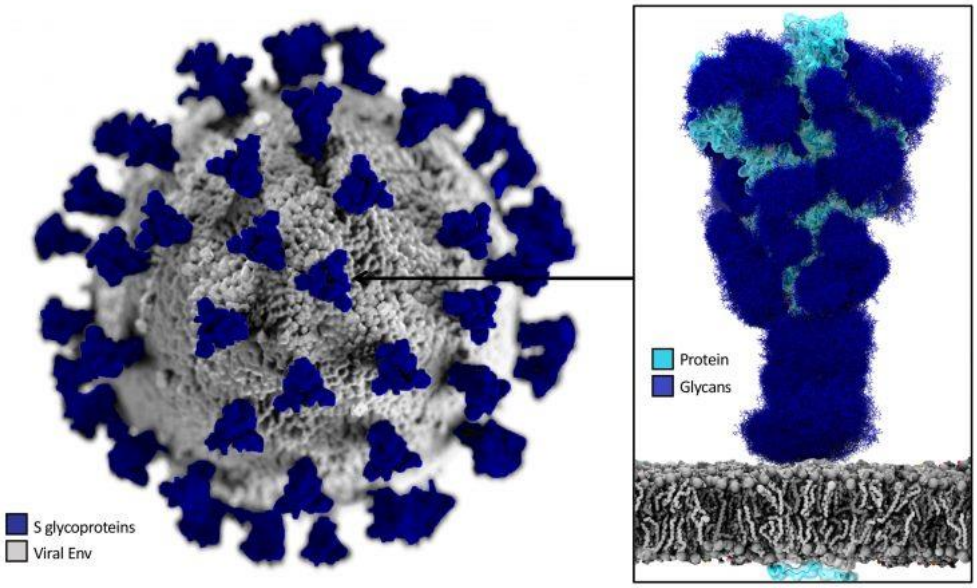

Figure 5. Graphical representation of the SARS-CoV-2 virus surface (grey) with the spike (S) proteins highlighted in blue [85].

It was found that protein glycosylation sterically hinders the interaction between antibodies and S in a significant manner [84]. MD simulations revealed a role of some N-glycans as modulators of the receptor binding domain (RBD) conformational plasticity. Deletion of these glycans elicits a destabilizing effect on the RBD conformation [85]. Furthermore, cryo-electron microscopy and binding assays identified a human mAb that has broad neutralizing activity by recognizing an epitope that includes a glycan conserved within the *Sarbecovirus* subgenus (including SARS-CoV-2) [86]. Overall, these works highlight the importance of glycans as essential structural elements for virus infectivity.

1.7.1 Surface Plasmon Resonance (SPR)

SPR analyses have emerged as powerful tools for the characterization of label-free biomolecular interactions, enabling the dynamics of complex formation and dissociation to be monitored in real-time. SPR has made significant progress in the last two decades and is now becoming a relevant technology for developing immunological assays for in-depth characterization of protein-glycan interactions.

SPR is a phenomenon that occurs once plane-polarized light with a certain angle of incidence propagates from a denser medium (high refractive index) into a less dense one (low refractive index), refracting the light beam towards the interface. By changing the incidence angles, in this case higher angles of incidence, all the light is reflected inside the medium of higher refractive index, a phenomenon described as total internal reflection (TIR). If the surface is coated by a noble metal (e.g. gold) this reflection is not total, with this component transformed into an electric field called evanescent wave, which penetrates about 200 nm into the lower refractive index medium, where the ligand happens to be immobilized and the analyte is flown at real time. The penetrating photons therefore will interact with gold surface electrons, and if possessed with correct quantum energy the latter are converted into plasmons. This energy transfer results in light no longer being reflected from the surface, viewed as an intensity loss of reflection and seen as a dip in the SPR reflection intensity curve. At a certain incidence angle, the momentum of the incoming photons matches the momentum of the surface plasmons with the electrons resulting in momentum resonance, thus giving the name of surface plasmon resonance. Importantly, the angle at which surface plasmons resonance occurs is called resonant angle, characterized by dip in intensity. Once the chemical composition of the surface changes, one expects the refractive properties of the medium to change and therefore the momentum of the incident photons to change resulting in a shift in the angle of the reflected light and the angle associated with the condition of resonance (**Figure 6**) [87].

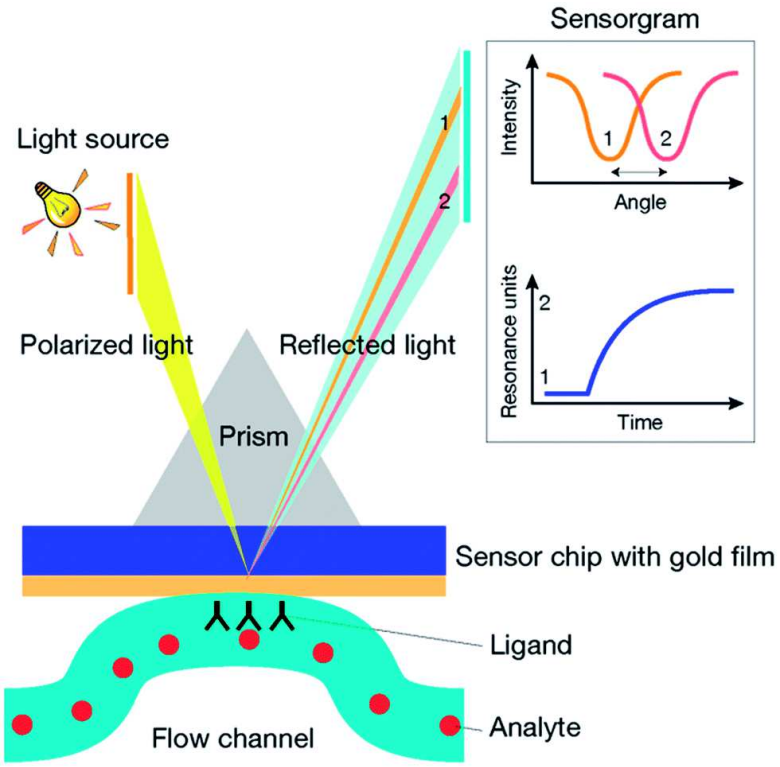

Figure 6. Schematic configuration of an SPR detector. The incident polarized light is coupled by a glass prism on the biosensor chip coated with a thin layer of gold and integrated with a flow channel for continuous flow of buffer. At a defined incidence angle, the SPR phenomenon is seen as a dip in the intensity of the reflected light, characteristic of the specific angle of reflection. The shift of the angle of reflection from position 1 to position 2 reveals a change in the composition of the medium near the gold film as a result of the binding between the ligand and the analyte. The angular variations are recorded in resonance units and plotted versus time in a sensorgram[87].

In a SPR experiment a ligand is immobilized on the surface of a sensor chip with an appropriate coupling chemistry. Then, an analyte is injected over the coated surface in a continuous flow. The binding event between the ligand and the analyte generates a response proportional to the bound mass evidenced by a variation in the refractive index of the solvent around the surface. As the analyte binds the ligand, the surface refractive index of the medium adjacent to the sensor increases, which leads to an increase of the resonance units. The formation and dissociation of the biospecific complex can be described using the direct estimation of the association rate constant (ka) and the dissociation rate constant (kd). At equilibrium, by definition, the amount of analyte that is associating and dissociating with the ligand is equal. After association, the analyte solution is replaced by running buffer, and the ligand-analyte complex is allowed to dissociate. The equilibrium dissociation constant is the ratio KD = kd/ka. By means of SPR analysis, insights into binding affinity and kinetics can be obtained, providing elements useful for investigating, selecting and tailoring target molecules (**Figure 7**) [88].

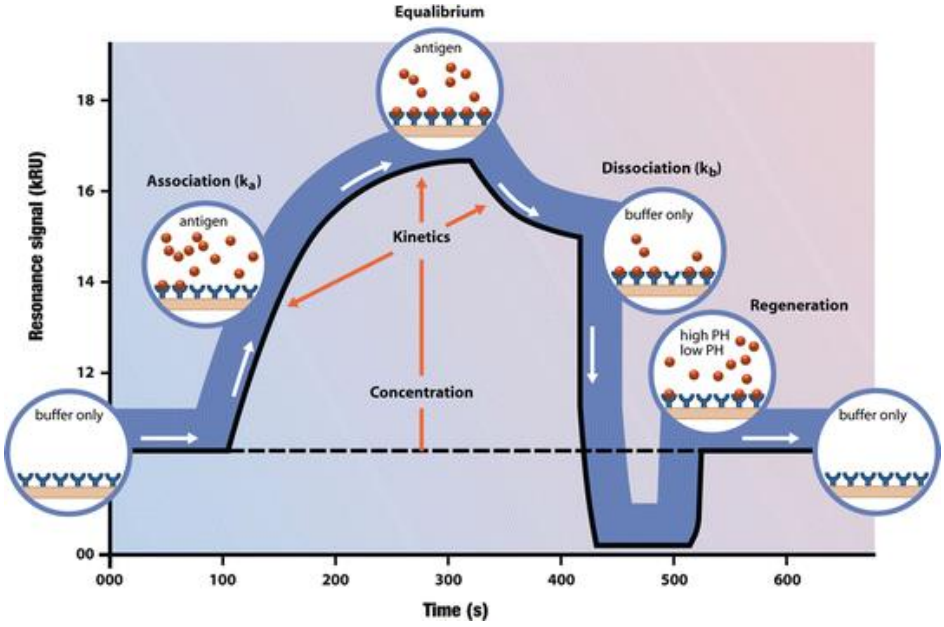

Figure 7. Real-time binding with SPR enables measurement of concentration, affinity, and kinetics [88].

Another application of SPR useful for polysaccharide epitope mapping is represented by a competitive SPR assay. A library of different antigens can be screened used as inhibitors of the binding between mAb and another antigen previously immobilized on the chip. The aim is to assess the ability of the competitors to block one another's binding between mAb and ligand immobilized on the chip. This approach has been successfully applied to support the identification and characterization of the conformational epitope of the type III polysaccharide from Group B *Streptococcus* (GBS), recognized by specific protective mAb elicited by vaccination [82]. In this case, oligosaccharides of different lengths complexed with the antibody were flowed onto a chip in which the polysaccharide had previously been immobilized. The measurement of the binding inhibition capacity of each oligosaccharide allowed to identify the minimum length of the epitope necessary for antibody recognition.

1.7.2 Saturation Transfer Difference (STD)- Nuclear Magnetic Resonance (NMR)

Nuclear Magnetic Resonance (NMR) represents a powerful technique to unravel binding process at a molecular level in solution. Therefore, it has become an essential tool for characterizing the biological processes of molecular recognition, relying on the information obtained either by looking at the resonance signals of the ligand or the protein [89]. Ligand-based NMR experiments provide methods to map glycotope moieties engaged in intramolecular interactions, augmented by the determination of both free and bound conformations in solution, thus offering opportunities for glycotope interactome interpretation and rational design of glycoconjugate vaccines.

In this context Saturation Transfer Difference (STD)-NMR has emerged as one of the most robust experimental techniques for the study of protein-glycan interactions [90]. Notably, STD NMR spectroscopy is a powerful tool that permits to:

- verify the presence of the interaction between small molecules and their receptor(s);
- analyze the binding process at molecular level;
- characterize the ligand region(s) directly involved in the binding process by deriving the epitope map.

This technique is applicable to solution systems in fast exchange, like small ligands with a medium-weak affinity to the receptors, exhibiting a K_D generally in the millimolar to micromolar range (10^{-6} -10^{-3} M) [91]. Some of the main advantage of this technique rely on the fact that the spectrum analysis only focuses on the ligand, and only small amounts of non-labeled protein and ligand are necessary, making this technique a very popular method of fragment-based vaccine design.

Sample preparation is often composed by a molecular receptor (large molecule with MW > 15kDa, in a concentration ranging from 10^{-5} to 10^{-6} M) in the presence of a large molar excess (typically from 1:10 to 1:1000 molar equivalents) of the ligand target to be studied [91]. On the one hand, molecular receptors with large molecular weights possess larger correlation times (τ_c), hence enhancing their spin diffusion, and increasing efficiency of protein saturation its transfer to the ligand. On the other hand, the efficiency of STD-NMR relies in the number of ligand molecules in solution when saturation is in place, therefore using a high ligand excess allows the transfer of saturation from one molecular receptor to a larger fraction of ligand molecules. This has the benefit of increasing the experiment sensitivity at the cost of using very

diluted samples of protein (μM range). Depending on the affinity of the system, both ligand to protein ratio, saturation time and the temperature of acquisition have to be finely tuned to achieve the best results. STD-NMR involves the acquisition of two experiments:

- 1D-^{1}H NMR spectrum without protein saturation, so-called *off-resonance* (I_0) spectrum
- 1D-^{1}H NMR spectrum, in which the protein was selectively saturated, for instances at 7-8 or -1 ppm, respectively in their aromatic and aliphatic protons, using a low power radio-frequency during a period of time (saturation time), yielding the so-called *on-resonance* spectrum (I_{SAT}).

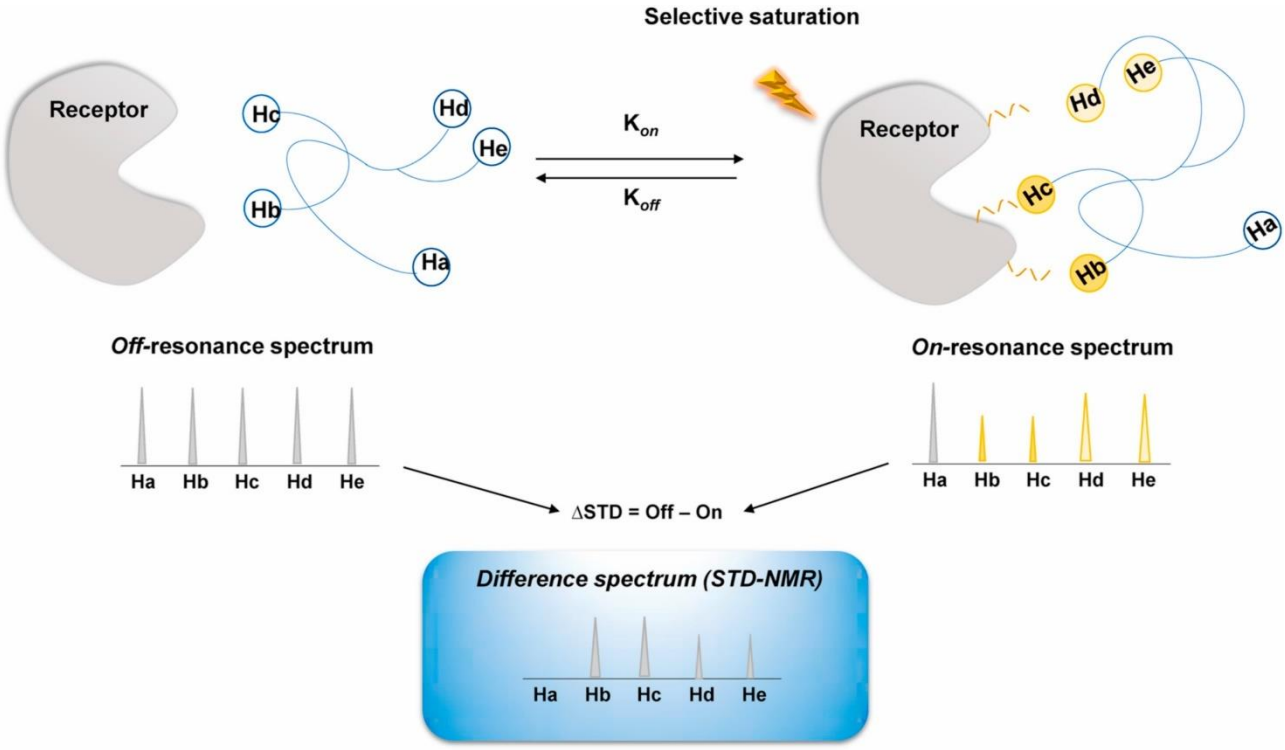

Figure 8. Schematic representation of Saturation Transfer Difference (STD)-NMR technique. On the left: the receptor and unbound small molecule that did not receive receptor saturation. On the right: the receptor is selectively saturatedThe magnetization is transferred from the receptor to the ligand protons (highlighted in yellow in the figure) by intermolecular NOE. Protons in close contact to the binding pocket receive a higher degree of saturation (Hb and Hc in on-resonance spectrum) with a following decrease of ligand signal intensities, indicative of the binding. On the contrary, protons far from the binding pocket do not receive magnetization from the protein and are not reduced in signal intensities (Ha). The Saturation Transfer Difference (STD)-NMR spectrum (in the blue box) obtained by subtracting the on-from the off-resonance spectrum, shows only the ligand signals involved in the binding process.

As referred above, in addition to the protein size and ligand excess, the time interval used to saturate the protein (saturation time-T_{SAT}) and the dissociation kinetics (K_D) will control the efficiency of the macroscopic transfer of saturation to the ligand (I_{SAT}). The macroscopic transfer of saturation is a result of the polarization of the protein to non-equilibrium state, and as a result of relaxation to equilibrium, intermolecular negative NOEs with the ligands protons take place in the bound state, mostly to protons in closer proximity to the binding pocket surface. Consequently, this protein to ligand transfer of saturation, under negative NOE, will reduce the intensity of the ligand resonance signal under on-resonance conditions (I_{SAT}), in comparison to the reference spectrum (I_0). The STD-NMR results from the subtraction of latter on-resonance from the off-resonance spectrum respectively ($I_{STD} = I_0 - I_{SAT}$). Since signals are reduced comparatively to the reference spectrum ($I_{SAT} < I_0$), the subtraction of the aforementioned spectra ($I_0 - I_{SAT}$) leads to positive difference signals, an indication of a binding event. Thus, in the resulting difference spectrum (I_{STD}), only the signals of the ligand receiving saturation transfer from the protein will remain, since it is expected that non-binding molecules have equal intensities in both spectra and the difference spectra cancels out ($I_0 - I_{SAT} = 0$). Therefore, it is important that the on-resonance irradiation frequency does not result in any ligand resonance irradiation. The STD intensities (I_{STD}) are calculated by following equation (1) [91]:

$$I_{STD} = \frac{I_0 - I_{SAT}}{I_0} \quad (1)$$

where I_0 is the intensity of a signal in the off-resonance experiment (the reference spectrum), I_{SAT} is the intensity of the signal in the on-resonance experiment (the saturated spectrum).

Since the signals of the ligand in a STD-NMR experiment do not show the same amount of saturation, STD-NMR can be used as a fingerprint to qualitatively detect binding and quantitatively assess the strength of this interactions. Efficiency of magnetization transfer from protein to ligand by intermolecular NOE in the bound state is correlated to the inverse sixth power of their distances. Hence, explaining for the differences of saturation transferred among different protons of the ligand, ultimately indicating differential spatial proximities between different moieties of the ligand when positioned in the binding pocket.

1.7.3 X-ray crystallography

X-ray crystallography allows to clarify the three-dimensional (3D) structure of a molecule at atomic resolution that is essential for the detailed understanding of its physiological functional. In 1926 James Sumner demonstrated that proteins can be crystallized, and must therefore adopt a regular, ordered lattice [92]. The very first crystal structure of a macromolecule, the sperm whale myoglobin, was solved in 1957 by Sir John Kendrew, first at 6 Å [93] later improved to 2 Å [94]. Since then, X-ray became the gold-standard method of choice to obtain atomic resolution information about macromolecules. X-ray crystallographic studies of ligand-antibody (Fab) complexes provided the most detailed structural pictures of specific binding reactions at the combining sites of antibody molecules [95]. Protein crystallography is based on the diffraction of X-rays by the electrons composing a biomolecule. X-rays are electromagnetic radiation of very short wavelength of around 1 Å (1 Å = 10^{-10} m) discovered by Wilhelm Rontgen in 1895. They can be produced using various laboratory sources or at synchrotrons. Synchrotrons are employed when very high-intensity and highly focused X-rays are desirable [96]. In the early 20th century Max von Laue revealed for the first time the diffraction pattern of a periodic crystal impinged with X-ray. Soon after, William Lawrence Bragg derived a general equation, known as the *Bragg's Law*, to describe the founding principle of image formation by X-ray diffraction. A diffraction pattern reflects the internal molecular composition of the crystal and can be used to calculate an electron density map. This map is used to progressively assemble and refine an atomic model, that is carefully validated before submission in the Protein Data Bank (PDB). The steps involved in the determination of a protein structure are illustrated in **Figure 9**.

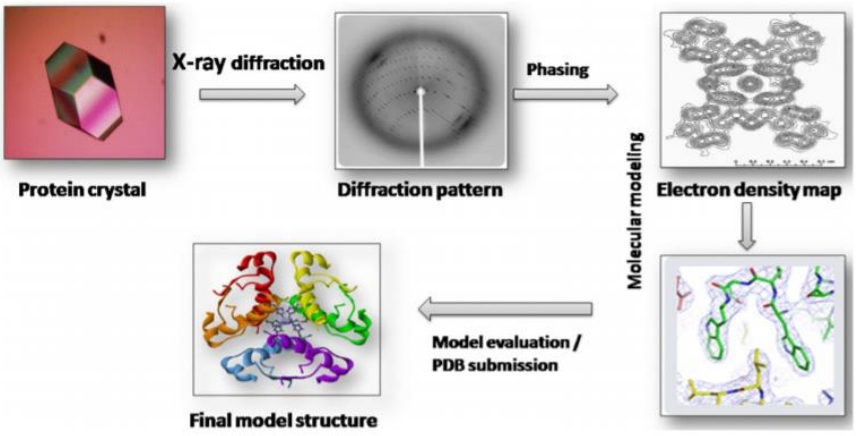

Figure 9. Schematic diagram showing the workflow for structural determination of protein by X-ray crystallography.

Protein crystallization

The first stage to obtain an X-ray crystallographic structure is to obtain a crystal of the protein of interest. A single molecule if exposed to an X-ray beam would cause the scattering of the incident radiation, nevertheless into a very weak signal. Thus, in order to magnify this signal, the molecules have to be arranged periodically into a crystal lattice, leading to a constructive interference of the scattered radiation and therefore to an amplified signal resulting in sharp diffraction spots. Importantly, the quality of the final model is directly influenced by the quality of diffraction, so the crystal quality regarding its purity and order are key for the successful tridimensional structural determination of the protein in question. Obtaining a good diffracting crystal is regarded as the bottle neck of solving a structure by X-ray crystallography. Several conditions can be considering as factors that affect protein crystallization such as: protein concentration and homogeneity, pH, precipitant, ionic strength, temperature, additives and ligands. Any of these factors can be determinant in finding a single crystal or no crystal at all.

The most common technique for growing protein crystals is through vapor diffusion and can be performed using hanging or sitting drop methods. In these methods, a drop containing a mixture of a precipitating solution (salt or polymer) and protein is placed in a sealed chamber over a reservoir that contains the precipitant solution. Because the concentration of the protein and the precipitant are reduced to half, water then evaporates from the drop to the reservoir until the osmolarity equilibrium is reached between the drop and the reservoir. The controlled dehydration causes a slow increase in the concentration of both the protein and precipitant in the drop, ideally placing the protein in the crystal nucleation zone of the phase diagram. Typically, the protein crystallization process can be divided in two steps: nucleation and crystal growth. During nucleation the protein solution is supersaturated leading to the increase collision of protein molecules against each other and eventually to form spontaneously small microscopic clusters of protein from which crystal eventually grow in the metastable zone. In addition, in high supersaturation regions protein aggregates and precipitates, while in the undersaturation zone, the protein is dissolved and will not crystalize. Therefore, the process of protein crystallization is mainly a trial-and-error procedure of sampling a wide chemical space of condition leading to slow protein precipitation until formation of crystals.

Due to the vast variables that influence the process of protein crystallization, it requires time and protein consuming. To overcome this, crystallization robots dispensers for automated

crystallization increase the number of conditions under testing, using small amounts of protein, when compared with the tradition manual drop casting.

Crystal symmetry and space groups

Crystals are three-dimensional, ordered and periodical assemblies of identical molecules, that are arranged in identical building blocks in a repeating pattern, disposed in all tridimensional spatial dimensions. By definition, the crystal can be decomposed into its smallest building blocks, defined as unit cell that can replicate the entire crystal by translation operations of its lattices. The unit cell can be described by a set of angles and lengths extending from the cell edges. The smallest volume of the unit cell containing all the structural information, and that can generate the whole unit cell, once duplicated and moved by crystallographic symmetry operators is denominated as asymmetric unit (ASU). This crystal ASU can contain one or more biological entities, and in some cases only part of functional unit. The dimensions of the unit cell can be described by three vectors (axis edges) a (x), b (y) and c (z) and three angles α, β and γ.

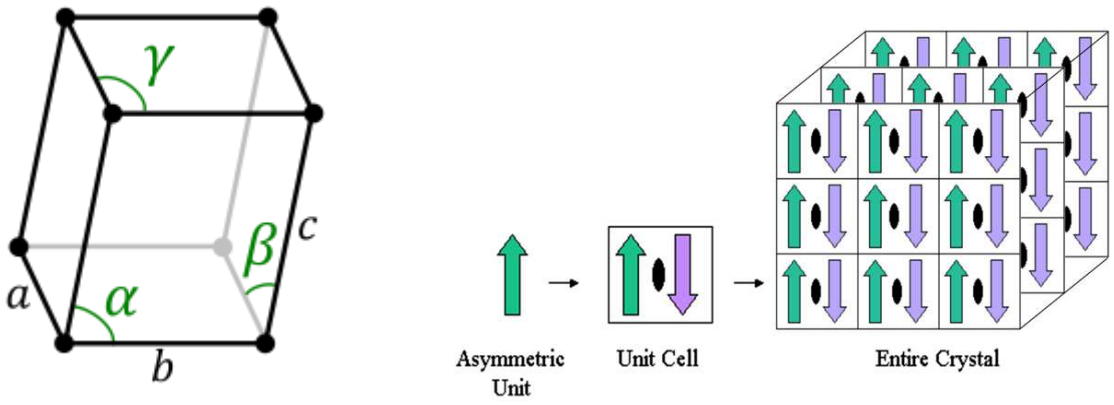

Figure 10. Crystal structure [97].

The edges that divide the crystal into identical unit cells are defined by lattice points, which connect each unit cell in the crystal structure, so the sets of planes most readily apparent in a crystal lattice are those determined by the faces of the unit cells. The position of each molecule in a crystal lattice is a lattice point. The internal symmetry of an elementary cell and its contents is described by its space group. The space group defines a set of symmetry operation that allow to convert the ASU in the crystal lattice. The combination of all symmetry operations with the

translational elements give 230 possible space groups. Space groups can be divided by four types of possible lattice centering's:

- Primitive (P)
- Centered (C)
- Body centered (I)
- Face centered (F)

that can be combined with seven crystal systems namely:

- Triclinic
- Monoclinic
- Hexagonal
- Trigonal
- Cubic
- Tetragonal
- Orthorhombic

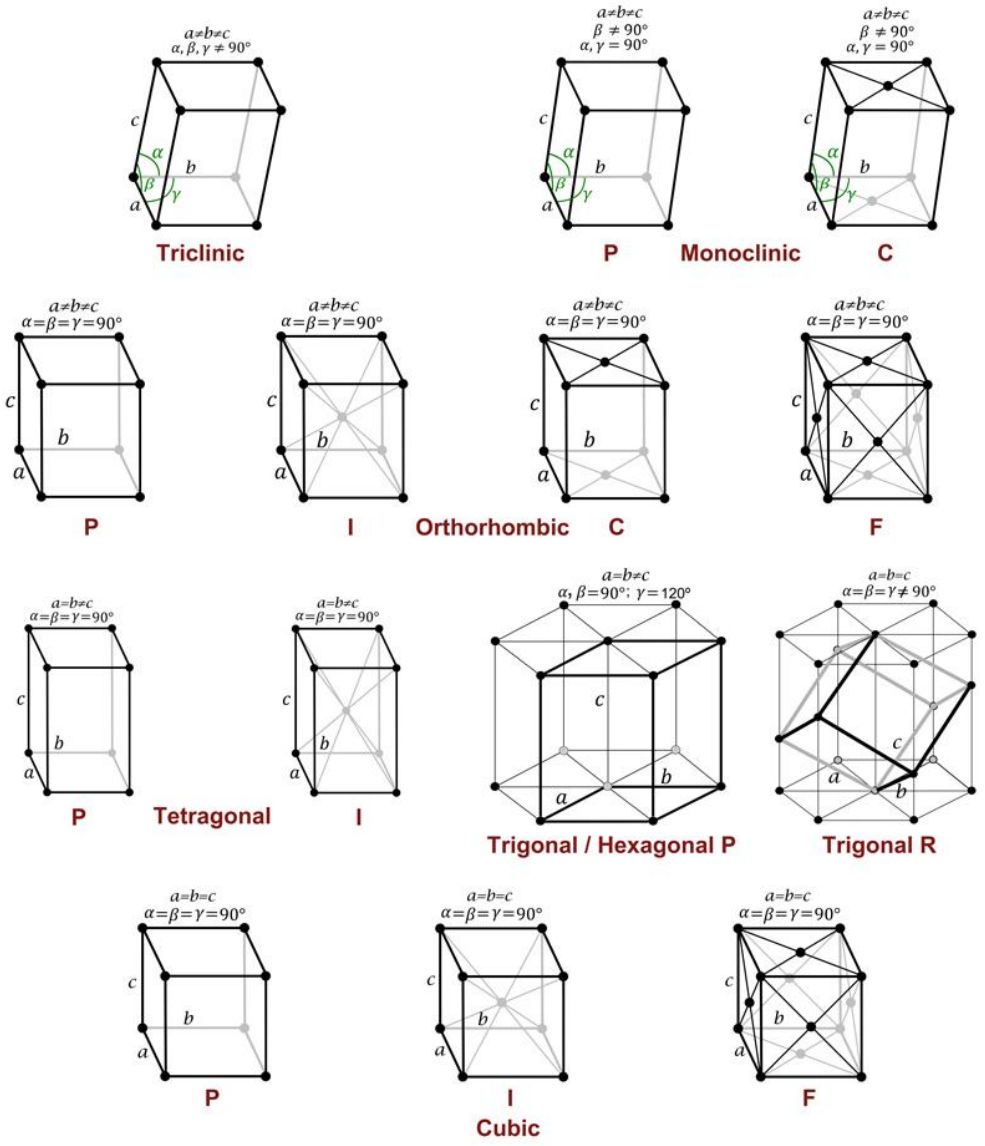

Figure 11. Representation of the different crystal systems (Triclinic, Monoclinic, Orthorhombic, Tetragonal, Hexagonal, Rhombohedral and Cubic), represented as the four different allowed unit cell (Primitive-P, Centered in the side-C, Centered in the body of the cell -I, centered in all faces of the cell -F. The spheres in the Bravais Lattice represent the lattice points corresponding not with atoms but with places in space that are indistinguishable from each other.

The internal symmetry of the biological element contents of the unit cell is described by symmetry operations such as *translations*, *rotations* and *reflections*, and their combinations such as centers of symmetry, screw axe and glide planes. A rotational symmetry operator is defined as a n-fold rotation of 360/n degrees over a symmetry element impinging the object, that transforms the object identical to its original one. These rotations can assume 1-, 2-, 3-, 4- or 6- fold axes. Translations on the other hand can be understood as movements along a specific

distance length of the axes of a given unit cell, allowing its superposition along a symmetric copy in the vicinal cell. Finally, screw axis results from a combination of rotation and translation. The symbol n_m represents a n-fold screw axis with a translation *m/n* of the unit translation. Therefore, molecules on a 3_1 screw axis in a unit cell, can be symmetrically rotated by 120º and translated by one third of the axial length in the direction of the rotation axis. Hence, the symmetry operations can be applied over the ASU thus generating the whole crystal, which in practical terms means one only needs to build the protein content of the ASU. Due to the chirality of aminoacids, mirror planes and inversions centers are not found in protein crystals, since those change the hand of the molecule. This limitations on the symmetry of unit cells containing chiral molecules reduces the number of spaces groups from the original 230 to 65.

Table 3. Different space groups in protein asymmetric units

Lattice type	Class	Space group	Cell restrictions	Angular restrictions
Triclinic	1	P1	a≠ b≠ c	
Monoclinic	2	P2, $P2_1$, C2	a≠ b≠ c	α= β= 90º γ
Orthorhombic	222	P222, $P222_1$, $P2_12_12$, $P2_12_12_1$, C222, $C222_1$, F222, I222, $I2_12_12_1$	a≠ b≠ c	α= β= γ= 90º
Tetragonal	4 422	P4, $P4_1$, $P4_2$, $P4_3$, I4, $I4_1$, P422, $P42_12$, $P4_122$, $P4_322$, $P4_12_12$, $P4_32_12$, $P4_222$, $P4_22_12$, I422, $I4_122$	a= b≠ c	α= β= γ= 90º
Trigonal	3 32	P3, $P3_1$, $P3_2$, R3, P312, P321, $P3_121$, $P3_221$, $P3_112$, $P3_212$, R32	a= b≠ c	α= β= 90º, γ= 120º
Hexagonal	6 622	P6, P61, $P6_2$, $P6_3$, $P6_4$, $P6_5$, P622, $P6_122$, $P6_522$, $P6_222$, $P6_422$, $P6_322$	a= b≠ c	α= β= 90º, γ= 120º
Cubic	23 432	P23, F23, I23, $P2_13$, $I2_13$, P432, $P4_132$, $P4_332$, $P4_232$, F432, $F4_132$, I432, $I4_132$	a= b= c	α= β= γ= 90º

Principles of protein crystal diffraction

Once a protein crystal is obtained, data collection is the next step in the process of determining the three-dimensional structure of the protein of interest. Protein crystals, which reveal large solvent channels, are fragile entities due to a high solvent content which can vary between 30 and 70%. Given their fragility, it is usually necessary to stabilize them before handling. To minimize the effects caused by radiation damage, data is collected at cryo-temperatures. To avoid the formation of crystalline ice during collection and rapid freezing of protein crystals in liquid nitrogen, the crystals can be immersed in a collection solution added with cryoprotective agents (ethylene glycol, sucrose, glycerol). Finally, in the data collection phase, a strategy should be optimized to obtain a data set with high redundancy, completeness and signal-to-noise ratio. Exposure time is a critical parameter and, when too short, the signal-to-noise ratio will be low, especially important for the faintest high-resolution reflections, while the long exposure time leads to highly saturated sports with increased susceptibility to radiation damage. The dataset is collected in snapshots taken during the rotation of the crystal, the greater the oscillation angle, the more reflections are collected on a single exposure, however if the oscillation is too large, the reflections will overlap on the detector; Crystals with higher mosaics require the use of lower rotation angles to have a complete profile of each point. The raw results of a diffraction experiment are a set of diffraction images stored as 2D grids of pixels containing individual reflection intensities. Most reflections are measured many times and their intensities must be averaged after all necessary corrections have been applied and appropriate scaling. This process is known as "*scaling and merging*", resulting in the indexing of Miller indices with unique reflection intensities, accompanied by a standard uncertainty. Multiple observation of the same reflection provides a means of identifying and rejecting potential outliers.

Once a monochromatic X-ray beam hits the crystal, the radiation is scattered by the electrons and the diffraction pattern is recorded in a detector. Each reflection contains information about the periodic arrangement of the molecules in the crystal, which can be reconstructed as electron density. Protein crystallography is based on the interaction phenomena of X-rays with electrons present in biomolecules. In 1913, W. L. Bragg derived a general equation known as Bragg's law. Consequently, an X-ray beam will only be diffracted when it impinges on a set of parallel planes in a crystal lattice, defined by the Miller indices (h, k, l), if a constructive interface of the scattered X-rays occurs:

$$\eta\lambda = 2d_{hkl}\sin\theta \tag{2}$$

where η is an integer, λ is the wavelength of the X-ray beam, d_{hkl} is the interplanar spacing between two lattice planes, and θ is the diffracting angle. Therefore, a diffraction pattern is formed if only the difference in path length for X-rays reflected from successive planes is equal to an integral number of wavelengths ($\eta\lambda$) of the impinging X-rays. The reflections from successive places emerge in phase with each other, interfering constructively to produce a strong diffracted beam. Otherwise, if this condition is not met, waves are out of phase and result in destructive interference (**Figure 12**). Every protein crystal can be decomposed in an infinite array of lattice planes, with this scatterers of x-ray radiation obeying to Bragg's law for discrete values of $\sin\theta$, thus the necessity to acquire the diffraction for the whole crystal under rotation. The maximum angle θ corresponds to the minimum distance d_{hkl} in the crystal that can be resolve, and is called the resolution limit of the diffraction pattern $d_{hkl,min}$=λ /$\sin\theta_{max}$.

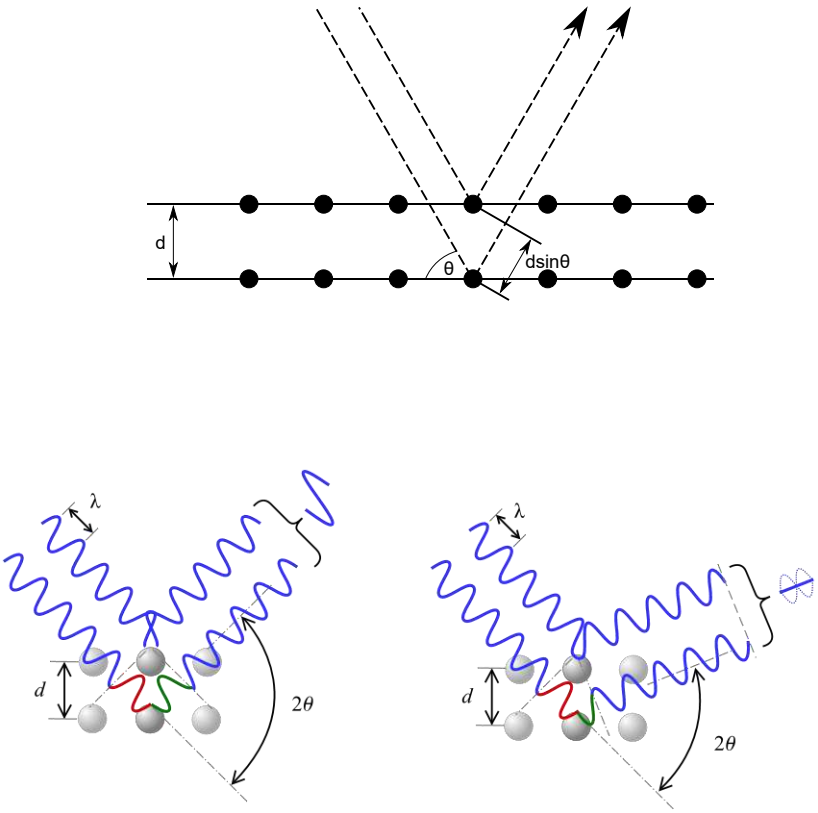

Figure 12. Bragg's Law.

According to Bragg's law, the angle of diffraction θ is inversely related to the interplanar spacing d_{hkl}, which implies that large unit cells give small angles of diffraction and hence produce many reflections that fall within a convenient angle from the incident beam. On the other hand, small unit cells give large angles of diffraction, producing fewer measurable reflections. Because of this inverse relationship between the spacing in the object and the angle of diffraction, the diffraction space is called "reciprocal space" whereas the diffraction pattern is called the "real space". In the reciprocal space, each point of coordinates (h,k,l) corresponds to a family of planes in real space. The Bragg's equation applied to the diffraction data, results in a list of d_{hkl} values that upon integration are associated with an intensity ($I_{h,k,l}$) obtained in a processed called indexing.

The method of molecular replacement allows the use of the phases from structure factors of a known protein as initial phases for a new protein as long as they share a common folding and at least a sequence identity of 30%. The principle behind molecular replacement relies on the use of protein structure models similar to the unknown one. Rotation and translation operation sample all orientation and position of the model in the unknown crystal to find which predicted diffraction best matches the observed diffraction. Using the phases of the model and the observed intensities an initial electron density map is built. Importantly, these phases will only be approximate since the two molecules are not truly identical, yet as they are structurally similar, the calculated phases may provide adequate estimates and a starting point for improvement and refinement of the unknown protein in the real and reciprocal space.

Structure modeling and model refinement

After the determining the initial phases, an electron map is calculated. If the initial phases are good, clear secondary structure features can be identified. Model building requires fitting the polypeptide chain into the strongest density in the map while maintaining geometric and stereo chemical properties. The first electron density map is calculated using the experimental amplitudes and the calculated phases.

The phase calculated varies from 0 to 1. A good phase will have a weighting factor near 1.0, and a smaller value for reflections whose the phase is less reliable.

The experimentally determined electron density maps show initial imperfections, mostly since the raw initial phases obtained are usually poor, challenging the following steps of structure solution. Thereby procedures of density modification such as solvent flattening, histogram

matching and noncrystallographic symmetry (NCS) averaging are used to improve initial phases. Density modification is an iterative procedure where the original phases are combined with new phase estimates. If the new phase estimates are better, then the new ρ(x,y,z) will be improved, and the new electron-density map will be more detailed. In other words, the iterative process of incorporating phases from successively better and more complete models converges toward a structure that fits the native data better.

At some point in the iterative improvement of phases, the map becomes clear enough that we can start to trace the molecular model of the protein. Using computer graphic tools such as COOT, we can build and manipulate a stick model of the know sequence within sections of the map. The resulting model will most certainly contain errors and undefined regions, at this point the objective is to correct as many of these errors as possible checking residue-by-residue.

Two types of maps can be calculated that reduce the overall model influence by subtracting the calculated structure factor amplitudes of the observed amplitudes. The Fo-Fc map contains both positive and negative density, depending on weather the contribution of the observed intensities to the ρ are larger or smaller than the contribution of the model in the unit cell. In other words, this means that the map tells us where the model should be adjusted to increase or decrease electron density in a certain region, by adding (in the case of positive density) or deleting (in the case of negative density) some atoms respectively. For instance, if an amino acid side chain in the model is in the wrong conformation, the Fo-Fc map will exhibit negative density coincident with erroneous model side chain and a nearby positive density indicating the correct position. Therefore, the Fo-Fc map emphasizes errors in the current model and removes the influence of the current model so that the original data can "indicate" where the model is wrong. However, if the model still contains many errors, the Fo-Fc map becomes very noisy. In order to minimize this, the double difference 2Fo-Fc are used. These are regular electron density maps of the protein, but with reduced model influence. Unless the model contains severe errors, this map is positive everywhere, and contours at carefully chosen electron density resemble a molecular surface appropriate for map fitting.

In general, a preliminary model of the protein contains errors and must be optimized to best fit the experimental data as well as known chemical information. Thus, refinement must be carried out in order to generate improved phases, resulting in a more accurate electron density map allowing for better model building. Often this is repeated in an iterative way until little or no further improvements are obtained. Refinement is the process of systematically altering the

model so that the observed and calculated data agree more and more closely, because these computations entail comparison of computed and observed structure factor amplitudes, these methods are referred as reciprocal space refinement.

In order to systematically improve the model, the simplest method is the least-squares refinement. In the cyclographic case, the parameters we seek are, for all atoms, the positions (x, y, z) that best fit the observed structure-factor amplitudes. Because the positions of atoms in the current model can be used to calculate structure factors |Fcalc|, we want to find a set of atom positions that are as close as possible to the |Fobs|. In least-squares refinement, we seek to minimize the function, F, which is the sum of the differences between the observed and calculated amplitudes for each hkl reflection.

However, for most protein structures there is a very poor observation-to-parameter ratio. Therefore, for each atom one refines introduce a set of restraints during refinement of its position (x,y,z) as is the case of temperature factor (B-factor) and its occupancy, and constraints (bond length, bond angle, close contacts).

The temperature factor is the measure of how much an atom oscillates around the position specified by the model. Atoms at the side-chain termini are expected to have higher degree of freedom of movement than those in the main chain. Diffraction is affected by this variation in atomic position, thus it is realistic to refine these values. From the temperature factors computed during refinement we gain some insight into the dynamics of our largely static model and also into errors in the model-building process as wrongly places atoms will exhibit higher B-factors, when compared to neighboring atoms.

The occupancy of an atom defines the fraction of asymmetric units where the atom is actually occupies the position specified in the model, and ranges from 0 to 1, where intermediate values indicate that an atom does not occupy that position in all asymmetric units. This parameter can be used to define alternate conformations of amino acid side chains. By including occupancies among the refinement parameters, we obtain estimates of the frequency of alternative conformations, and thus additional information about the dynamics of the protein molecule.

As the model converges to the correct structure, the difference between the amplitudes decreases, as does the Rfactor. Values of R range from zero, for perfect agreement of calculated and observed intensities, to about 0.6 when a set of measured amplitudes is compared with a set of random amplitudes.

During refinement however, the R-factor can be artificially decreased by simply increasing the number of adjustable parameters, independently of how many of those parameters are correct. Over-fitting can be measure using a cross-validation in the form of Rfree. In this method, a random subset of reflection (5%), is set aside from the rest of the reflection working set. This residual measure how well the current model predicts a random set of measured intensities that were not included in the refinement. During the different stages of refinement, the behavior of Rfactor/Rfree should decrease and converge. A divergence greater than 20% in the Rfactor/Rfree is an indicator of model over-fitting and thus the refinement procedure is not correct.

X-ray crystallography is useful for studying the interactions between an antibody and its bacterial polysaccharide target providing essential information for the development of more specific and effective antibody therapies and vaccines. Since mAbs are too flexible for crystallization experiments, crystals preparation of Fab-antigen complexes allow to characterize the Fab binding site, the antigenic epitope and identify the details of the antigen-antibody interaction [98].

CHAPTER 2: *Haemophilus influenzae* type b

2.1 INTRODUCTION

Haemophilus influenzae is a Gram-negative coccobacillus part of the nasopharynx microbiota in healthy adults, children and infants [99]. It can be found in an encapsulated (typable) form that are further divided into six serotypes (*a-f*) based on the chemical structure of its capsular polysaccharide (CPS). The unencapsulated strains are indicated as non-typable (NTHi) and are responsible for the majority of cases of otitis media and sinusitis [100]. Serotype b (Hib) is the most familiar and predominant form which infects mostly children and immunocompromised individuals. Other serotypes such as a, e and f are also isolated although less frequently than type b, while types c and d are rarely identified. Hib causes severe invasive infections in humans such as epiglottitis, sepsis, pneumonia and meningitis. CPS is made up of polyribosyl-ribitol-phosphate (PRP) repeating units (RUs) and represents the most virulent factor of infections [101].

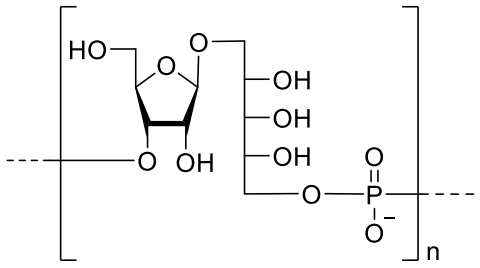

Figure 13. Hib CPS repeating unit structure (poly-3-β-D-ribosyl-(1→1)-D-ribitol-5-phosphate) [102].

Polysaccharide capsule prevents bacterial phagocytosis and acts as an effective shield from the action of complement. As the majority of polysaccharide-based vaccines, the purified PRP used as vaccine against Hib infections was immunogen in adult but failed to induce protective antibodies in young children [103, 104]. Bacterial polysaccharides are T cell-independent antigens that can induce a short-term immune response. The conjugation of polysaccharides to carrier proteins enables an involvement of T-cells leading to the generation of an immunological memory that makes vaccines immunogenic even for children and infants [105]. Although this concept was discovered in 1930, its application to a commercial product occurred only in 1987, when Hib PRP was conjugated to *Diphteria Toxoid* (DT) protein resulting in the

first glycoconjugate vaccine ever developed. Since then, several bacterial vaccines able to induce immunological memory thereby ensuring an extended protection including young children, were introduced [106]. Currently, Hib glycoconjugate vaccines with different carrier proteins are available in global market either in single form or in combination with other vaccines (**Table 4**) [99].

Table H4. Licensed monovalent and combination Hib vaccines used globally [24, 99]

	***Trade name*/ Manufacturer**	**Carrier protein**	**Carbohydrate**	**Other Components**
Monovalent	*ProHIBiT* Merck Sharp&Dohme	DT	Size-reduced CPS	/
	PedvaxHIB Merck Sharp&Dohme	OMP	Size-reduced CPS	/
	ActHIB and *OmniHIB* Pasteur Merieux Vaccines	TT	Native CPS	/
	HibTITER Lederle-Praxis	CRM_{197}	Oligosaccharide	/
	Hiberix GSK	TT	Native CPS	/
Combined	*Infanrix hexa* GSK	TT	Native CPS	DT, aP, HB, IPV
	Hexacima/Hexyon/Hexaxim Sanofi Pasteur	TT	Native CPS	DT, aP, HB, IPV
	Vaxelis MCM Vaccine Co.	OMP	Size-reduced CPS	DT, TT, aP, HB, IPV
	Infanrix-IPV/Hib GSK	TT	Native CPS	DT, aP, IPV
	Pentacel Sanofi Pasteur	TT	Native CPS	DT, aP, IPV
	Quinvaxem Berna	CRM_{197}	Oligosaccharide	DT, TT, PT HB
	Menitorix GSK	TT	Size-reduced CPS	MenC
	MenHibrix GSK	TT	Native CPS	MenC, MenY

DT, diphtheria toxoid; TT, Tetanus Toxoid; PT, pertussis toxoid; aP, acellular pertussis; HB, hepatitis B; IPV, inactivated poliovirus

Most licensed glycoconjugate vaccines are composed of poly- or oligosaccharides extracted from bacteria, however Hib is also the target of the first synthetic glycoconjugate vaccine, Quimi-Hib, licensed in Cuba in 2004. Such vaccine is composed of a synthetic antigen made by an average of seven repeating units of PRP conjugated to thiolated *Tetanus Toxoid* (TT) carrier protein through a 3-(maleimido)-propanamide linker [107]. Over the years, Hib oligosaccharides obtained both from depolymerization of natural polysaccharide [46, 108-110] and by chemical synthesis [111-113] have been used for structural studies aimed at identifying the minimal epitope able to induce an immune response. Recent studies suggest that conjugated oligosaccharides with a polymerization degree (DP) long enough to cover the native polysaccharide epitope can give a better response than a polysaccharide conjugated product [46, 110, 114]. Furthermore, the use of oligosaccharides provides a clearer and more identifiable composition of a vaccine [115]. In 1983 Anderson et al. reported that Hib oligosaccharides conjugated to carrier proteins with an optimal glycosylation degree may be more likely to activate T-helper cells than conjugates formed by the corresponding polysaccharide [108]. They showed that Hib oligosaccharides of three different size ranges (average DP9, 19, 31) conjugated to CRM_{197} were well immunogenic in rabbits [108]. Subsequently, they demonstrated that a oligosaccharide conjugate formed by an average (av) length of 20 RU (avDP20) resulted in high titers in 1 year old infants after the second immunization [116]. In 1997 Chong et al reported a comparison between low-glycosylated TT-conjugates of synthetic Hib dimer and trimer oligosaccharides tested in a rabbit model. The study clearly indicated that at least three repeating units are required to achieve high immunogenicity [113]. Recently, Baek et al demonstrated that a tetramer (4RU - octasaccharide) resembles the polysaccharide in terms of immunogenicity and antibody recognition [101]. The authors synthesized oligosaccharides from tetramer up to decamer through a [2+2] elongation strategy. Tetra-, hexa-, octa- and decamer were obtained through a one-pot iterative approach involving the dimer and a H-phosphonate aminopentyl linker. The CRM_{197} conjugates of these deprotected oligosaccharides were tested in rabbit and the sera were analyzed by glycan array assay. Tetramer and octamer revealed the highest immunogenicity, while a linear and marked length-dependent trend was not observed. This study suggested that four repeating units could completely cover the Hib polysaccharide epitope and represented an optimal length for vaccine design. [101]. In addition to the saccharide length, also the saccharide to protein ratio might play an important role on the immunogenicity of a glycoconjugate vaccine [105]. Anderson reported a comparison between Hib oligosaccharide conjugates of different lengths demonstrating that an avDP7 conjugate with a high number of

chains loaded on the protein was more active in infants than longer oligosaccharide conjugates with a lower loading [46]. A high glycosylation degree allows a multiple exposure of the epitope and consequently the saccharide length appears less impacting, compensated by the so-called multivalence effect. This effect suggests that also short oligosaccharide fragments, when exposed many times on protein surface, can lead to a good antibody response [79, 117]. Hence, once the minimal length is identified, even very short oligosaccharides conjugated to carrier proteins with an appropriate glycosylation degree can act as effective vaccine antigens. Detailed information on the structural requirements necessary for saccharide recognition are key to facilitate the design of new carbohydrate-based vaccine candidates.

2.2 AIM OF THE STUDY

Glycoconjugate vaccines are generally obtained by conjugating native or size-reduced capsular polysaccharide to carrier proteins. Elucidating the polysaccharide (PS) minimal epitopes recognized by functional antibodies mediating protection from infection is crucial to guide the design of optimized carbohydrate-based vaccine. Generally, the antigenic determinants and the structural details of the minimal epitope targeted by specific functional antibodies elicited by glycoconjugate vaccines are unknown. Structural glycobiology studies using oligosaccharides (OS) in complex with functional monoclonal antibodies could represent a powerful tool to gain information on PS immunological determinants at the atomic level. In the last few years, structural studies aimed to map polysaccharide antigenic determinants and epitope conformations have been applied to different bacteria. Recently it was demonstrated that a length of five to six RUs contains the minimal structural and immunogenic epitope of *N. Meningitidis* serogroup X (MenX) capsular polysaccharide [118]. In our group, a combined techniques strategy was used to study at atomic level the minimal epitope of *Group B Streptococcus* type III revealing a sialylated epitope spreaded in two adjacent repeating units [82]. The same principle enforced on *N. Meningitidis* serogroup A identified the O-Acetylated trisaccharide as the minimal antigenic epitope [83]. The aim of our work was to apply a similar approach to unravel the structural antigenic determinants of Hib PS. Recently, it has been reported that a length of 4RU is able to resemble the polysaccharide in terms of immunogenicity [101], however, the optimal immunogenic oligosaccharide length remains elusive. A glycoconjugate vaccine with a high glycosylation degree allowing multiple exposure of the epitope could reveal that even a shorter length can cover the minimal PS epitope. Herein, short and well-defined Hib oligosaccharides originating from the depolymerization of the native polysaccharide have been used to elucidate the minimal epitope recognized by a functional human monoclonal antibody (hmAb) and to facilitate the study of the relationship between immune response and antigenic structural characteristics. A multidisciplinary strategy combining SPR, STD-NMR and X-ray crystallography has been applied to acquire information on antigen-antibody interaction. Finally, the selected oligosaccharides were conjugated to carrier proteins to evaluate *in vivo* their immunogenicity.

2.3 MATERIAL AND METHODS

Selection of oligosaccharides

- Oligosaccharides with a chain length of 2-5 repeating units were obtained by depolymerization of natural polysaccharide as published by Ravenscroft et al. [119]. Hib polysaccharide was hydrolyzed with acetic acid and fragments of different lengths were separated by anion exchange chromatography using a Mono Q column [119]. The chain length of each oligosaccharide was confirmed by Mass-Spectrometry while the point of cleavage between ribose and ribitol was confirmed by $^{1}H/^{31}P$-NMR: the absence of phosphomonoester species detected by ^{31}P-NMR excludes a cleavage at the level of phosphodiester linkage.

- A Hib long oligosaccharide with an average molecular weight of 28000 Da (avDP80) was obtained by treatment of the native polysaccharide with $NaIO_4$ (1:0.08 mol/mol) for 30 minutes at 4°C. After purification in size-exclusion G15 resin, sugar and aldehyde groups generated quantification were measured by colorimetric Ribose assay and microBCA based on a glucose standard curve, respectively. An activation of about 20% is measured from the ratio between moles of monomer and moles of aldehyde generated.

HmAb and Fab production

The recombinant human monoclonal antibody (hmAb) anti-Hib PS was produced by Takis SRL starting from published nucleotide sequences of a human IgG mAb [120]. The hmAb, called CA4, was isolated from a fusion between a mouse-human heterohybridoma cell line and peripheral blood lymphocytes from an adult immunized with Hib CPS vaccine. This hmAb demonstrated functional activity against Hib bacteria *in vitro* and *in vivo* [120]. The Fab used comes from the mentioned above hmAb and was produced in two ways: hmAb digestion by papain enzyme (following the Pierce™ Fab Preparation Kit protocol) and production in mammalian cells (Expi293F).

Oligosaccharides biotinylation

Hib DP2, DP3, DP4 and avDP80 previously lyophilized were dissolved in a mixture of H_2O and DMSO (1:9) and added of Biotin Hydrazide (10 eq) and $NaBH_3CN$ (40eq) **(Scheme1).** The solution was kept at 37°C for 3 days and purified through size-exclusion in G10 resin. The

product was checked by NMR and colorimetric Q-Tag assay. Sugar quantification was measured by colorimetric Ribose assay.

SPR analysis

Binding and kinetics were determined by SPR using a BIACORE X100 system. Biotinylated Hib OS avDP80, DP2, DP3 and DP4 were immobilized on a streptavidin-coated sensor chip (GE Healthcare) through a streptavidin-biotin capture using 1M NaCl, 50mM NaOH buffer for surface activation and 1M NaCl, 50mM NaOH, 50% isopropanol buffer to deactivate remaining active groups on the chip surface and remove non-covalently bound ligand. Biotinylated Hib avDP80 was used at 10 µg/mL reaching an immobilized surface density of 277 resonance units. Binding competition was performed by incubating each competitor with the hmAb before injection. For each sample the experiment was performed using a constant concentration of mAb and decreasing concentrations (two-fold dilutions) of competitor. The ability of the competitor of inhibiting the mAb binding to immobilized Hib avDP80 is expressed as a percentage or reduction of binding level compared to not-competed mAb.

Biotinylated Hib DP2, DP3 and DP4 were used at 100nM reaching an immobilized surface density of 52, 18 and 29 resonance units, respectively. Kinetics experiments with the Fab fragment were performed using 2X diluted solutions. All experiments were conducted in 10mM HEPES (pH 7.2), 150mM NaCl, 3mM EDTA, 0.005% Tween20 at 25° C and at a flow rate of 45 µL/min. After each cycle of hmAb and Fab flow, the chips were regenerated with 3.5M $MgCl_2$ and a contact time of 120 seconds. Sensorgram data were analyzed using BIAevaluation software (Biacore).

STD-NMR

STD-NMR experiments were carried out on a Bruker 600 MHz NMR instrument equipped with a TBI cooled probe at controlled temperature (± 0.1 K). Data acquisition and processing were performed using TOPSPIN 1.3 and 3.1 software, respectively. Suppression of water signal was achieved by excitation sculpting (2 msec selective square pulse). Proton-Carbon Saccharides resonances were assigned collecting both 1D and 2D experiments, using standard pulse sequences. To avoid pitfalls in the interpretation of STD-NMR spectra, a negative control spectrum was always recorded in absence of mAb (ligand and buffer) at the very same condition (concentration and pH) of the mAb-saccharide samples. The STD negative controls were always subtracted to the relative mAb-saccharide STD spectrum, obtaining the STDD

experiments. STD-NMR technique was applied to Hib DP2-hmAb complex (100:1 mol/mol) and experiments were carried out following the parameters reported in **Table 5**. The hmAb was purified through PD-10 desalting columns packed with Sephadex G-25 resin and exchange in Tris-HCl buffer 50mM pH 8.0 through 2 mL Zeba Spin desalting column. The hmAb solution was then added to lyophilized DP2 oligosaccharide.

Table 5. Parameters for STD-NMR acquisition

Parameters acquisition	
Temperature	308K
D20	2 sec
D1	2 sec
NS	80
L4	80
D29	20 msec
P11	5 msec
SPW13	500uW (0.0005 W)
P13	15 msec
Irradiation	7.5ppm
OS:mAb (mol)	100:1

X-Ray

Protein crystallization

Human Fab CA4 was purified in 20mM Tris-HCl, 150mM NaCl, pH 8.0, and concentrated to 20 mg/mL using centrifugal filter devices with a 10 kDa cutoff Amicon membrane. DP2- and DP3-Fab complexes (15:1 saccharide/Fab molar ratio) were prepared by incubating the lyophilized sugars with the Fab solution at room temperature. Crystallization screenings were

performed using a sitting-drop vapor-diffusion format at 293 K, by mixing equal volumes (200 nL) of the complexes with crystallization reservoir solutions using a Crystal Gryphon liquid handling robot (Art Robbins Instruments). DP2-Fab crystals were obtained after 6 days using a reservoir made of 0.01M Zinc sulfate heptahydrate, 0.1M MES 6.5, 25 % v/v PEG 500 MME. DP3-Fab crystals were obtain after 4 days in a reservoir of 0.01M Nickel(II) chloride hexahydrate, 0.1M Tris 8.5, 20 % w/v PEG 2000 MME. All crystals were soaked into a cryoprotection solution composed by 25% v/v ethylene glycol and 75% reservoir solutions and flash-cooled in liquid nitrogen for subsequent data collection at 100 K.

Structure determination

X-ray diffraction data of Fab-DP2 complex were collected at Diamond Light Source (Didcot, Oxforshire, UK), on the beamline I03 equipped with an Eiger2 XE 16M detector. For Fab-DP3 complex, diffraction data were collected at the European Synchrotron Radiation Facility (ESRF), Grenoble, France on the beamline ID30A-1, using a PILATUS3 2M detector. Diffraction data were integrated with DIALS [121] and scaled with the software Aimless [122] from the CCP4 program suite [123]. Crystals of both complexes belonged to the orthorhombic C2221 space group, with approximate cell parameters a= 60.67 Å, b=131.59 Å, c=145.1 Å and one copy of the Fab-OS complex in the asymmetric unit. The structure of the complex Fab-DP2 complex was determined by molecular replacement in Phaser [124], using the coordinates of Fabs with PDB codes 3KYM and 6AZM as template models. The refined coordinates of the Fab CA4 were used for molecular replacement of the DP3 complex. Refinement of both structures and manual model building were performed using Phenix.refine [125] and Coot [126], respectively.

Structure quality

The final models were inspected and validated with Molprobity [127]. The buried surface areas and the root mean square displacements were calculated with PISA [128] and Coot [126], respectively. Atomic interactions/contacts between the oligosaccharides and the Fab were calculated with MOE software (version 2020.0901, Chemical Computing Group, Montreal, QC, Canada) and manually inspected. Figures were generated using PyMOL (PyMOL Molecular Graphics System, version XX; Schrödinger, LLC; http://www.pymol.org). Data collection and refinement statistics are reported in **Table 9.**

Tetanus Toxoid (TT) conjugation of DP2-DP5 oligosaccharides

DP2, DP3, DP4 and DP5 were aminated with adipic acid dihydrazide (ADH), activated with succinimidyl diester of adipic acid (SIDEA) and finally conjugated to *Tetanus Toxoid* (TT) protein (Scheme1). The previously lyophilized oligosaccharides were dissolved in 100 mM sodium phosphate buffer at pH 6.2, added with ADH (saccharide:ADH 1:4 w/w) and $NaBH_3CN$ (saccharide: $NaBH_3CN$ 1:10 w/w) and the reactions were stirred at room temperature for 3 days. Purification was performed by size exclusion in G10 resin, quantification was measured by Ribose colorimetric assay (90% yield) and the total amount of amino groups generated was determined by 2,4,6-Trinitrobenzene Sulfonic Acid (TNBSA) colorimetric assay using a standard ADH curve (70-80% amination). The oligosaccharides were lyophilized and resolubilized in a mixture of water and DMSO (1: 9), followed by the addition of triethylamine (5 eq) and SIDEA (12 eq) and the reactions were stirred for 3 h at room temperature. Next, each sample was transferred to a 15 mL Falcon cold Ethyl acetate (EtOAc) (1:5 v/v) was added to allow for sugar precipitation. After 30 min at 0° C the sample was centrifuged for 10 min (4° C, 4500 G), the solvent was extracted and the residual precipitate was dissolved again in EtOAc. This procedure was repeated 8 times and finally the remaining solid was frozen and lyophilized. The resulting active esters were analyzed by NMR to verify the level of activation of each oligosaccharide (80-90%). As final step, conjugation was performed by adding lyophilized activated sugar (200eq) to TT protein and incubating the solution overnight at room temperature. Conjugation was monitored by size-exclusion HPLC using a TSK4000PW column with 100mM sodium phosphate buffer with 100mM Na_2SO_4 and 5% acetonitrile at pH 7.2 and confirmed by SDS-Page and Western Blot. The conjugates were purified from the free unreacted saccharide using the 30KDa Amicon membrane. The protein content in the purified glycoconjugates was determined by micro-BCA colorimetric analysis and the saccharide content was estimated by HPAEC-PAD analysis.

SDS-PAGE analysis

Sodium Dodecyl Sulfate-Polyacrylamide gel electrophoresis (SDS-PAGE) was performed on 3-8% pre-casted polyacrylamide gel (NuPAGE Invitrogen) using tris acetate as running buffer (NuPAGE Invitrogen). 5µg of protein were loaded for each sample. Hib CRM conjugate was used as positive control. After electrophoretic running with a voltage of 150V for about 45 min, the gel was stained with blue Coomassie.

Western Blot analysis

SDS-Page was run as described before and gel was transferred on cellulose with iBlot gel transfer stacks nitrocellulose kit and blocked with PBS 1x pH 7.2+BSA 3%. HmAb CA4 was used as primary antibody (dilution 1:1000, 1 h) followed by several washes with PBS 1X + tween20 0,05% buffer. Anti-Human IgG-alkaline phosphatase antibody (Sigma) was used as secondary antibody (dilution 1:2000, 30min) followed by several washes with PBS 1X + tween20 0,05% buffer. Western-Blot was finally developed with AP conjugate substrate kit (BIORAD).

HPAEC-PAD analysis for total saccharide quantification of Hib OS-TT conjugates

The total saccharide quantification of Hib samples has been performed by HPAEC-PAD analysis and consists in the acidic hydrolysis of Hib oligosaccharides to the monosaccharide components, which are Ribose and Ribitol. For the saccharide quantification the Ribitol moiety has been used, applying the convertor factor Ribitol/saccharide of 2.42. A standard curve of commercial Ribitol as standard has been built in the concentration range 0.1-4.0 µg/mL. Each sample was prepared targeting the calibration curve midpoint. A sample of Hib-CRM or Hib PS, having known concentration, was used as positive control.

Standards and samples, all in duplicates, have been hydrolyzed with 0.3 M HCl in oven at 100 °C for 2 hours, chilled at +4°C for 30 minutes and added with NaOH 2M to a final 0.25 M NaOH. All analytical samples were filtered by 0.45 µm Phenex filter before analysis. HPAEC-PAD analysis was performed on CarboPac MA1 column (4 × 250 mm; Dionex) coupled with MA1 guard column (4 × 50 mm; Dionex) by isocratic elution with 580 mM NaOH. Detection was performed by using a quadruple wave form for carbohydrates with Ag/AgCl as reference electrode. The resulting chromatographic data were elaborated by using Chromeleon™ software vs 7.2.

Evaluation of Hib glycoconjugates immunogenicity in a Rat model

Seven groups of eight rats were immunized by intramuscular (IM) injection with 1 µg dose in saccharide content of each glycoconjugate using alum hydroxide as adjuvant. Hib polysaccharide-TT (used as control) and Hib DP5-TT conjugates were tested both with and without adjuvant. Rats received the vaccines at days 1, 14 and 28. Bleeding were performed at days 0, 27 and 42.

ELISA analysis of Rat sera

Microtiter plates (96 wells, NUNC, Maxisorp) were coated with 10µg/well of Hib capsular polysaccharide in PBS 1x. Plates were incubated overnight at 2–8°C, washed three times with PBST (0.05% Tween-20 in PBS pH 7.4) and saturated with 250 µL/well of PBST-B (2% Bovine Serum Albumin-BSA in PBST) for 90 min at 37 °C. The plates were then aspirated to remove the solution. Two-fold serial dilutions of sera in PBST-B were added to each well. Plates were then incubated at 37°C for 2h, washed with PBST, and then incubated for 1h at 37°C with anti-rat IgG-alkaline phosphatase antibody (Sigma) diluted 1:2000 in PBST-B. After washing, the plates were developed with a 4 mg/mL solution of p-Nitrophenyl Phosphate in 1M diethanolamine pH 9.8, at room temperature for 30 min. The absorbance was measured using a SPECTRAmax plate reader with wavelength set at 405 nm. IgG concentrations were expressed as relative ELISA Units/mL (EU/mL) and were calculated as the reciprocal of sera dilutions giving a final OD of 1AU.

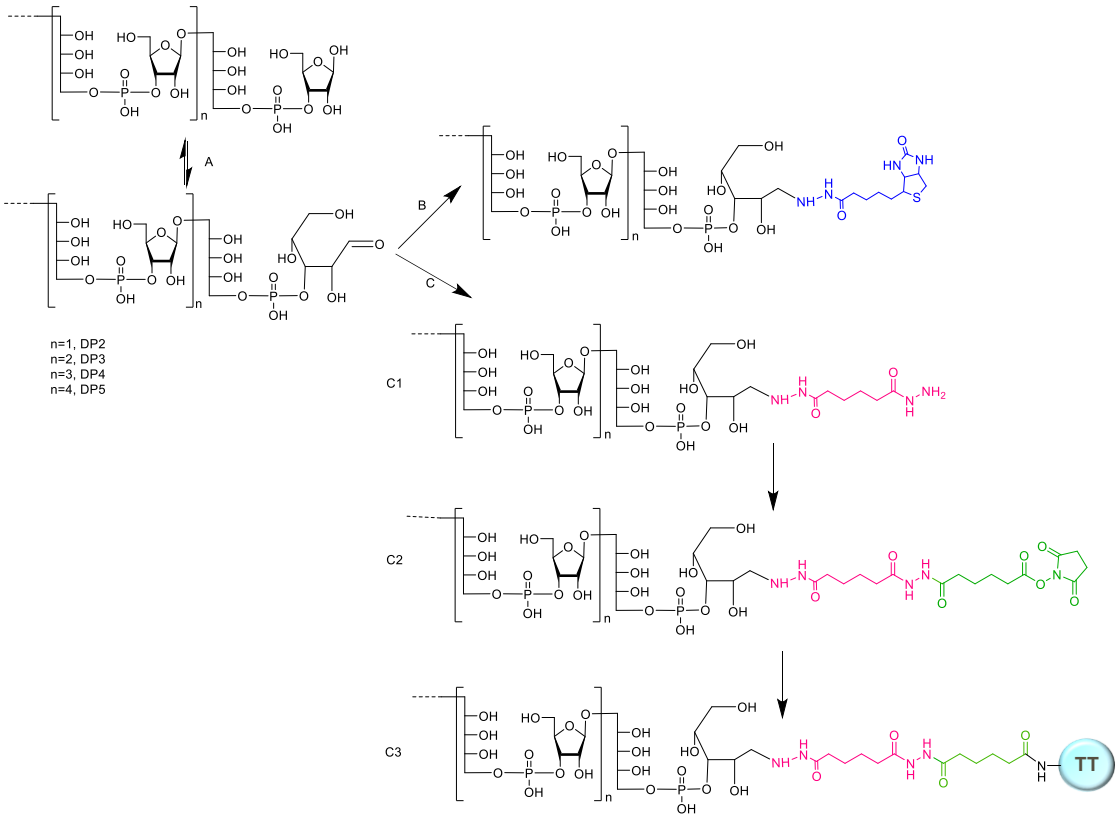

Scheme 1. **A)** Sugar forms in water [119]; **B)** Biotinylation; **C)** Conjugation steps: amination (C1), SIDEA activation (C2) and TT-conjugation (C3).

2.4 RESULTS

2.4.1 Selection of Hib oligosaccharides for structural studies by SPR technique

In order to characterize the interaction between Hib PS and functional antibodies at the atomic level, a monoclonal antibody was produced as recombinant from published nucleotide sequences of a functional human IgG2 mAb specific for Hib capsular polysaccharide, named CA4 [120]. Moreover, a fragment antigen binding (Fab) from the same sequences was produced to facilitate the epitope characterization. To identify the Hib PS epitope recognized by the selected human monoclonal antibody (hmAb), a set of Hib oligosaccharides were generated through acid hydrolysis of natural polysaccharide as already described [119] and isolated by ion exchange chromatography. NMR analysis showed that the hydrolysis conditions generates ribose at the reducing end with a cleavage between ribose and ribitol groups. Additionally, this finding was confirmed by the absence of phosphomonoester form in P-NMR spectra. The resulting structure of the generated oligosaccharides repeating unit is reported in **Figure 14** and oligosaccharides with a length of 2-5 repeating units (DP2-DP5) have been selected for structural studies. The length was confirmed by Mass Spectrometry analysis.

A

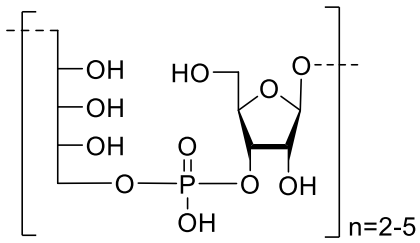

B

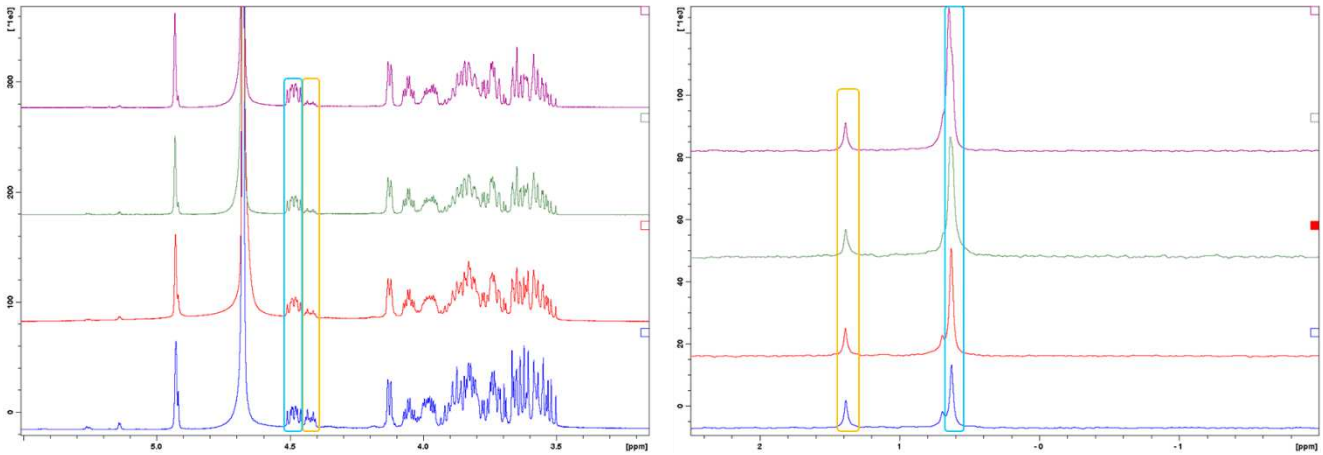

Figure 14. A) Hib oligosaccharides structure obtained by hydrolysis of native PS; **B)** $^{1}H/^{31}P$-NMR characterization of Hib DP2 (blue), DP3 (red), DP4 (green), DP5 (purple). Signals of H3-ribose in-chain and terminal protons in are circled in light blue and yellow, respectively (left panel). The relative intensity of the end-H3 proton signal decreased with increasing chain length. Signals of phosphate groups of terminal RU and in-chain are circled yellow and light blue, respectively (right panel).

To initiate the rational design of Hib minimal epitope, competitive SPR experiments were performed as starting point to investigate whether the available fragments covered the saccharide epitope recognized by the hmAb. Hib DP2, DP3, DP4 and DP5 were used as competitors of the binding between the hmAb and a biotinylated Hib longer oligosaccharide (MW 28KDa, avDP80) immobilized on a streptavidin (SA)-Chip. Hib oligosaccharide avDP80 and Hib polysaccharide have been used as positive controls in the competition. The percentage of hmAb binding inhibition was plotted against the concentration of each inhibitor tested.

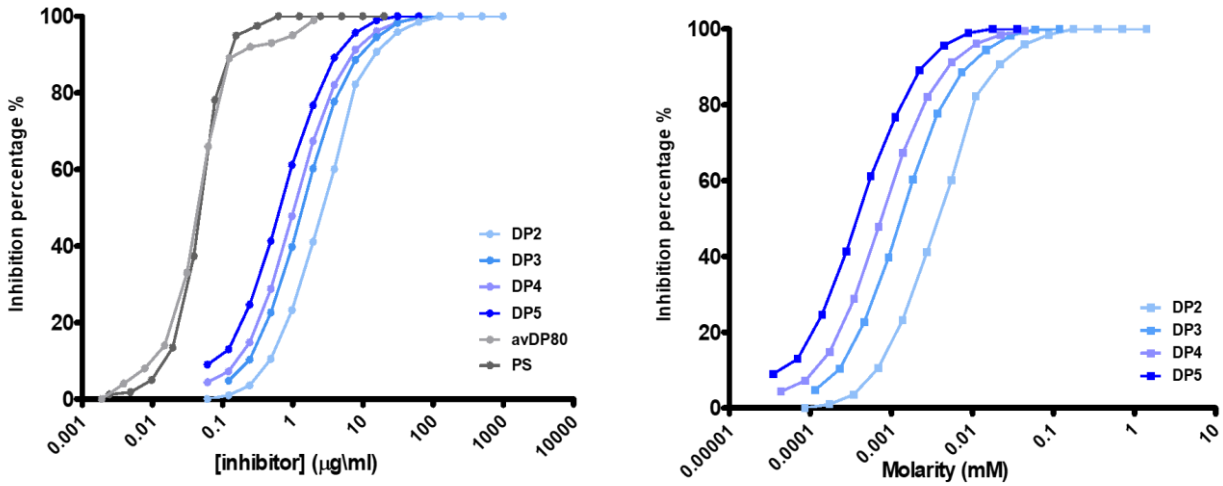

Figure 15. Competitive SPR curves: specific length-dependent recognition by CA4 hmAb.

Table 6. IC50 for the interaction of CA4 hmAb with Hib OSs and PS

	DP2	DP3	DP4	DP5	avDP80	PS
IC50 (µg/mL)	2,43	1,26	1,03	0,67	0,04	0,04

Competitive SPR displayed hmAb recognition of all short oligosaccharides with a comparable binding affinity. All tested lengths were sufficient to fully inhibit the binding of hmAb to the immobilized avDP80 oligosaccharide. All short oligosaccharides, including the shortest DP2, reached 100% of inhibition of the binding with less than two logs of concentration difference with the polysaccharide. Nevertheless, the curves showed a slight shift towards lower concentrations needed for binding inhibition directly related to the increase in saccharide chain length, as highlighted clearly considering IC50 results reported in **Table 6**. The length-dependent recognition of the different fragments could be explained by the multivalent

presentation of the repeating units along the polysaccharide; moreover the high degree of polymerization of polysaccharide also determines an avidity effect considering the bivalent mAb interaction [87].

Overall, this analysis confirmed a length-dependent affinity of anti-Hib antibody but also indicated that DP2 already contains the Hib PS portion necessary for high-affinity antibody binding and could be used for further structural analysis. In order compare the affinity towards the hmAb, KDs affinities to Fab fragment were evaluated for Hib DP3, DP4 and avDP80. To correlate the affinity data with competitive results, we need to take in consideration the differences between the two assays. In competitive SPR the biotinylated PS was immobilized on a SA-Chip and the intact oligosaccharides complexed with the hmAb were injected over the chip in a continuous flow. For the kinetic experiment of each short oligosaccharide, each antigen had to be biotinylated to achieve immobilization on a SA-Chip. The biotinylation reaction consists of the covalent binding of biotin to the terminal end of the oligosaccharides and this has an impact on the length of each fragment as the ribose of the final RU is blocked in the open form (**Scheme 1**). Consequently, the last repeating unit of each oligosaccharide is no longer complete but lacks the ribose at the reducing end. Considering that, biotinylated DP4 and DP3 were used to evaluate the affinity towards the Fab fragment of DP3 and DP2 respectively. For the DP2, corresponding to one and a half repeating unit, it was not possible to carry out a kinetic experiment with the Fab, probably due to the fact that the fragment is too short to cover the epitope, thus confirming that two consecutive repeating units are needed for a specific mAb recognition. Biotinylated Hib DP3 and DP4 (corresponding to DP2 and DP3 plus a half unit), showed high Fab affinities comparable to that of the longer oligosaccharide avDP80 (**Table 7**). These results confirmed that two repeating units (DP2) could represent an optimal length to be used in structural studies aimed at dissecting at atomic level the interaction with the specific hmAb.

Table 7. KD affinities of Hib DP3, DP4 and avDP80 binding to Fab CA4

Hib oligosaccharides	**KD**
DP3-Biotin	3,16E-06
	5,72E-06
	6,15E-06
DP4-Biotin	8,57E-07
	5,35E-07
	1,01E-06
avDP80-Biotin	7,22E-07
	2,06E-07
	2,72E-07

2.4.2 Epitope mapping by STD-NMR of Hib DP2 fragment complexed with CA4 hmAb

To map the interactions of Hib DP2 oligosaccharide with the protective hmAb, proton Saturation Transfer Difference NMR (^{1}H STD-NMR) studies were undertaken on DP2-hmAb complex. STD difference (STDD)-NMR spectra were derived by subtracting the STD-NMR spectrum of the glycan in the bound state with the mAb (ligand/protein 100:1 molar ratio) to the reference spectrum in the unbound state (**Figure 16**). The experimental NMR temperature was raised up to 308K to brought kinetics closer to the ideal range of revelation, with K_D normally ranging between 10^{-3} to 10^{-6} M [91]. The spectrum evidenced signals arising from both ribose and ribitol suggesting the engagement of the whole DP2 molecule in the binding. Looking at STD effects throughout the structure, we observed that H1, H2, and H4 protons of ribose together with H5 and H5' protons of ribitol have similar STD intensities ranging between 75% and 100%: these are the positions most involved in the binding with the hmAb. H4, H1 and H1' positions of the ribitol are clearly involved in the hmAb binding showing smaller STD intensities between 50% and 75% while lower intensities (but still higher than 25%) correspond to the H5 and H5' protons of ribose and the H2 and H3 protons of the ribitol. Taken together, these results unambiguously showed that both the two Hib repeating units, and within each repeating unit both ribose and ribitol, directly interact with the hmAb, with only minimal differences observable between the involvement of different protons of the two residues (**Figure 16**). To investigate whether longer oligosaccharides could lead to conformational changes highlighting further positions involved in hmAb binding, few STD-NMR trials have been performed using longer Hib DP3 and DP4 complexed with the hmAb (data not shown), but it was not possible to obtain a good resolution as for the DP2 since they required further settings optimization. However, the preliminary spectra showed a comparable profile to the DP2 spectrum, indicating that the shortest oligosaccharide in our panel was sufficient to map the positions of the Hib repeating unit involved in the binding.

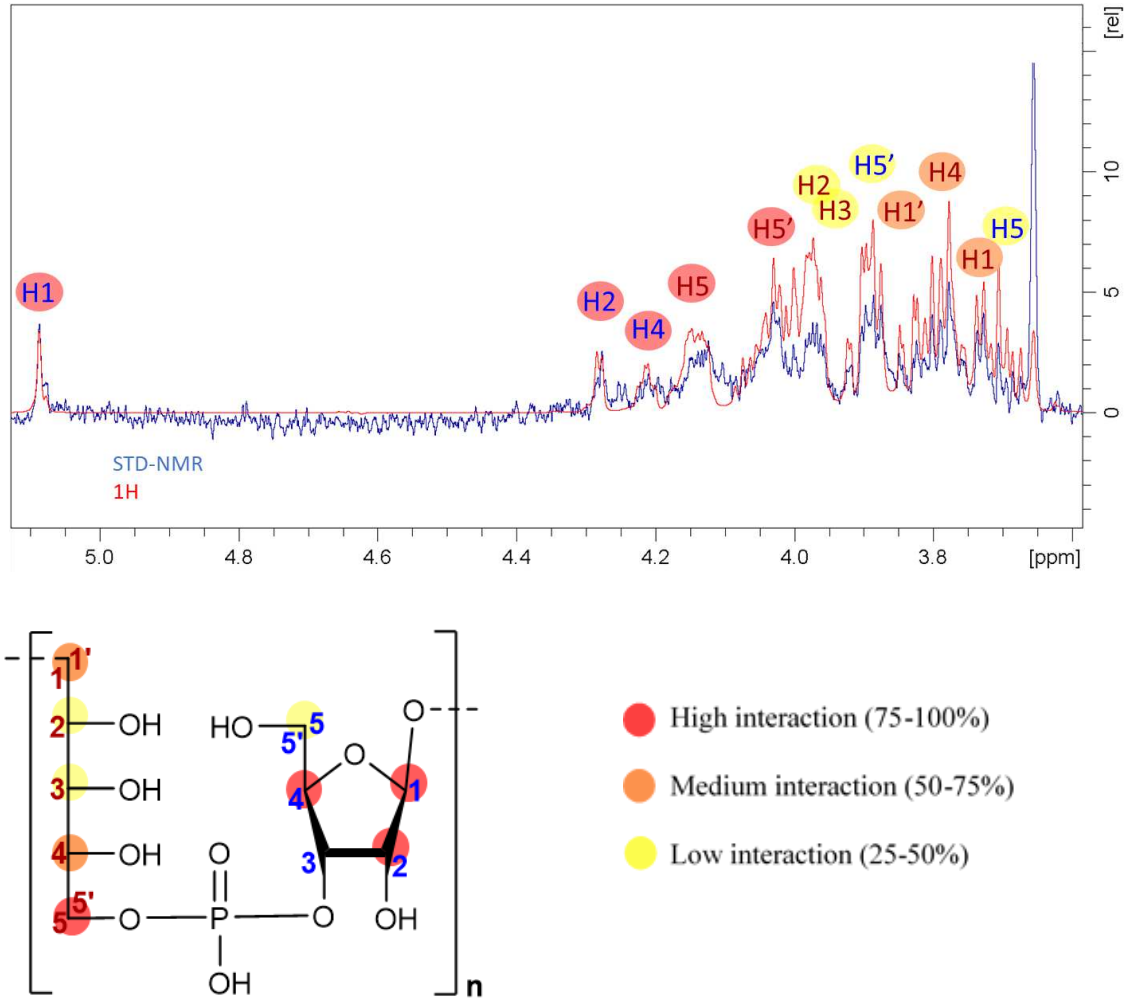

Figure 16. A) STD-NMR epitope mapping on Hib DP2-hmAb complex; **B)** Structure interpretation of the DP2 protons closely interacting with the hmAb represented with different colors based on their involvement.

Table 8. ^{1}H frequencies of DP2 residues protons.

Saccharide	Proton	^{1}H frequence
Ribose (in chain)	H1	3.69
	H1’	3.85
	H2	3.96
	H3	3.93
	H4	3.76
	H5	3.97
	H5’	4.09

Saccharide	Proton	^{1}H frequence
Ribitol (in chain)	H1	5.05
	H2	4.24
	H3	4.60
	H4	4.17
	H5	3.87
	H5’	3.66

Calibration on HDO 4.79ppm

2.4.3 Three-dimensional structures of human Fab CA4 in complex with DP2 and DP3 oligosaccharide (OS) fragments

X-ray crystallography was used to facilitate the 3D-structural interpretation of Hib PS-hmAb interactions. Crystals of DP2 and DP3 oligosaccharides in complex with the human Fab CA4 were determined in the orthorhombic space group $C222_1$, at 2.3 and 2.7 Å resolution respectively, with one single Fab copy in the asymmetric unit. The structures were refined to final *Rwork/Rfree* values of 21.2/26.5% (Fab-DP2 complex) and 22.5/28.9% (Fab-DP3 complex).

For convenience, Ribitol (Rib-ol) and Ribose (Ribf) moieties of the OS fragments are individually indicated as A', B', A'', B'', A''', B''' starting from the Ribitol of the first repeating unit. Superposition of the two complexes reveals that the overall fold of the antibody is essentially identical irrespective of the length of the bound OS, exhibiting a root mean square deviation (RMSD) of 0.32 Å for the pairwise superposition of 435 Cα atoms. The two polypeptide chains, heavy (H) and light (L) chains, of both Fab complexes show unambiguous electron density. Additionally, in the DP2-bound complex, there is clear electron density for the entire disaccharide ligand. For the DP3 OS, after the first cycles of refinement, additional electron density became visible at the end of the Ribf B'', sorrounding the O1 of the initially fitted dimer, clearly indicating that the third RU of the DP3 fragment protrudes outside the antibody cleft occupied by the DP2 **(Figure 17)**. As this extra density is not well-resolved for the entire length of the third RU, we decided to refine only the ordered Rib-ol A'''. For completeness, the floppy Ribf B''' and the phosphodiester bridging Rib-ol A'''- Ribf B''' is included in the final model with zero site occupancy.

Starting from the description of the DP2 complex, the total surface area occluded from the bulk solvent upon formation of the Fab-DP2 complex is ~ 870Å^2 (360 Å^2 from the Fab paratope and 510 Å^2 from the glycan). More in details, DP2 glycan is accommodated into a Fab small groove-shaped binding site delineated exclusively by the H chain complementarity determining regions (CDRs) H1, H2, H3. The long 16-residue CDR H3 is likely oriented to shield the epitope from interactions with the Fab L chain. DP2-Fab binding affinity is the result of contributions arised mainly by polar and electrostatic interactions. Indeed, all major functional groups of the sugar participate in direct or water-mediated Hydrogen Bonds (HBs) with the Fab. On the Fab side, it is noteworthy the key contribution of Arg53, from CDR H2, in binding the saccharide.

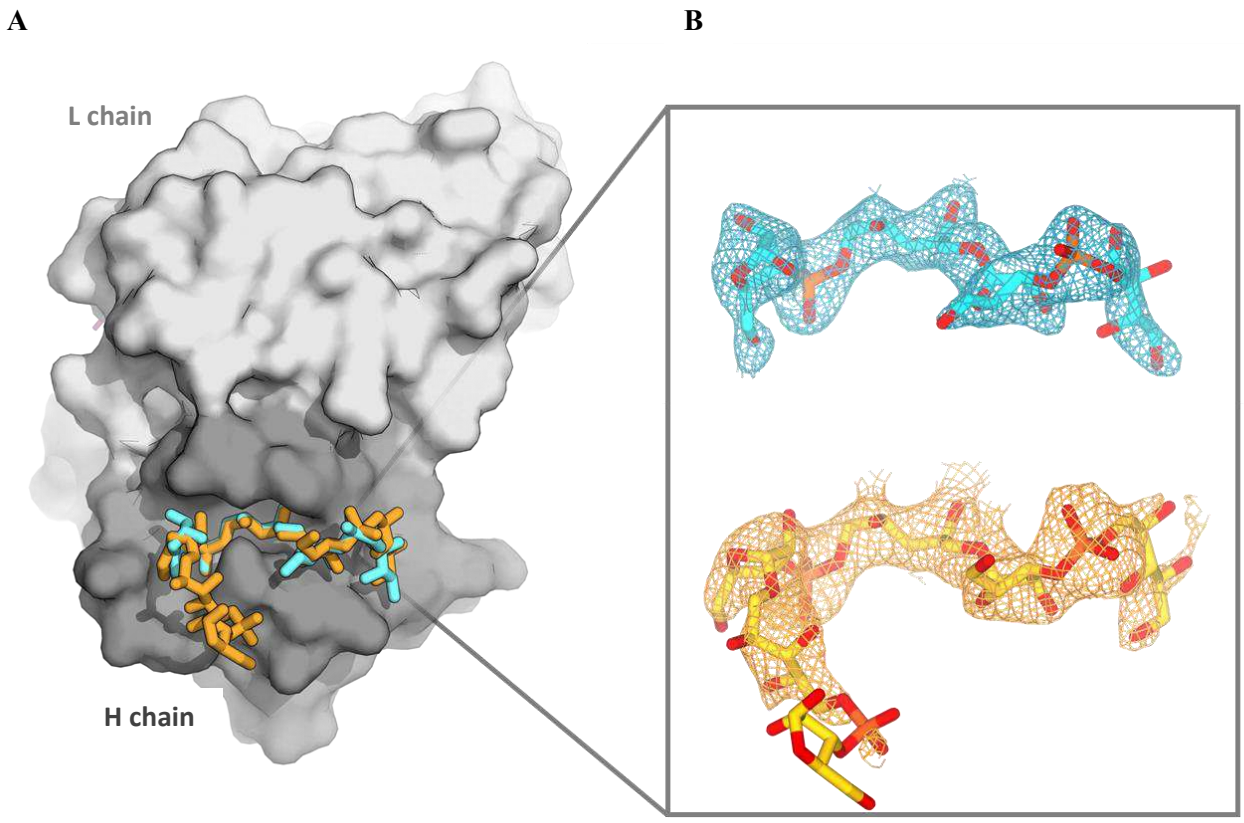

Figure 17. A) Fab CA4 binding pocket withoverlapping of the two Hib structures; the Fab is depicted as surfaces while DP2 (cyan) and DP3 (yellow) fragments are represented by sticks**. B)** Electron density for DP2 and DP3; strcutures are represented with sticks coloured by element (phosphate in orange and oxygen in red).

As concerns the sugar, the first RU A'-B', Rib-ol-A' is able to establish two direct H-bonds with Thr28 backbone and sidechain (CDR H1) through its hydroxyl groups at positions 1 and 2 while its OH groups at positions 3 and 4 are water mediated bridged to Arg98 (CDR H3). The phosphodiester group between A' and B' is not involved in relevant interactions with the Fab, while the Ribf-B' interacts with Gly102, Thr31 and Arg53 through its OH-1, OH-2 and OH-5 groups, respectively. Moving to the most engulfed RU A''B'', the Rib-ol-A'' is stabilized by 5 direct HBs with CDR H2 and H3: the OH-2 group is within HB distance from Asn99 sidechain and Met103 backbone, the OH-3 interacts with both Ser33 backbone and Asn99 sidechain while the OH-4 group makes a HB with Met103 backbone carbonyl. H-bonds of the central phosphodiester group A''-B'' are established with sidechains of CDR residues Arg53 and Thr106. The Ribf B'' moiety interacts with Pro104 backbone of CDR H3 through its OH-2 while its OH-5 group is water-mediated bridged to Ser52 and Ser54 sidechains. Noteworthy, the DP2 conformation is also stabilized by four intramolecular H-bonds, two of which involving

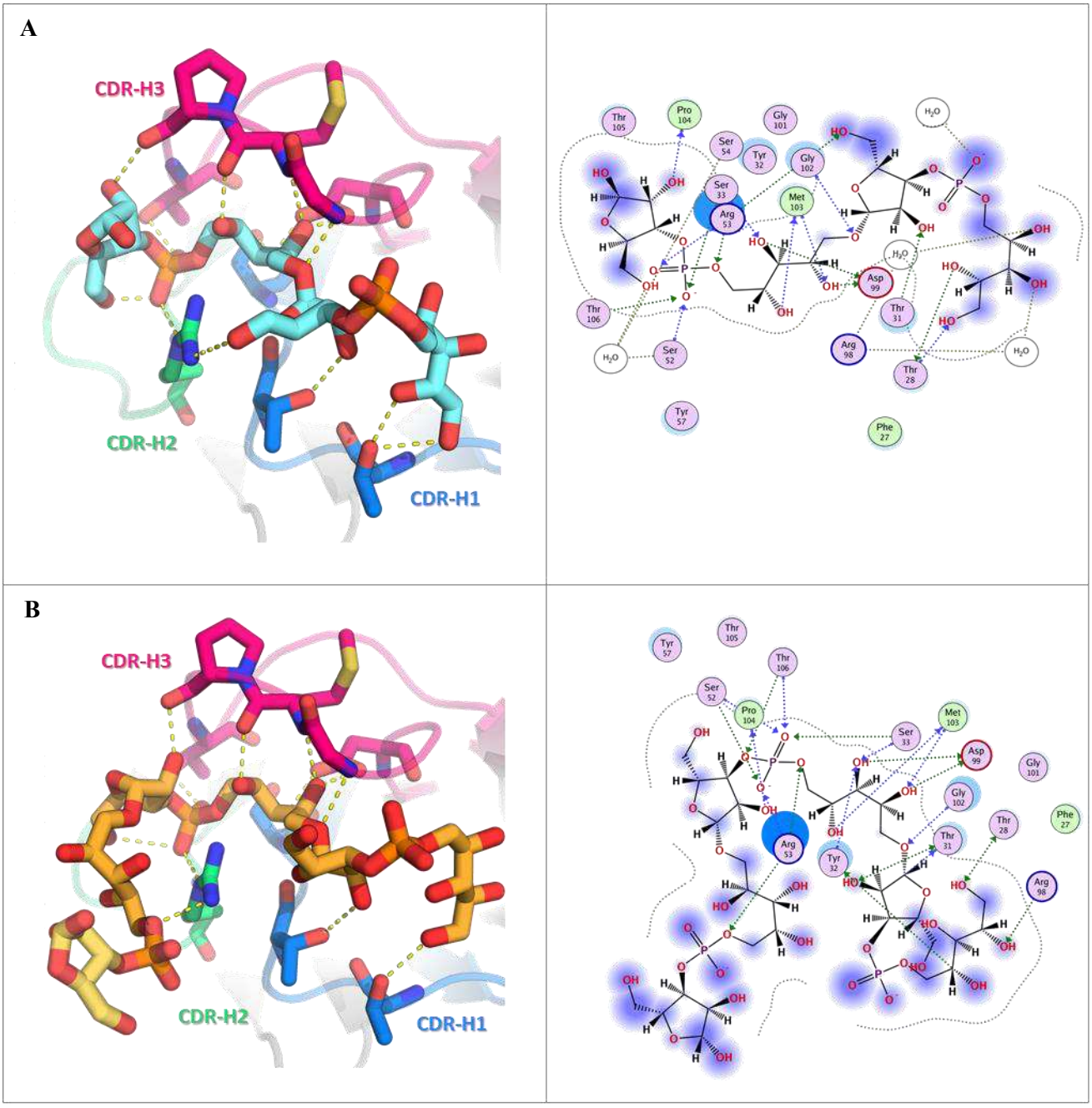

Figure 18. A) Hib DP2-Fab interactions; B) Hib DP3-Fab interactions. Letf panels: binding site representation with more involved residues and sugar depicted as sticks. Right panels: all Hydrogen bonds interactions carried out by DP2 and DP43 fragments with the H chain.

the phosphodiester groups. The A''-B''phosphodiester is bridged to Ribf B'' OH-5 group, while the A'-B' phosphodiester approaches the Rib-ol-A' OH-4 group. Additionally, intramolecular interactions are possible also between Ribf B' OH-2 group and Rib-ol-A' OH-2.

In addition to H-bonds, the Fab-DP2 binding is mediated by the electrostatic interactions between the positively charged Fab binding pocket and the negatively charged phosphodiester moieties of the saccharide (**Figure 19 panel A**).

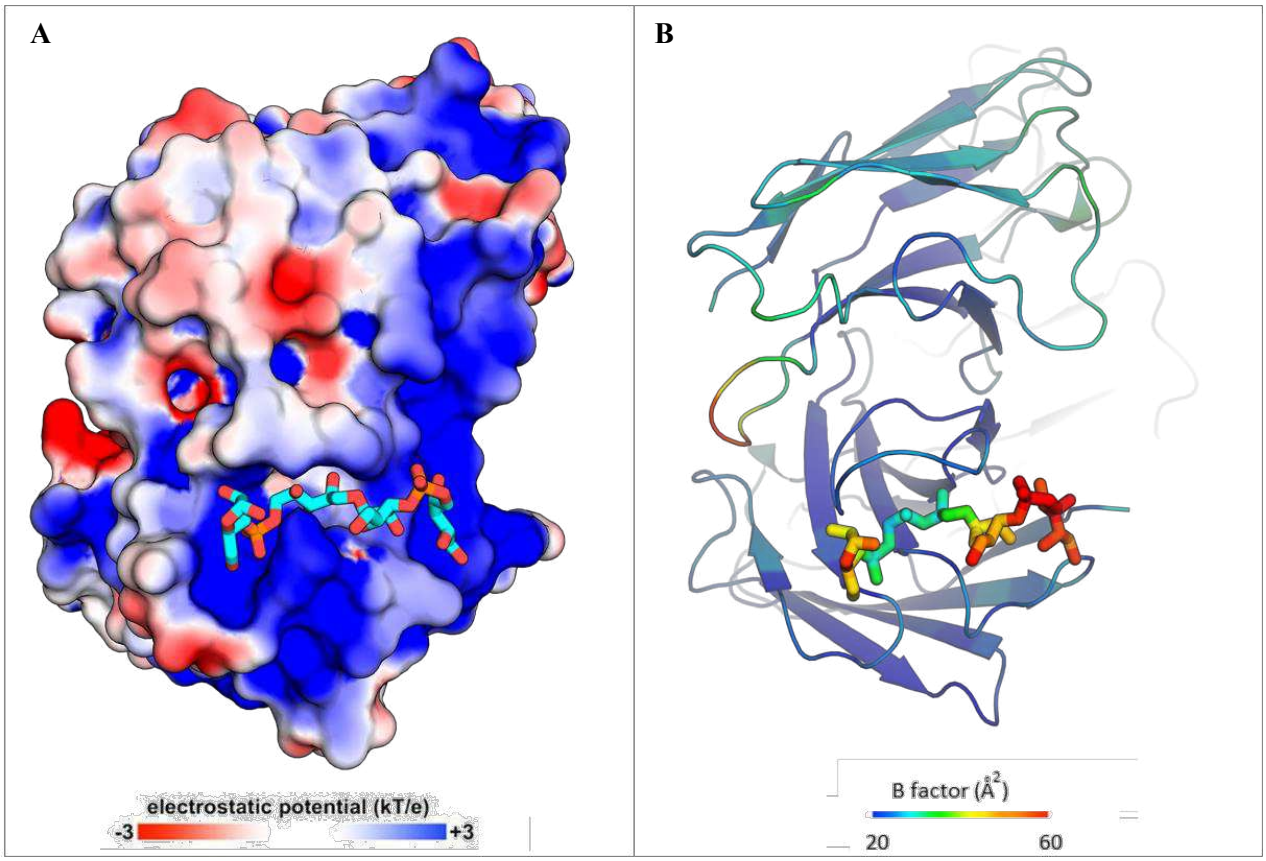

Figure 19. A) Surface electrostatic potential distribution of the Fab; **B)** B-Factor values for Fab and Hib DP2.

Although the difference in length, the DP3 and DP2 oligosaccharide adopt very similar bound conformation to the antibody. Of note, only the Rib-ol-A' group shows slightly different orientations in the two structures, likely as a consequence of its flexibility. In support of this, B-factor values reveal that this moiety is quite mobile, especially in the DP2 structure (**Figure 19 panel B**). As a consequence of the similar binding mode of the two OS fragments, the majority of the interactions established by the DP2 are nearly identical in the complex Fab-DP3, suggesting that the first two RUs represent the crucial anchoring core for Hib carbohydrate recognition. Notably, although the change in conformation, DP3 Rib-ol-A' engages the same interactions established by the same group in DP2, being able to contact both Thr28 and Arg98 residues. The only relevant difference between DP3 and DP2 is in the Ribf-B' which loses its interaction with the key Arg53 residue. As concerns the third RU of DP3, it extends out of the binding pocket, resulting in only one weak interaction with the antibody, i.e. the H-bond

between the Rib-ol-A''' OH-5 group and Arg53 (CDR H2) sidechain. This finding demonstrates that the third RU (especially the Ribf B''' group) is relatively free and mobile since it is not critical for antibody binding, explaining the diffuse electron density for this portion of the DP3 OS.

Table 9. Data collection and refinement statistics

	Fab CA4-DP2	Fab CA4-DP3
Crystal		
Space group	C 2 2 2_1	C 2 2 2_1
Cell dimensions		
a, *b*, *c* (Å)	60.66, 131.59, 145.1	60.80, 131.22, 144.95
Data collection		
Beamline	DLS I03	ESRF ID30A-1
Wavelength (Å)	0.976	0.965
Resolution (Å)	51.50-2.29 (2.33-2.29)	65.64- 2.74 (2.87-2.74)
Total reflections	207267 (5801)	53118 (6956)
Unique reflections	26582 (1252)	15060 (2007)
R_{merge}	0.16 (1.16)	0.18 (0.94)
R_{meas}	0.19 (1.45)	0.21 (1.11)
$I/\sigma(I)$	7.3 (1.1)	5 (1.2)
$CC_{1/2}$	0.99 (0.38)	0.94 (0.58)
Completeness (%)	99.7 (93.4)	96.8 (98.1)
Redundancy	7.8 (4.6)	3.5 (3.5)
Wilson B-factor (Å)	37.09	36.55
Refinement		
Resolution (Å)	51.50-2.29	65.64-2.74
No. reflections	26531	14988
R_{work} / R_{free}	21.2/26.5	22.5/28.9
No. atoms		
Protein	3309	3284
Ligands	49	67
Water	213	59
B factors		
Protein (H, L chains)	36.27/ 40.49	39.22/44.41
Ligands	44.70	52.06
Water	37.83	36.84
R.m.s. deviations		
Bond lengths (Å)	0.01	0.004
Bond angles (°)	1.08	0.631
Clash scores	5.49	5.67
Ramachandran[#]		
Favored (%)	95.14	96.02
Allowed (%)	4.63	3.51

[a] Values in parentheses are for highest-resolution shell
[#] Measured using Molprobity

2.4.4 Glycoconjugates preparation and *in vivo* evaluation

To complete the characterization of Hib minimal epitope, Hib oligosaccharides immunogenicity was assessed in vivo following glycoconjugates preparation. Therefore, Hib DP2, DP3 and DP4 were conjugated to the carrier protein in order to correlate structural studies with the identification of a minimal immunogenic epitope. Fragments were first aminated with adipic acid dihydrazide (ADH), activated with succinimidyl diester of adipic acid (SIDEA) and finally conjugated to *Tetanus Toxoid* (TT) protein using a saccharide:protein molar ratio of 200:1. The oligosaccharides were conjugated to the protein through the reducing end ribose as reported in **Scheme 1**, consequently impacting the last repeating unit as already explained for biotilination. Hib DP2, DP3 and DP4 conjugates therefore contain one, two and three repeating units respectively, plus an additional half RU. Conjugation reactions were monitored by HPLC, SDS-Page and Western Blot (**Figure 20**).

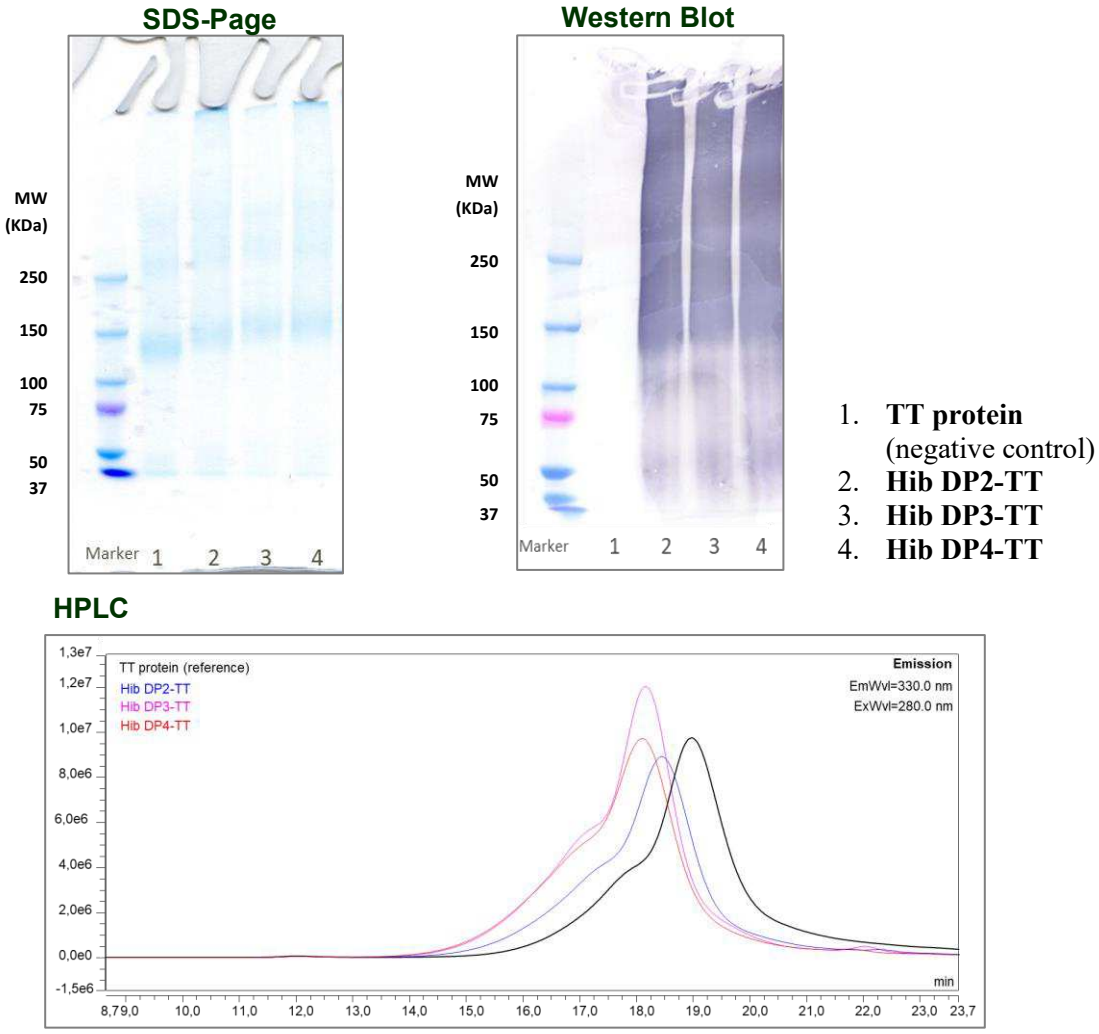

Figure 20. SDS-PAGE gel electrophoresis, Western Blot and HPLC analysis of Hib-TT glycoconjugates.

The formation of the conjugates was initially followed by SDS-Page in which, despite the reference TT itself gives a smear (line 1), it was possible to appreciate a slight and linear increase in molecular weight (lines 2-4). Subsequently, conjugation was confirmed by HPLC analysis in which a difference of the conjugates peaks compared to the reference TT peak is visible, with a gradual shift increase passing from DP2 to DP4, indicating an increase in the molecular weight corresponding to the sugar loading on the carrier. Finally, the Western Blot analysis showed that all four conjugates were well recognized by the selected hmAb anti-Hib PS. After purification from the free unreacted saccharide in Amicon 30K, the conjugates have been sterile filtered and analyzed by micro-BCA colorimetric assay and HPAEC-PAD analysis for the quantification of protein and saccharide content, respectively, and calculate the saccharide:protein molar ratio. As summarized in **Table 10**, Hib DP2-TT and DP3-TT conjugates have comparable glycosylation degree with an average of 7 saccharide chains attached per mole of protein, while Hib DP4-TT present a lower glycosylation with an average of 5 chains. Finally, endotoxins content was measured by LAL Test.

Table 10. Hib-TT glycoconjugates quantification

Conjugates	**[Protein] µg/mL** *microBCA*	**[Saccharide] µg/mL** *HPAEC-PAD*	**Sacc/Prot (w/w)**	**Sacc/Prot (mol/mol)**	**Endotoxins (EU/µg)** *LAL Test*
Hib DP2-TT	1711	58,7	0,034	**7,2**	3,1
Hib DP3-TT	1292	68,1	0,053	**7,5**	3,2
Hib DP4-TT	1552	75,8	0,049	**5,2**	1,5

To investigate the effects of the saccharide length on the PS immunogenicity, all Hib glycoconjugates were tested *in vivo* in a rat model. Rats were immunized with three IM injections two weeks apart and sera post third immunization were collected and analyzed by ELISA assay to determine the IgG binding levels towards native Hib polysaccharide. The results reported in the **Figure 21** demonstrates an increasing antibody level moving from DP2 to DP4. As expected, DP2-TT conjugate, consisting of one and a half Rus, is unable to elicit IgG titers. Titers elicited by DP3 confirms what has been seen with the structural analysis, namely that two repeating units are sufficient to cover the minimal immunogenic epitope of Hib polysaccharide. DP4-TT conjugates, corresponding to three and a half RUs, shows the most

promising immunogenicity. The extra repeating unit probably functions as a linker ensuring a better exposure of the epitope which could be more shielded by the protein in the DP3-TT conjugate. Overall, these results highlighted the finding that 2 Hib repeating units represent the minimal PS portion able to elicit a specific immune response.

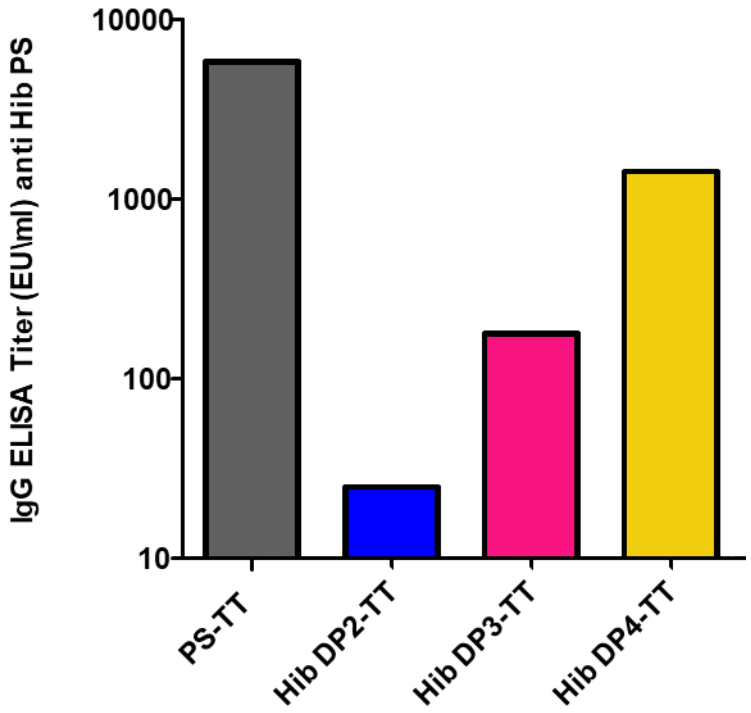

Figure 21. Anti-Hib PS IgG titers of Rat sera post III immunization measured by ELISA assay.

2.5 DISCUSSION

Conjugate vaccines have been one of the major developments of the last 40 years [129]. Many aspects can influence the immunogenicity of glycoconjugates, such as the saccharide:protein ratio, the conjugation strategy, the nature of the spacer and protein carrier and the size of the saccharide moiety, that is one of the most important. Hence the identification of bacterial polysaccharides minimal epitope is crucial to guide the rational design of modern and efficacious glycoconjugates vaccines. Traditional glycoconjugates are composed of long poly- or oligosaccharides containing many copies of the repeating unit. However, immunogenic PS epitopes involved in the interaction with specific antibodies usually comprise precise glycan structures, often not longer than six or eight sugar units (45 year-old paradigm established by Kabat) [42], although even oligosaccharides as short as tetra- or disaccharides have been shown to possess the minimal structural requirements for raising functional antibodies [130-132]. The nature of the repetitive protective epitopes present in the PS is difficult to define, mostly because of the difficulty in obtaining crystals from sugars. In this study, we determined the molecular structure of a protective epitope of Hib PS. Our work focused on the use of short and well-defined oligosaccharides (DP2-DP5) to study and characterize the minimal saccharide epitope directly involved in binding of a protective and functional humanized monoclonal antibody (hmAb), named CA4 [120], as representative of anti-Hib human Ab repertoire. Indeed, this antibody belongs to one of the most abundant family of anti-Hib antibodies derived from the VκIII (A27) gene [133] and was selected on the basis of its *in vitro* and *in vivo* functional activity against Hib bacteria [120]. A multi-disciplinary approach including SPR, STD-NMR and X-ray crystallography was applied to gain information on the structural antigenic determinants of Hib capsular polysaccharide. SPR studies have driven the elucidation of antigenic minimal epitope, revealing that all short Hib oligosaccharides used, including a saccharide as short as two repeating units, are well recognized by the protective hmAb with a slight length-dependent behavior from DP2 to DP5 which further increase with longer oligosaccharide and polysaccharide. These findings directed the STD-NMR studies on DP2-hmAb complex, which provided information on sugar moieties involved in the interaction. STD-NMR results confirmed the good recognition of DP2 antigen indicating the contribution of all sugar protons in binding the hmAb with a particular involvement of H1, H2, and H4 protons of ribose together with H5/5’ protons of ribitol group. X-ray crystallography was used to facilitate the 3D-structural interpretation of Hib PS-hmAb binding. Despite the power of the technique, relatively few crystal structures of carbohydrate-antibody complexes have been

solved so far with the majority of them describing murine or rabbit antibodies [82, 83, 134-138] and only 5 X-ray complexes including human antibodies [98]. Here, we used a Fab fragment derived from the full length humanized CA4 IgG for co-crystallization studies with Hib oligosaccharides to explore fine details on the protein-ligand interaction. The crystal structure of Fab-DP2 complex clearly shows that the antibody participates in a groove-type binding of the DP2 ligand using the three H chain CDRs and without any involvement of its L chain. To the best of our knowledge, such exclusive participation of the H chain in the binding is quite unusual for glycans and is not in agreement to what previously described for anti-Hib A2 Abs, the most abundant family of anti-Hib Abs, where the contribution of the L chain to the sugar binding has been postulated to be important for antigen recognition [139], suggesting that, although the apparent simplicity of this capsular polysaccharide structure, multiple Hib epitopes may be expected with different antibodies [140, 141]. The DP2 is recognized by the hmAb in a rather extended conformation, in an epitope region corresponding to its entire structure. Indeed, all the sugar residues of the dimer are involved in polar and/or electrostatic interactions with the antibody, with the internal Ribf-B'-Rib-ol-A'' groups giving the most important contributions. Since the antibody binding pocket revealed potential free space available to accommodate longer OS fragments, we also determined the 3D structure of the same Fab fragment in complex with the DP3 in order to evaluate whether longer OS may establish an increased number of antibody-contacting interactions. However, the DP3 bound almost identically to DP2, with only two RUs able to establish direct contact to the Fab, suggesting that two RUs of the native Hib polysaccharide are required for optimal mimicry of Hib epitopes, at least with the CA4 family of antibodies. This hypothesis is consistent with the weak electron density observed for the third RU of the DP3, especially for the Ribose moiety, which protrudes outside the binding pocket, and may explain the comparable affinity demonstrated by all the short OS fragments tested with this antibody.

Altogether, these findings strengthen our hypothesis that two RUs represent an optimal saccharide length for antibody recognition. Whereupon, our goal was to identify the minimal immunogenic epitope and to find out if the *in vivo* results could be correlated with the structural information. Despite several studies have been reported in literature, the optimal saccharide length to ensure a protection against Hib infections is not yet clear. The commercial QuimiHib vaccine is formed by a synthetic antigen comprised of an average of seven repeating units [107]. Over the years it has been demonstrated that also shorter oligosaccharides can give good immunogenic results. Recently, it has been shown that four repeating units resembles the native

polysaccharide in terms of immunogenicity and recognition by anti-Hib antibodies [101]. Some previous work on shorter oligosaccharides has reported that a length of three repeating units could be considered as optimal saccharide length to mimic the polysaccharide epitope [111, 113]. A result comparable to our structural studies was reported by Pillai et al. Indeed, competitive ELISA experiments performed using different sized Hib oligosaccharides as PS competitors to bind human monoclonal and polyclonal antibodies, suggested that DP2 oligomer may also contain an optimal length for full filling of the antibody binding sites [142]. To clarify Hib minimal immunogenic epitope, DP2-DP4 oligosaccharides were conjugated to TT carrier protein and tested *in vivo* using a rat model. As previously mentioned, conjugation with the carrier protein blocks the terminal ribose of the sugar in open form, causing the loss of half a repeating unit and therefore the length reduction of each oligosaccharide used for conjugation. Consequently, DP2, DP3 and DP4 conjugates are composed, respectively, of one, two and three repeating units plus a half. Sera analysis performed by ELISA assay showed that antibody titer increases with the saccharide length for DP2 to DP4 fragments. As expected, DP2-TT conjugate did not elicit anti Hib-PS IgG titers, revealing that one and a half RUs is not sufficient to generate any immunogenicity. Conversely, titers elicited by Hib DP3-TT conjugate indicate that two repeating units represent the minimal immunogenic epitope confirming what is clearly suggested by the structural studies. Among all OS conjugates tested, DP4-TT generates the highest immunogenicity, probably due to a better presentation of the minimal epitope granted by the presence of the additional RU. To conclude, our studies demonstrated that 2RUs represent the smallest PS fraction capable of eliciting recognition by an anti-PS antibody and *in vivo* immunogenicity. This finding represents a starting point for the future development of a modern and specific next generation Hib vaccine. Identification of the structural basis of carbohydrate minimal epitopes for the immune recognition paves the way for designing modern glycoconjugate vaccines with short specific oligosaccharides obtainable by synthetic, chemoenzymatic or bioengineering methods [132].

CHAPTER 3: *Staphylococcus aureus*

3.1 INTRODUCTION

Staphylococcus aureus is a Gram-positive coccal (round-shaped) bacterium that appears as grape-like clusters, when viewed through a microscope, and produces large and round colonies, often with a golden pigment, when grown on blood agar plates [143]. *S. aureus* is both a pathogen and a human commensal flora of skin and mucosal surface that asymptomatically colonizes approximately 30% of the population [144]. It is capable of infecting nearly all host tissues including bloodstream, lower respiratory tract, bones, various skin and other soft-tissue and that can lead to severe morbidity and mortality [144]. Infections started when a breach of the skin or mucosal barrier allows staphylococci access to adjoining tissues or the bloodstream. Whether an infection is contained or spreads depends on a complex interplay between *S. aureus* virulence determinants and host defense mechanisms [145]. Treatment options for *S. aureus* are becoming limited due to a its unique ability to rapidly acquire antibiotic resistance to virtually any antimicrobial molecule that has been developed. *S. aureus* has been included among the ESKAPE pathogens (*Enterococcus faecium, S. aureus, Klebsiella pneumoniae, Acinetobacter baumannii, Pseudomonas aeruginosa* and *Enterobacter* species) recognized as the leading cause of antibiotic-resistant infections occurring worldwide in hospitals [146]. Since the 1960s, there has been a spread of methicillin-resistant *S. aureus* (MRSA) strains that are more prevalent in hospitals than methicillin-sensitive *S. aureus* (MSSA) and are more difficult to treat. Since the 1980s, new strains known as community-associated (CA-) MRSA strains, have also emerged that cause severe skin lesions and respiratory infections [147]. In recent years there has been a reduction in transmission as a result of local and national campaigns to strengthen both basic and more intensive infection controls such as hand hygiene, barrier nursing, decolonization and isolation of MRSA patients detected through routine culture and screenings [147]. Today, there are a number of newly developed antimicrobial agents that show good anti-MRSA activity, such as lipoglycopeptides and new anti-staphylococcal cephalosporins, but their efficacy will be jeopardized by their use increase [148]. In addition, there are no authorized vaccines or immunotherapies on the market despite the considerable efforts made by public and private initiatives.

S. aureus pathogenicity is driven by the wealth of virulence factors and its ability to adapt to different environments. Virulence factors have been identified as viable therapeutic targets for

treatment, as they play key roles in cell viability and virulence [144]. The majority of *S. aureus* clinical isolates worldwide expresses Capsular Polysaccharide 5 and 8 (CP5 and CP8), shown to be critical for bacterial survival in the blood. CPs are important in immune evasion and represent one of the main targets of vaccines [149, 150]. Additional *S. aureus* strains can express a wide array of potential virulence factors, including surface proteins that promote adherence to damaged tissue, bind proteins in blood to help evade antibody-mediated immune responses, and promote iron uptake (**Figure 22**). Among these antigens, we find *staphylococcal protein A* (SpA), *Clumping factor A* and *B* (ClfA and ClfB), *Iron-regulated surface determinant A* and *B* (IsdA and IsdB), *Serine–aspartate repeat protein D* and *E* (SdrD and SdrE), and *Manganese binding protein C* (MntC). Moreover, *S. aureus* is able to secrete toxins that, in contrast to the protective and passive role of the cell-wall associated virulence factors mentioned above, play active roles in disarming host immunity causing tissue damage and septic shock. These toxins include the *Panton-Valentine Leukocidin* (PVL), *staphylococcal enterotoxin A* and *B* (SEA and SEB) and *α-Hemolysin* (Hla) [151], which appears to play a prominent role in causing pneumonia and skin lesions in animal models of *S. aureus* infection [152]. Hla antigen used in clinical trials was detoxified by an amino acid substitution at position 35 resulting in a mutated protein unable to form pores [153].

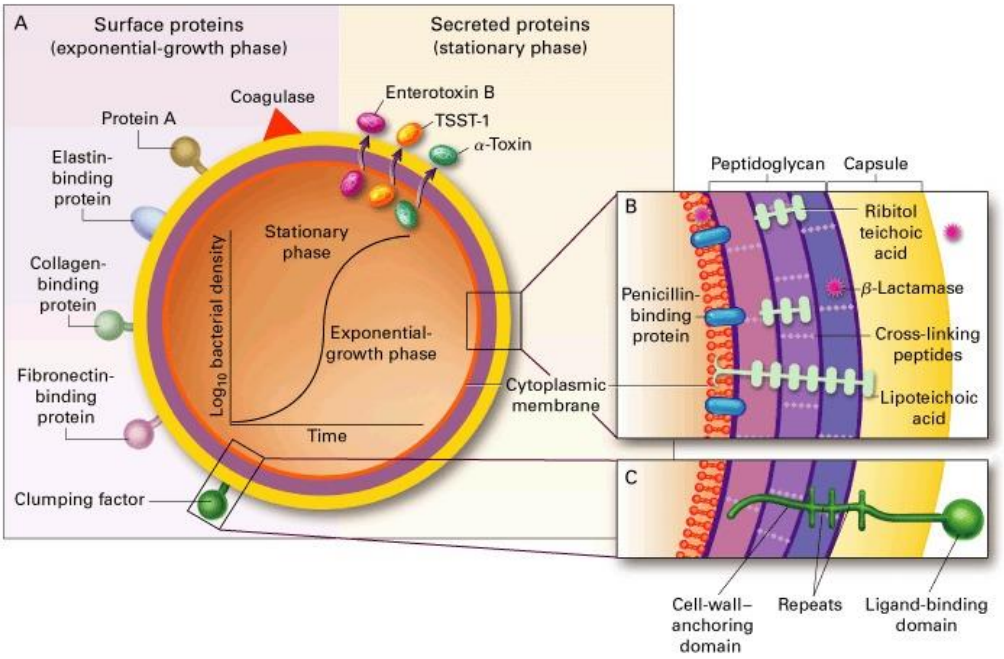

Figure 22. Structure of *S. aureus*. **A)** surface and secreted proteins; **B, C)** cross sections of the cell envelope [145].

Capsular polysaccharides

Several bacteria, as well as *S. aureus*, present an extracellular capsule composed of long polysaccharide chains known as capsular polysaccharides (CPs). Capsules are the bacterial structure first recognized by the immune system, therefore, encapsulated bacteria have developed an immune evasion property which is exploited in the development of vaccines. Although as many as 11 serotypes of capsule were described, serotype 5 (CP5) and serotype 8 (CP8) are the most clinically relevant and therefore the major effective vaccine targets. CP5 and CP8 polysaccharide repeating units share similar trisaccharide of D-N-acetyl mannosaminuronic acid (ManNAcA), L-N-acetyl fucosamine (L-FucNAc), and D-N-acetyl fucosamine (D-FucNAc). The trisaccharide structures are identical in monosaccharide composition and sequence, and they differ only in the glycosidic linkages between the sugars and the sites of O-acetylation (**Figure 23**) [72]. In CP5 repeating unit the O-acetyl is beared by α-fucosamine whilst in CP8 it is hold by the β-mannosaminuronic acid.

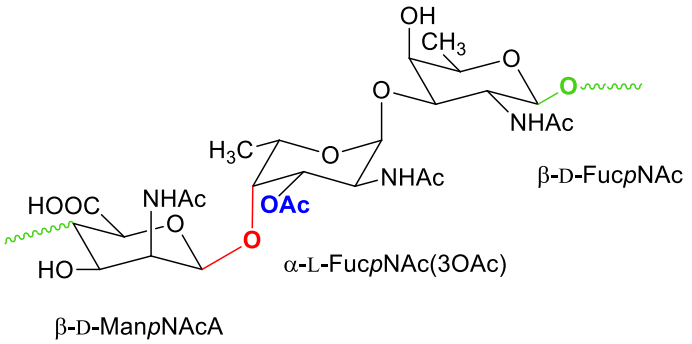

→4)-β-D-ManNAcA-(1→4)-∝-L-FucNAc(3OAc)-(1→3)-β-D-FucNAc-(1→

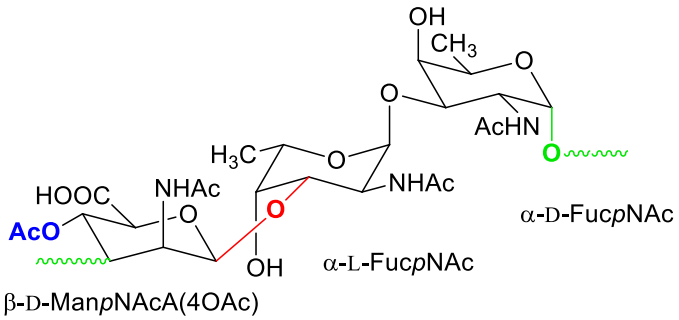

→3)-β-D-ManNAcA(4OAc)-(1→3)-∝-L-FucNAc-(1→3)-∝-D-FucNAc-(1→

Figure 23. *S. auereus* CP5 and CP8 repeating units.

3.1.1 S. aureus vaccines

The enormous burden of *S. aureus* infections and emerging antimicrobial resistance makes a vaccine to prevent these infections a worthy goal. Several vaccine candidates have been tested in clinical trials in recent years but none of them succeeded in showing efficacy against the infection in phase III trials. The antigens tested so far were mainly bacterial surface associated and secreted proteins or capsular polysaccharides (CPs). The first vaccine based on *S. aureus* CPs, called StaphVAX, was produced at Nabi Biopharmaceuticals and consists of CP5 and CP8 conjugated to nontoxic recombinant Pseudomonas aeruginosa exoprotein A (rEPA). Phase III clinical trials showed that StaphVAX offered no significant protection against bacteremia over the placebo control, thus halting further development of the vaccine [154, 155]. Vaccines tested so far in efficacy trials, which targeted single antigens and contained no adjuvants, were likely insufficient to cope with the complexity of this pathogen since its pathogenicity is due to several virulence factors, each playing different roles in the disease progression. A 4-component vaccine candidate, SA4ag, developed by Pfizer includes CP5, CP8, Clumping factor A (ClfA), and Manganese transport protein C (MntC) [156-158]. Although SA4Ag was deemed highly immunogenic, it failed in clinical stage IIb as it was unable to cause any reduction in the incidence of *S. aureus* bloodstream infections, surgical site infections, or all-cause mortality in patients who have had elective spinal surgery [159]. GSK developed a similar vaccine candidate that includes four antigens: CP5, CP8, ClfA and an additional detoxified hemolysin (HlaH35R), instead of MntC included in the Pfizer product. Furthermore, the polysaccharides developed by GSK are conjugated to the carrier protein TT, instead of CRM_{197} as in the case of Pfizer. This vaccine has reached phase I trial where it was found to induce strong IgG responses but weak cellular immune responses in recipients, with no effect on colonization level over two years. No safety concerns arose during this study, but this vaccine was not further developed [160]. Further multivalent vaccines have been developed and are now in clinical stages. **Table 11** reports the recently developed *S. aureus* vaccines. A combination of five recombinant *S. aureus* antigens was recently developed by Olymvax and is now in clinical phase II. The vaccine, named rFSAV, includes Hla, SEB, MntC, IsdB and SpA antigens and its efficacy was tested in murine preclinical studies with promising results [161]. Moreover, Integrated BioTherapeutics have developed a heptavalent product consisting of seven *S. aureus* toxoids which was proven able to confer protection to both mice and rabbits against *S. aureus* skin infection. Lastly, a new GSK vaccine consisting of five antigens including bioconjugates and recombinant proteins has been also developed and has recently started a clinical phase II [162].

Table 11. *Staphylococcus aureus* vaccines enrolled in clinical trials

Company	Vaccine	Phase	References
GSK	SA-5Ag: Unspecified Recombinant Protein; bioconjugates; adjuvanted	I/II: ongoing	[162]
Novadigm Therapeutics	NDV-3A: Als-3p; alum	II: ongoing	[163]
Olymvax	rFSAV: Hla, SpA, SEB, IsdB, MntC; alum	II: ongoing	[161]
Pfizer	SA4Ag: CP5-CRM_{197}, CP8-CRM_{197}, ClfA, MntC	IIb: failed	[159]
Integrated Biotherapeutics	STEBvax: rSEB; alum	I: completed in 2015	[164]
Integrated Biotherapeutics	IBT-V02: SEB, SEA, TSST-1, LukS, LukF, LukAB, Hla; alum	I: scheduled	[165]

Another approach in vaccine development is represented by passive immunization which consists in the transfer of specific antibodies to the various *S. aureus* antigens. Passive immunization with monoclonal antibodies as therapeutic and short-term prophylactic treatments for *S. aureus* is an area of keen interest in developing therapies [166]. Several studies have been conducted over the years using poly- and monoclonal antibodies targeting different *S. aureus* antigens [151, 166]. A recent example is the anti-Hla monoclonal antibody developed by Aridis, Tosatoxumab, which has been shown to be well tolerated in clinical phases I and II and is currently in phase III in patients with *S. aureus* ventilator associated pneumonia (VAP) in addition to the standard of care treatment [166, 167].

3.2 AIM OF THE STUDY

The medical need for a *Staphylococcus aureus* vaccine is clear. Purified serotype 5 and 8 capsular polysaccharides offer promise as target antigens for a vaccine to prevent staphylococcal infections. In fact, staphylococcal capsules are important in the pathogenesis of *S. aureus* infections enhancing virulence by impeding phagocytosis and resulting in bacterial persistence in the bloodstream of infected hosts [168]. Polysaccharide-based vaccines induce antibodies that can overcome this virulence mechanism by enabling the organism to be opsonized and subsequently phagocytosed [156]. It is therefore important to study the aspects that can influence the immunogenicity of CP5 and CP8 glycoconjugates, highlighting the most important clinical quality attributes (CQA) to be taken in consideration during the development of this type of vaccines. In this study, the saccharide size, the saccharide:protein ratio and the PS O-acetylation moieties have been analyzed in detail. In particular, in addition to the role of O-acetylation in PS immunogenicity already demonstrated in previous publications [73], this study points out the importance of O-acetyl moieties in polyclonal antibody recognition that has been related to the 3D structure predicted by MD simulation experiments. Moreover, the selection of the best monoclonal antibodies able to discriminate acetylated and not-acetylated CP5 and CP8 PS structures has been performed in order to generate optimal tools to follow the development of a potent *S. aureus* vaccine.

3.3 MATERIAL AND METHODS

Preparation of CP5 and CP8 oligosaccharides

CP5 and CP8 PSs were hydrolyzed with 5% acetic acid at 90 °C for 8h and 60h, respectively, and neutralized with 2M NaOH. The hydrolyzed samples were purified in size exclusion G10 resin and oligosaccharides of different lengths were separated by anion exchange chromatography into different pools using an Hi-Trap Q FF column. Each pool was purified with a G10 resin column and their average molecular weight was estimated by HPLC using a TSK3000PW column and Pullulan standards. For both CP5 and CP8, the pool composed of shorter oligosaccharides was further separated by MonoQ column into more homogeneous pools. Lengths and percentage of O-acetylation were estimated by 1H-NMR and a pool of an average length of 3 repeating units was selected for structural studies. For CP5 only, longer pools from Hi-Trap Q FF were used for the preparation of Hla-conjugates.

Preparation of de-O-acetylated polysaccharides and oligosaccharides

CP5 and CP8 natural polysaccharides and shorter oligosaccharides were de-O-acetylated by incubation with 5mM (for CP5) or 25mM (for CP8) NaOD, at room temperature. The samples were incubated with different duration time depending on the degree of targeted O-acetylation:

- CP5: 75% (20 min), 50% (2,5h), 25% (7,5h), 0% (65h)
- CP8: 75% (1h), 50% (7h), 25% (20,5h), 0% (65h).

The reactions were neutralized with HCl 2M and the percentage of acetylation was measured by ^{1}H-NMR. All polysaccharides and oligosaccharides were purified in 30KDa and 10KDa Amicon membrane, respectively.

HPAEC-PAD analysis for total saccharide quantification of CP5 and CP8 samples

The total saccharide quantification of Staph CP5 and CP8 samples has been performed by HPAEC-PAD analysis and consists in the acidic hydrolysis of the CP5 and CP8 polysaccharide or oligosaccharide structures to their monosaccharide components, which are N-Acetyl-Fucosamine (FucNAc) and N-Aceyl-Mannosaminuronic. For the saccharide quantification the FucNAc moiety has been used. A standard curve of CP5 or CP8 standard polysaccharides is built in the concentration range 0.1-3.0 µg/mL. Each sample has been prepared targeting the calibration curve midpoint. Commercial FucNAc has been used as positive control.

Standards and samples, all in duplicates, have been hydrolyzed with 4 M HCl in oven at 100 °C for 3 hours ± 5min, dried under vacuum (SpeedVac Thermo) at 55 °C for 3 hours, then solubilized in water and finally filtered by 0.45 µm Phenex filter. HPAEC-PAD chromatography has been performed on CarboPacPA1 column by isocratic elution in 16 mM sodium hydroxide followed by a washing step with 500 mM sodium hydroxide and recondition; detection was performed by using a quadruple wave form for carbohydrates with Ag/AgCl as reference electrode. The resulting chromatographic data were elaborated by using Chromeleon™ software vs 7.2.

Preparation of CP5-Hla conjugates

CP5 OSs avDP15 and avDP33 were aminated with ammonium acetate (NH_4OAc), activated with SIDEA and finally conjugated to Hla protein.

The previously lyophilized oligosaccharides were dissolved in 100 mM sodium acetate buffer at pH 6.5, added with NH_4OAc and $NaBH_3CN$ and the reactions were stirred at 37°C for 5 days. Purification was performed by size exclusion chromatography using a G15 resin and the total amount of amino groups generated was determined by TNBSA assay using a standard 6-aminocaproic acid curve (60% amination). The oligosaccharides were lyophilized and resolubilized in a mixture of water and DMSO (1: 9), followed by the addition of triethylamine (5 eq) and SIDEA (12 eq) and the reactions were stirred for 3 h at room temperature. Next, each sample was transferred to a 15 mL Falcon cold Ethyl acetate (EtOAc) (1:5 v/v) was added to allow for sugar precipitation. After 30 min at 0 ° C the Falcon was centrifuged for 10 min (4° C, 4500xg), the solvent was extracted and the residual precipitate was dissolved again in EtOAc. This procedure was repeated 8 times and finally the remaining solid was frozen and lyophilized. The resulting active esters were analyzed by NMR to verify the level of activation of each OS pool (60%). As final step, conjugation was performed by adding Hla to lyophilized activated sugar (saccharide:protein 200:1eq) and incubating the solution overnight at room temperature. Conjugation was confirmed by SDS-Page and Western Blot. The conjugates were purified from the free unreacted saccharide through precipitation with NH_4SO_4. After sterile filtration, the protein content in the purified glycoconjugates was determined by micro-BCA colorimetric analysis and the saccharide content was estimated by HPAEC-PAD analysis.

SDS-PAGE analysis

Sodium Dodecyl Sulfate-Polyacrylamide gel electrophoresis (SDS-PAGE) was performed on 4-12% pre-casted polyacrylamide gel (NuPAGE Invitrogen) using MOPS 1X as running buffer (NuPAGE Invitrogen). 5µg of protein were loaded for each sample. Hla protein alone was used as positive control. After electrophoretic running with a voltage of 150V for about 45 min, the gel was stained with blue Coomassie.

Western Blot analysis

Two SDS-Page were run as described before using Hla protein alone and CP5-TT conjugate as positive and negative control depending on the secondary mAb analyzed. Gels were transferred on cellulose with iBlot gel transfer stacks nitrocellulose kit and blocked with PBS 1x pH 7.2+BSA 3%. Rat anti-CP5/R1 mAb and an anti-Hla rat mab were used as primary antibody (dilution 1:1000, 1h) followed by several washes with PBS 1X + tween20 0,05% buffer. Anti-Rat IgG-alkaline phosphatase antibody (Sigma) was used as secondary antibody (dilution 1:2000, 30min) followed by several washes with PBS 1X + tween20 0,05% buffer. Western-Blot were finally developed with AP conjugate substrate kit (BIORAD).

Evaluation of CP5-Hla glycoconjugates immunogenicity in a mouse model

Four groups of 10/15 female BALB/c mice were immunized by intramuscular injection with 1µg dose in saccharide content of each conjugate using AS01 as adjuvant. A CP5-Hla bioconjugate was used as reference. Mice received the vaccines at days 1 and 29. Bleeding were performed at days 27 and 49.

Luminex Immunoassay

Three weeks after the second dose, individual IgG titers in mice sera were analyzed using the Luminex technology. The assay analysed Hla and CP5 PS antigens simultaneously using magnetic beads coated with Hla protein and CP5 capsular polysaccharide. Protein antigens were covalently conjugated to the free carboxyl groups of microspheres using an N-hydroxysulfosuccinimide-enhanced carbodiimide (EDC) -mediated conjugation chemistry. CP5 and CP8 were biotinylated using Biotin-Hydrazide and EDC, purified and subsequently conjugated to Streptavidin beads. The assay read-out was a mean of mean fluorescence intensity (MFI). For all sera, serial dilutions were manually prepared starting from 1:100, 8 dilutions 3-fold and loaded onto single 96 wells plate with an adequate number of coupled microspheres (~2500). One replicate of each dilution was tested. Antigen specific antibodies in sera of

immunized mice were revealed by an anti-mouse IgG Phycoerythrin-labelled secondary antibody and MFI were measured using a Luminex 200 Reader. Results were expresses as Relative Luminex Units (RLU)/mL using a pool of positive sera as Standard. Data were analyzed using Bioplex Manager Software (BioRad).

SPR analysis

Binding analyses were performed by SPR using both BIACORE X100 and T200 systems. Biotinylated CP5 and CP8 PSs were immobilized on a streptavidin-coated sensor chip (GE Healthcare) through a streptavidin-biotin capture using 1M NaCl, 50mM NaOH and 1M NaCl, 50mM NaOH, 50% isopropanol. Biotinylated CP5 and CP8 PSs were immobilized at 20µg/mL to a final surface density of 71 and 31 resonance units, respectively. Competitive SPR experiments were performed using acetylated and deacetylated PSs and OSs as competitors incubated with the relative mAb/pAb and flowed on the chip. Competitors that interact with the mAb inhibit the mAb binding to the PS immobilized on the chip and the inhibition is measured as a percentage with respect to mAb not inhibited. For each sample the experiment was performed using a constant concentration of mAb and decreasing concentrations of competitors. The experiments were conducted in 10 mM HEPES (pH 7.2), 150 mM NaCl, 3 mM EDTA, 0.005% Tween20 at 25° C and at a flow rate of 45 µL/min. After each cycle of mAb binding, the chips were regenerated with 3.5 M $MgCl_2$ and Glycine-HCl, and a contact time of 120 seconds. Sensorgram data were analyzed using BIAevaluation software (Biacore).

Phagocytosis assay (Anti-CP8 mAbs)

S. aureus CP8 biotinylated polysaccharide and *Neisseria meningitidis* Serogroup C (used as negative control) were incubated with fluorescent neutravidin beads in a round-bottom 96 well microplates overnight at 4°C. Beads were subsequently spun down and washed twice in DPBS-1% BSA in order to remove excess unbound antigen and then resuspended in the buffer. Saturation of the beads surface was determined experimentally, via incubation with different amounts of antigen. Beads were incubated with different amount of each monoclonal antibody serially diluted in blocking solution for 2 hrs at 37°C under 250 rpm shaking, in order to allow the immunocomplexes formation. Following equilibration in blocking solution THP-1 cells, a human monocytic cell line expressing multiple isoforms of Fcγ receptors, were added to each well in a final ratio beads:cells of 10:1 and the plate was incubated for 1hr at 37°C. At the end the plate was centrifuged at standard cell culture conditions and a volume of Trypan Blue, 0.2%

final, was added to wells, for quenching the fluorescence of adherent ICs, just before to be assayed by flow cytometry on a BD FACS CantoII. Data were collected with FACSDiva 8.0.1 and analyzed with FlowJo (Becton Dickinson, version 10.0.7 for Apple system). A phagocytic score was finally determined by gating samples on events representing cells and calculated by determining the percentage of beads-positive cells and multiplying by their mean fluorescence intensity (% PE beads-positive cells x iMFI).

OPKA assay (Anti-CP5 mAbs)

Functional activity of anti-CP5 antibodies was estimated by Opsono Phagocytic Killing Assay (OPKA). Assay was run in round-bottom 96 well microplates using *S. aureus* bacteria, test serum dilution, HL-60 human phagocytic cells and Guinea Pig Low Tox complement. A positive control (anti-capsule serum) and a negative control (without serum) were included in each test plate. Opsonophagocytic (OPK) titers were expressed as the reciprocal serum dilution mediating 50% bacterial killing, estimated through linear interpolation of the dilution-killing OPKA data. The 50% of bacterial killing was calculated as the [CFU mean of the negative control (Bacteria + HL60 + Complement without serum) at time T90 (0% killing) + CFU mean of the positive control at T90 (100% killing)]/2. The lower limit of quantification (LLOQ) value for this assay was a titer of 100.

NMR experiments

The NMR experiments were acquired with a Bruker Advance 800 MHz spectrometer equipped with cryoprobe head. The mAbs were exchanged in the working buffer (standard PBS 1X in D_2O at pD 8.0). The STD NMR experiments were carried out at 310K using a standard sequence from Bruker library. Suppression of the water signal was achieved by excitation sculpting (2 ms selective square pulse). For each ligand/protein sample the on-resonance protein saturation was obtained using a Gaussian shape pulse of 50 ms with a total saturation time of 2 s at two different frequencies (aliphatic region δ 0 ppm and aromatic region δ 7 ppm). The relaxation time was set at 3s and the experiments were acquired with 16 number of scans and 180 loops. The absolute STD (STD-AF) values were evaluated for the NMR signals of the ligand and the proton signal with the strongest STD effect was used as reference. Consequently, the relative STD intensities (STD%) were calculated, allowing us to map the ligand-binding epitope reported in the discussion.

MD simulations

CP5 (3 RU) and CP8 (3 RU) initial molecules were built using the GLYCAM carbohydrate builder web tool (http://glycam.org). The unusual O-acetylation, N-acetylation decorations and the COOH were added using the MAESTRO (Schroedinger) suite of programs. The parameters and partial atomic charges of the molecule were calculated with the antechamber module. The resulting geometries were taken as starting structures for the MD simulations in explicit solvent. The molecules were solvated in a theoretical box of explicit TIP3P waters and the solute atoms were positioned at least at 10 Å from the solvent box edge. Energy minimization of the solvent followed by an energy minimization of the entire system without restraints was then performed. The system was then heated up to 300 K during 100 ps followed by 2 ns dynamics at constant temperature of 300 K, controlled by the Langevin thermostat, and constant pressure of 1 atm. Minimization, equilibration, and production phases were carried out by the pmemd.cuda module of AMBER 16. The actual 500 ns MD simulations were performed using GAFF.2 force field. Once the trajectories have been generated and stored, the analysis of the simulations was performed using cpptraj module from AMBERTOOLS 16; data processing and 2D plots were carried out using GNUplot software.

3.4 RESULTS

3.4.1 Glycoconjugates immunogenicity influenced by saccharide length and glycosylation degree

Classically, Staph glycoconjugates vaccines have been prepared via conjugation of the capsular polysaccharide to common carrier proteins such as CRM (non-toxic mutant of diphtheria toxin) and TT (*Tetanus Toxoid*). However, it is well documented that protein carriers additionally induce an immune response against themselves and may therefore have a potential dual function: as providers of T-cell helper epitopes and as protective antigens per se [22, 25]. Wacker et al. showed that the glycoengineering *S. aureus* CP5-Hla (*S. aureus* α-toxin) bioconjugate induced in rabbits and mice specific antibody titers against the glycan and the protein moiety both with protective activity [169]. Thus, taking into consideration Hla as a good carrier for CP5, we have studied how other important glycoconjugate variables such as sugar size and saccharide/protein ratio could modulate the immunogenicity of a CP5-Hla vaccine against *S. aureus.* The CP5 polysaccharide was hydrolyzed to obtain smaller oligosaccharides. Since acid hydrolysis is not selective for a specific glycosidic bond, cleavage can occur at different points in the repeating unit and indeed it was not possible to obtain well-defined oligosaccharides. The strategy to obtain more defined CP5 oligosaccharides was to separate the hydrolyzed samples on the basis of the only negative charge available in the repeating unit, consisting of the carboxyl group of the N-acetyl aminomanuronic acid residue (ManNAcA). Through an anionic column, the oligosaccharides were differentiated based on the different number of ManNAcA residues which correspond directly to the number of charges present in the oligosaccharide itself. For our purpose, we selected two main populations of CP5 oligosaccharides with an average degree of polymerization (avDP) of 15 and 33, avDP15 and avDP33, which have been used for conjugation with Hla carrier protein. Oligosaccharides were subjected to reductive amination with ammonium acetate (NH_4OAc), activation with succinimidyl diester of adipic acid (SIDEA) and finally conjugation to Hla protein (**Figure 24**).

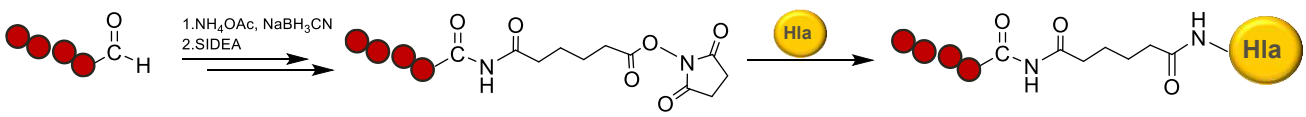

Figure 24. Conjugation strategy: reductive amination with NH_4OAc, activation with SIDEA and conjugation with Hla protein.

The shortest pool avDP15 was used to obtain two different conjugates, one highly glycosylated and one lowly glycosylated, while the longest avDP33 was used to obtain one single conjugate (**Figure 25**). Conjugation was monitored by SDS-Page and Western Blot.

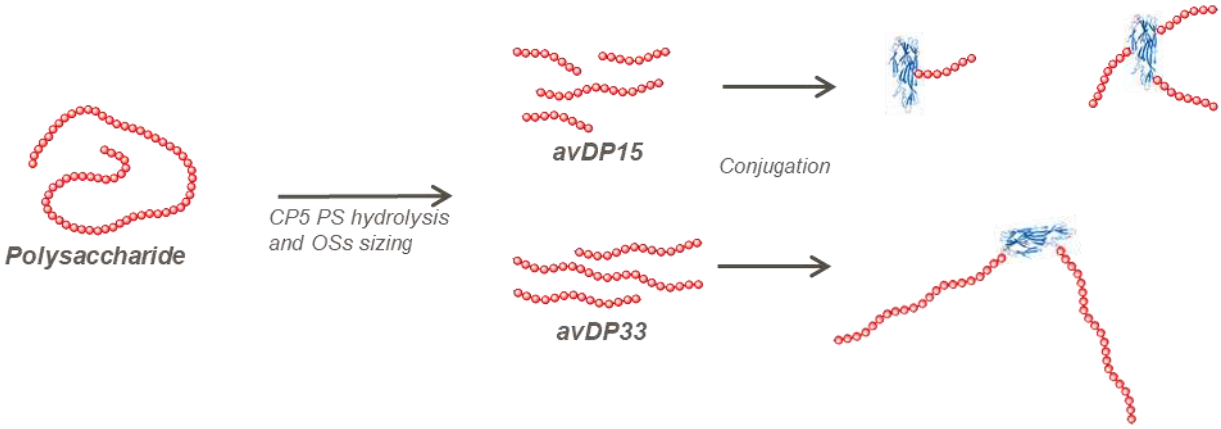

Figure 25. CP5-Hla conjugates design: CP5 polysaccharide hydrolysis with length-based oligosaccharides sizing and final conjugation to Hla carrier protein.

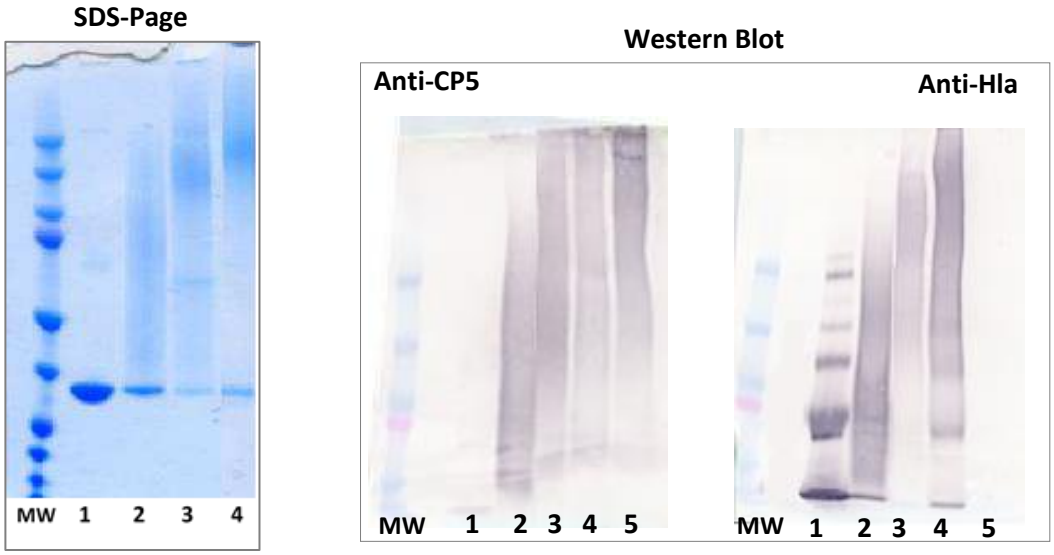

1=Hla; **2=** CP5-Hla (high glycosylation); **3=** CP5-Hla (low glycosylation); **4=** CP5-Hla (longer chain); **5=** CP5-TT

Figure 26. SDS-PAGE gel electrophoresis and Western Blot analysis of CP5-Hla glycoconjugates.

The formation of the conjugates has been followed by SDS-Page in which it is possible to appreciate a slight and linear increase in molecular weight (lines 2-4). Western Blot analysis showed that all three conjugates are well recognized by both the anti-CP5 and anti-Hla rat mAbs (**Figure 26**). After purification from the free unreacted saccharide through precipitation with ammonium sulfate $(NH_4)_2SO_4$, the conjugates have been sterile filtered and analyzed by micro-BCA colorimetric assay and HPAEC-PAD analysis for the quantification of protein and saccharide content, respectively, and calculate the saccharide:protein ratio (**Table 12**).

Table 12.CP5-Hla conjugates quantification

Antigen	Saccharide avDP	Sacc/Prot w/w	Sacc/Prot av molar ratio
CP5-Hla bioconj (Reference)	7-8	0,15	1:1
CP5-Hla chemical conj (low glycosylated)	15	0,24	0.8:1
CP5-Hla chemical conj (high glycosylated)	15	0,59	2:1
CP5-Hla chemical conj (longer chain)	33	1,18	1:1

Groups of 10 or 15 mice received two doses of the conjugates adjuvanted with AS01 (a liposome-based adjuvant which contains two immunostimulants, 3-O-desacyl-4'-monophosphoryl lipid A and QS-21, saponin fraction extracted from Quillaja saponaria Molina) [170]. Animals receiving a CP5-Hla bioconjugate as reference. Three weeks after the second dose, individual IgG titers were measured by Luminex assay using full-length biotinylated CP5 or Hla protein coupled to fluorescent beads.

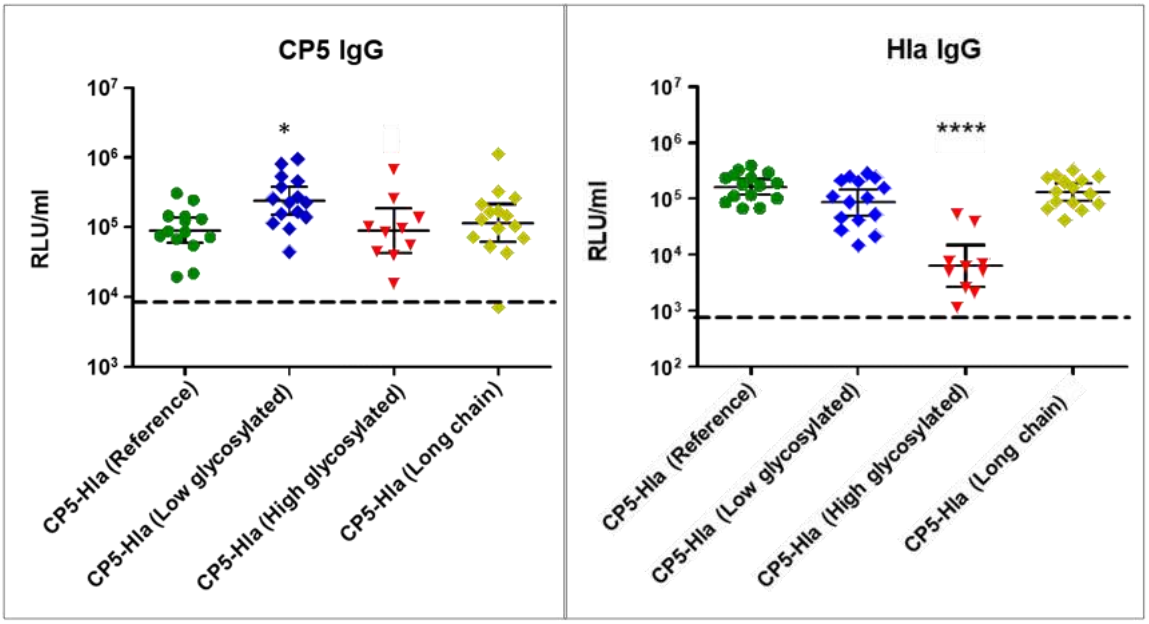

Figure 27. Luminex assay immunoglobulin G (IgG) titers in mouse serum samples collected after 2 vaccine doses, reported as arbitrary units (AU); bars represent the geometric mean titers with 95% confidence intervals from serum samples. Statistical analysis by Kruskal-Wallis test reported for each group compared to the reference (*P < .05; **P < .01; ***P < .001 **** P < .0001).

For CP5 titers, data show that both saccharide size and saccharide/protein ratio don't have a significant effect on immunogenicity (**Figure 27**): conjugates with longer chain and higher glycosylation elicit similar IgG titers comparable with the reference while the lowly glycosylated conjugate appears slightly more immunogenic. The anti-Hla titers underline that high glycosylation has an impact on the protein epitopes resulting in a significantly lower immunogenicity compared to the reference and this is probably due to the small size of the protein. Considering that Hla is a *S. aureus* protein used with a dual role of carrier and antigen and then Hla epitopes should be preserved, high glycosylation conjugate proves not to be an ideal solution since there's no added value in CP5 immune response. No effects were observed for the other formulations. Therefore, these studies point out that there isn't a marked role of saccharide length and saccharide/protein ratio in the anti-saccharide immune response and that only high glycosylation conditions should be avoided not to impact the protein immunogenicity.

3.4.2 Evaluation of O-acetylation recognition by polyclonal antibodies sera

Bacterial polysaccharides often contain a number of substituents, such as O-acetyl and phosphate groups, which may play a key role in the composition of immunodominant epitopes [61]. Bhasin *et al.* reported that CP5 O-acetylation rendered *S. aureus* more resistant to opsonophagocytic killing by human neutrophils than the de-O-acetylated CP5 [171]. More recently it has been shown that the generation of antibody responses to *S. aureus* requires the presence of O-acetyl modifications on the CPS [73]. Hence, we focused our attention at O-acetyl group present in CP5 and CP8 polysaccharide repeating units. CP5 and CP8 natural PSs and shorter OSs were completely de-O-acetylated by incubation with NaOH. To elucidate the importance of O-acetylation in the anti-CP5 and anti-CP8 immune response in rabbits and humans, we tested the recognition of fully acetylated and deacetylated antigens in polyclonal sera from subjects immunized with CP5-TT and CP8-TT conjugate vaccines by competitive SPR experiments. Sera have been preincubated with PSs (for human sera) and OSs (for rabbit sera) 100% and 0% O-acetylated serially diluted and then binding experiments were run in a chip where a specific biotinylated capsular PS were immobilized. PAbs from two rabbits immunized with specific monovalent PS-TT vaccines were tested after preincubation with fully acetylated and deacetylated short oligosaccharides used as competitors.

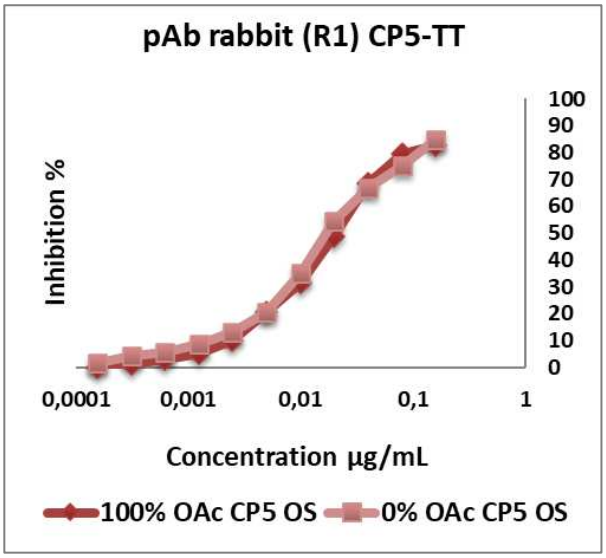

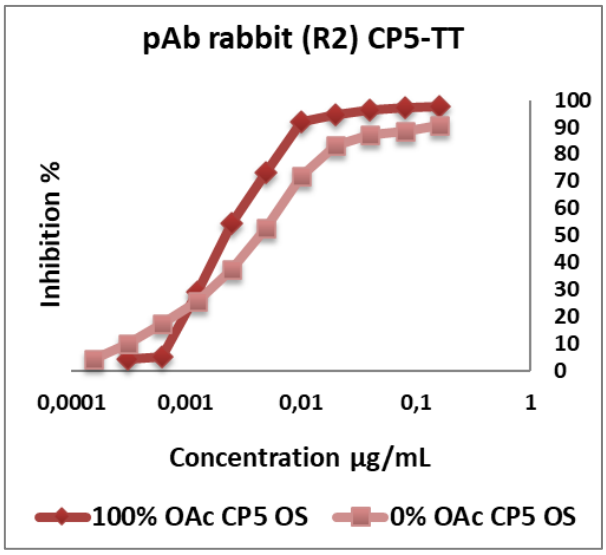

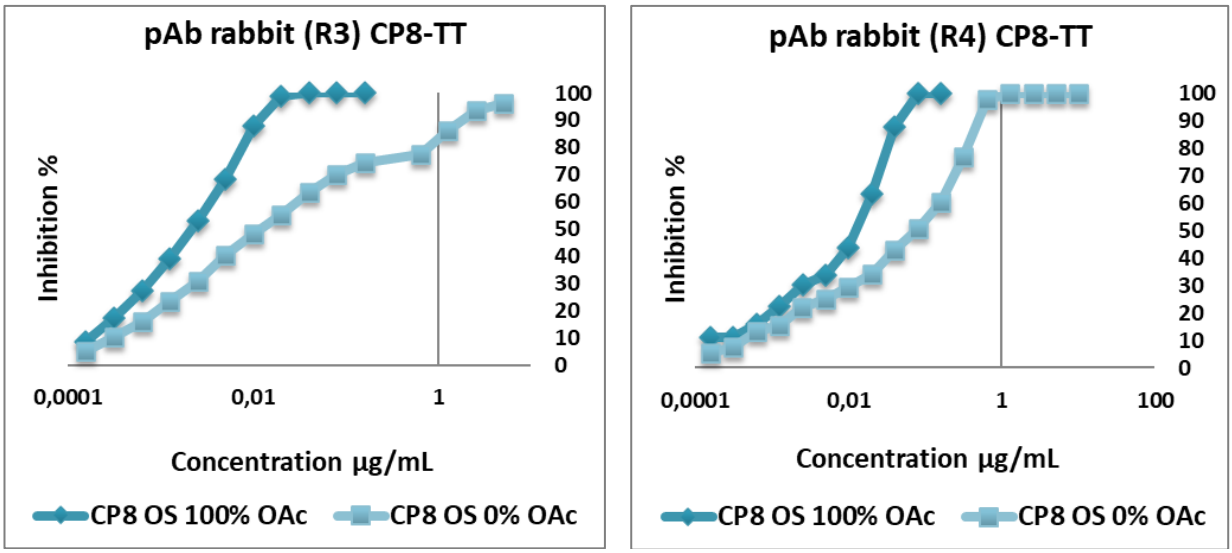

Figure 28. Competitive SPR experiments: 0% and 100% CP5 and CP8 OSs recognition by rabbit sera

The anti CP5 sera appear to be composed of antibodies that recognize equally both acetylated and deacetylated epitopes (**Figure 28**). On the other hand, both anti-CP8 sera are composed of a greater quantity of antibodies recognizing the acetylated epitope. At high concentrations even the totally deacetylated oligosaccharide reaches a complete inhibition of the binding showing an ability to cover the recognized polysaccharide epitope, but the presence of acetyl group considerably increases the affinity and therefore the recognition by the antibodies.

Subsequently, four human sera from subjects immunized with the GSK vaccine composed of 4 antigens (CP5-TT, CP8-TT, HlaH35L and ClfA) [160] were tested using fully acetylated and deacetylated polysaccharides as competitors. The affinity of each serum was tested for the two different serotypes.

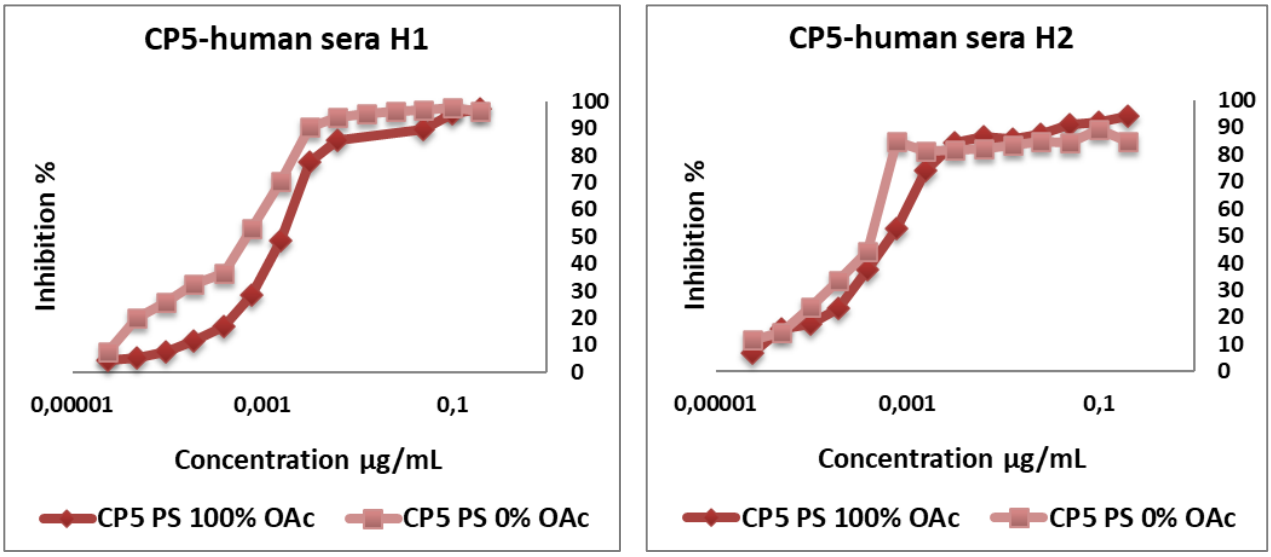

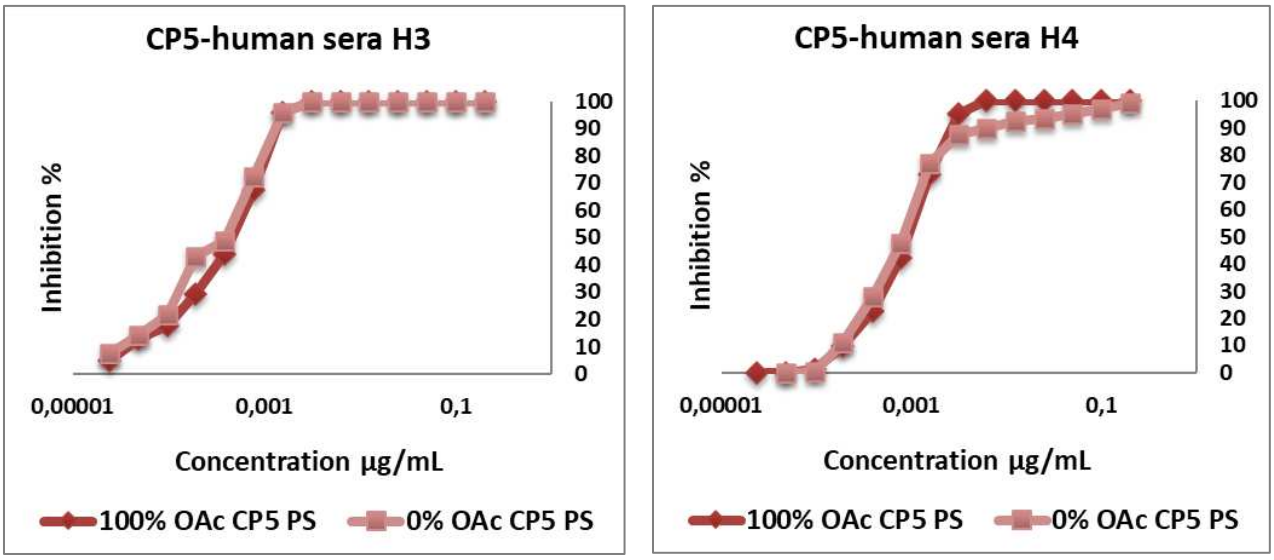

Figure 29. Competitive SPR experiments: 0% and 100% CP5 OSs recognition by human sera.

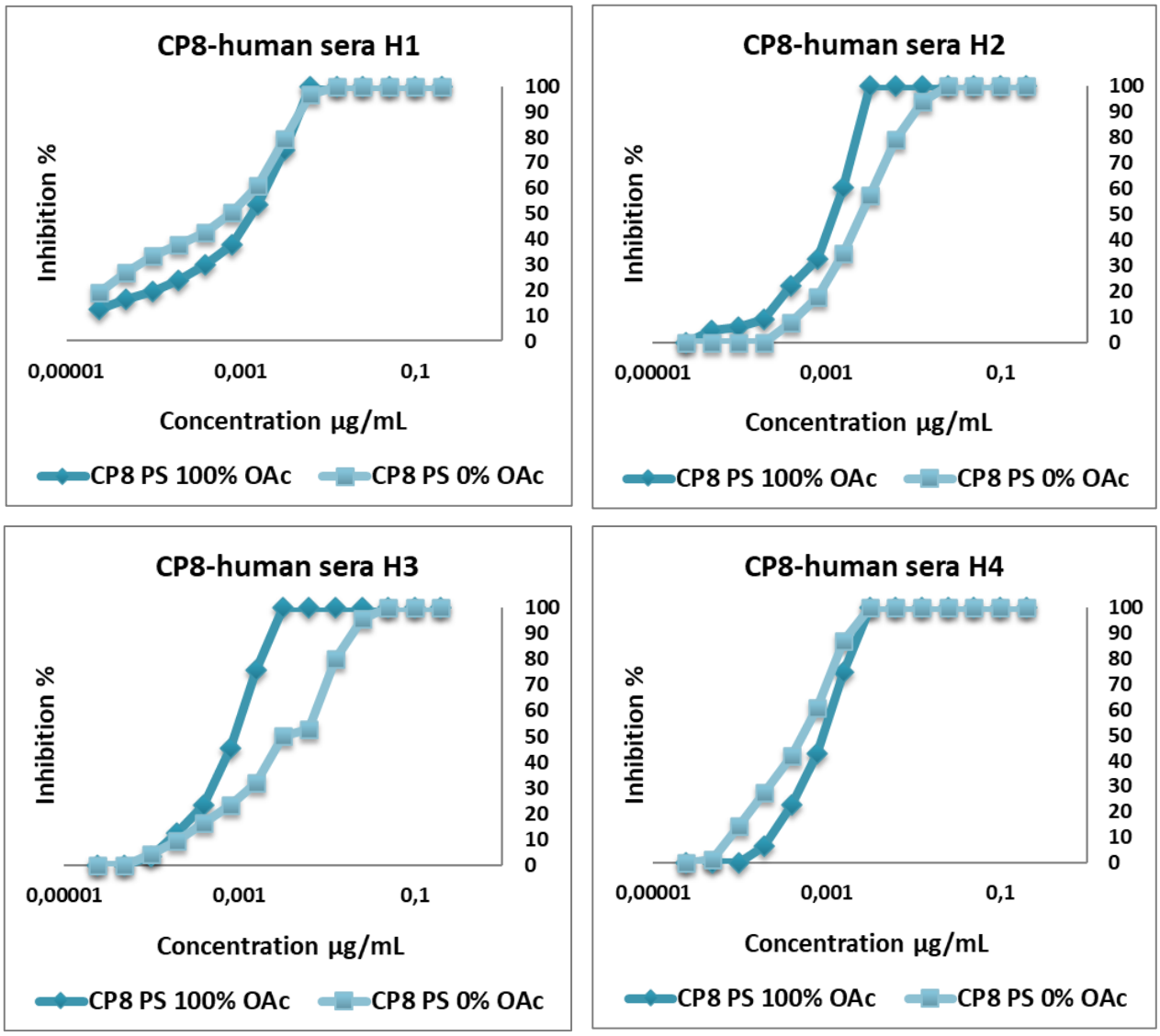

Figure 30. Competitive SPR experiments: 0% and 100% CP8 OSs recognition by human sera.

The results partly reflect what seen with rabbit experiments. All sera tested show no recognition differences towards acetylated and deacetylated CP5 polysaccharide (**Figure 29**), while a different behavior has been observed for CP8 (**Figure 30**): sera 2 and 3 show greater recognition for the acetylated epitope, confirming the results observed with rabbit sera. Therefore, O-acetylation has a different influence in the epitopes of CP5 and CP8, with a clearly high impact for CP8 polyclonal antibody recognition.

3.4.3 MD simulations of the free ligands

With the aim of investigating the behaviour of CP5 (3 RU) and CP8 (3 RU) in solution, 500 ns of Molecular Dynamics simulation were performed using GAFF.2 force field in explicit water. In order to unravel the dynamic features at the glycosidic linkage the dihedral angles were studied along the simulation (**Figure 31**).

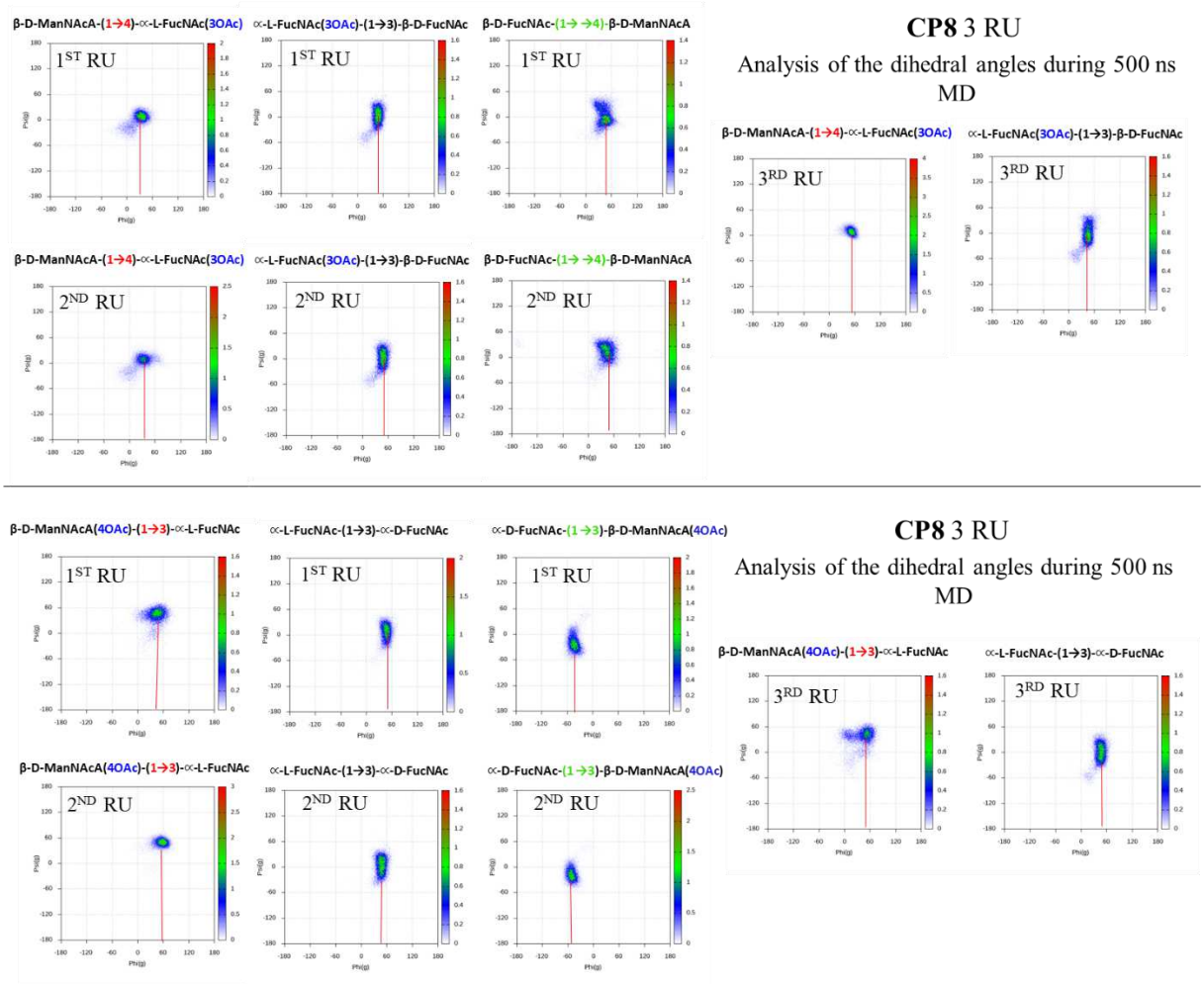

Figure 31. ϕ/ψ plot for all the glycosidic linkages of the MD trajectory (500 ns simulation time in explicit water with the GAFF.2 force field) for the initial structures of CP5 3RU (above) and CP8 3RU (below). Φ highlighted with red line.

The results indicate that in explicit water both CP5 and CP8 assume a typical exo-syn conformation around the ϕ torsion angle, which is strongly stabilized by the exo-anomeric effect. The ψ torsion angle mostly populates the syn+ conformation (ψ = +60°), although minor excursions to other regions of the conformational map (syn-, -60°) are also possible.

As general aspect, the global shape of both CP5 and CP8 is governed by the low variability of ψ. During the simulation, the oligosaccharides always maintain an extended structure with no relevant secondary structural element detected.

Inter-residue distances (Å) along the MD trajectory were calculated and the maximum distance between the first sugar residue (R1) and the last one (R9) rarely goes beyond 35 Å for CP5 as well as for CP8 (**Figure 32**). The different dispositions of the OAc group do not modify the flexibility comparing CP5 and CP8.

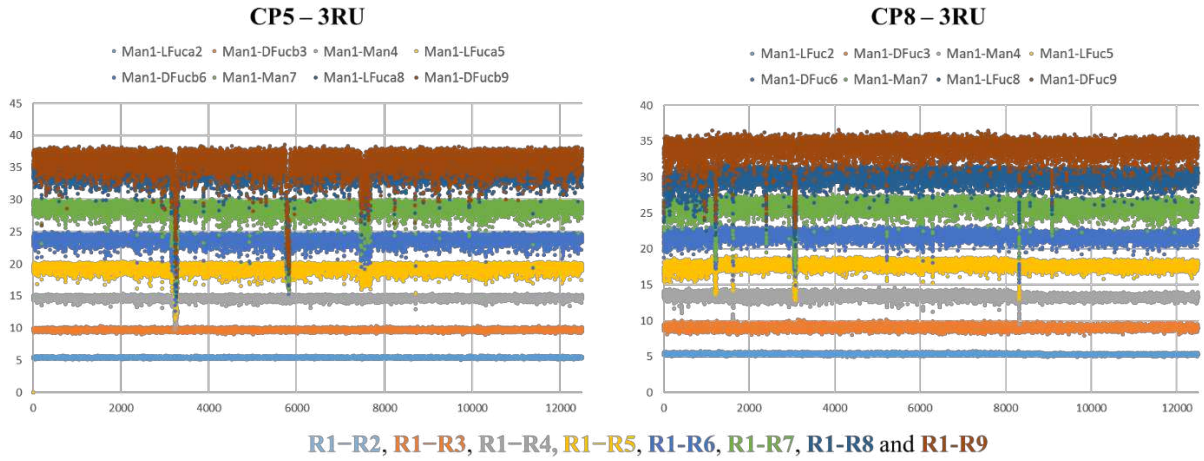

Figure 32. Calculated inter-residue distances (Å) along the MD trajectory. From bottom to top: distances between the centre of residue 1 and that of residue 2 (R1−R2), R1−R3, R1−R4, R1−R5, R1−R6, R1-R7, R1-R8 and R1-R9.

Taken altogether, the results from the MD simulation shows that the energy profile for CP5 and CP8 keeps the ϕ torsion in the exo-anomeric conformation and explores different conformations (± 60°) around ψ = 0.

Finally, the fluctuation of the OAc groups along the MD compared to a fixed reference (starting point of the MD) was analysed through RMSD (Root Mean Standard Deviation). However, no significant fluctuation was detected (data not shown) indicating that the spatial distribution of the acetyl groups is defined by the inter-residues glycosidic linkages.

Interestingly, the acetates of beta-1,4; alpha-1,3; alpha-1,3 linked CP8 are pointing on the same direction, while in the beta-1,4; alpha-1,3; beta-1,4 linked CP5 the acetate groups are more disordered. This is even more evident when the surface distribution of charge is displayed (**Figure 33**). Such a strong difference in the O-acetyl exposition can be responsible of guiding

the recognition in different ways. From this observation, a more hydrophobic-mediated interaction can be supposed for CP8 PS.

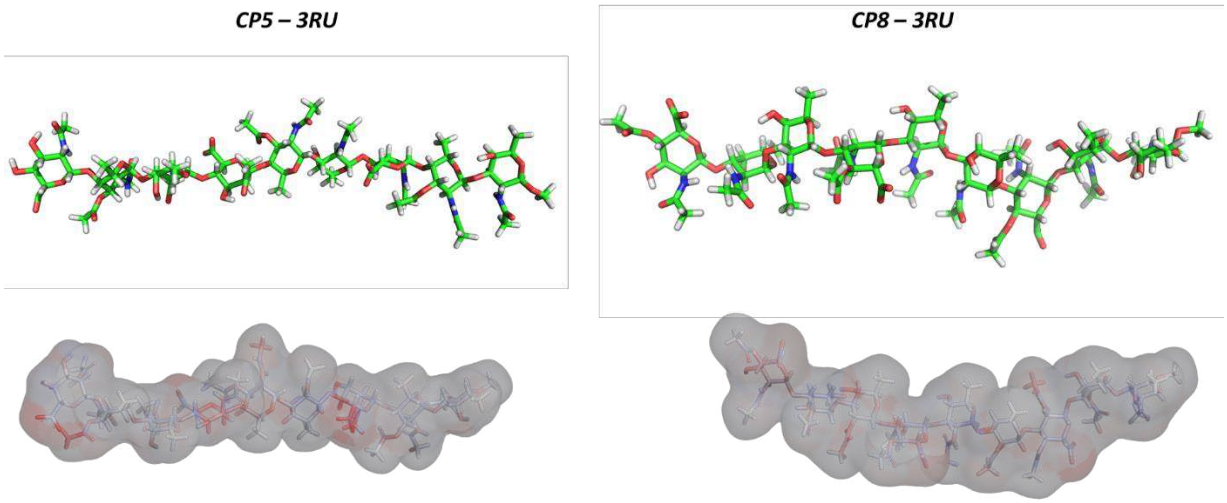

Figure 33. MD frames of CP5 and CP8 displayed in sticks (above). Smoothed-surface charge representation presented in the lower panel.

3.4.4 Importance of O-acetylation for monoclonal antibodies recognition

After testing the influence of acetyl groups in recognition by polyclonal antibodies, we investigated the CP5 and CP8 epitopes recognized by specific monoclonal antibodies (mAbs) to discover differences in the involvement of O-acetyl moieties in binding. A panel of anti-CP5 and anti-CP8 mAbs have been selected to study their affinity towards the differently acetylated epitopes. Deacetylated and fully acetylated CP5 and CP8 PSs were used as competitors of the immobilized PS for the binding with the mAbs. Screening revealed that some antibodies showed greater preference for the acetylated or deacetylated epitope, while others did not display difference in the recognition of the two polysaccharides (**Table 13**).

Table 13. CP5 and CP8 PSs recognition by different antibodies

MAbs	Immunogen	Isotype	Epitope recognition
Anti-CP5/R1	CP5 conjugated	Rat	**OAc>deOAc**
Anti-CP5/M1	CP5-DT	Mouse	**OAc<deOAc**
Anti-CP8/R2	CP8 conjugated	Rat	**OAc<deOAc**
Anti-CP8/R3	CP8 conjugated	Rat	**OAc<deOAc**
Anti-CP8/R4	CP8 conjugated	Rat	**OAc=deOAc**
Anti-CP8/M2	CP8 conjugated	Mouse	**OAc=deOAc**
Anti-CP8/M3	CP8-DT	Mouse	**OAc>deOAc**
Anti-CP8/M4	CP8-TT	Mouse	**OAc>deOAc**
Anti-CP8/M5	CP8-KLH	Mouse	**OAc<deOAc**

OAc= O-Acetylated; deOAc= de-O-acetylated.
anti-CP5 and anti-CP8 mAbs are highligted in yellow and green, respectively.
Antibodies selected for SPR experiment with OSs and functional studies are circled in light orange.

Among all mAbs tested, we selected for each serotype one mAb that binds preferentially the acetylated epitope and another mAb that recognize preferentially the deacetylated epitope to study more in details their affinity towards differently O-acetylated oligosaccharides to better appreciate differences (highlighted in red in **Table 13**). Short oligosaccharides were deacetylated targeting different levels of O-acetylation (0%, 25%, 50% and 100%) and together with fully O-acetylated ones were used as competitors of immobilized PS in SPR experiments (**Figure 34**).

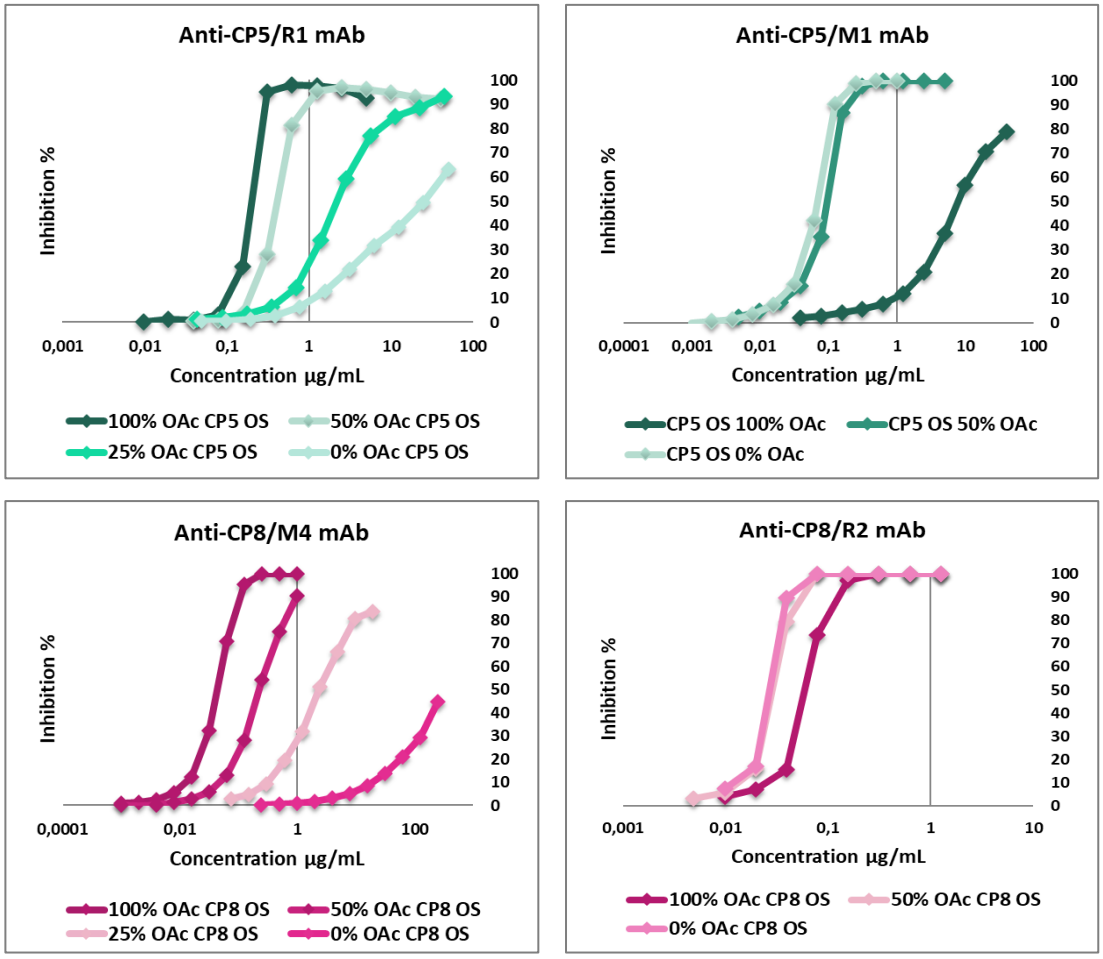

Figure 34. Competitive SPR experiments: differently O-acetylated CP5 and CP8 OSs recognition by monoclonal antibodies.

All the differently acetylated CP5 and CP8 oligosaccharides are recognized by the relative mAbs: anti-CP8/M4 and anti-CP5/R1 mAbs confirmed that all fragments are well recognized but a decrease in the degree of acetylation leads to a proportional reduced affinity with the antibody, highlighting the importance of the acetyl moiety for the interaction with this mAbs.

Conversely, anti-CP5/M1 and anti-CP8/R2 mAbs show less gradual difference; a similar recognition was observed for OSs with 50% and 0% of OAc while the affinity towards the fully acetylated OS is significantly reduced, especially in the case of CP5. The selected mAbs were then compared in terms of functional activity using two different assays. The functional activity for the anti-CP5 mAbs was investigate by OPK assay and for the anti-CP8 mAbs was measured by a flow cytometry-based assay as surrogate. After immobilizing CP8 PS on fluorescent microspheres, the latter are complexed with the relative mAb and the ability of THP-1 cells to phagocytize the immune-complex was measured by cell associated fluorescence.

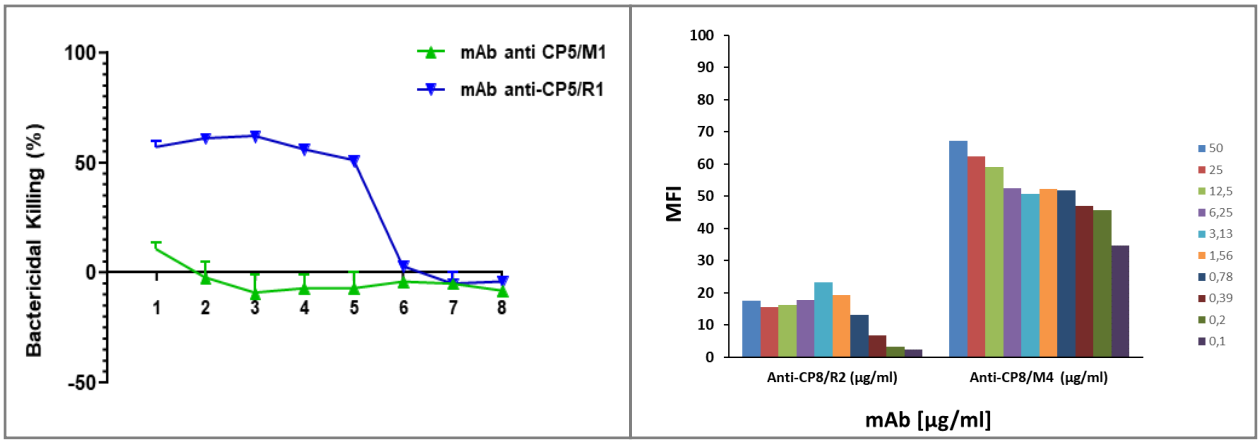

Figure 35. Functional assays for anti-CP5 anti anti-CP8 mAbs.

In both cases, the mAb targeting the acetylated epitope clearly showed a higher functional activity compared to the mAbs that binds preferentially the deacetylated epitopes (**Figure 35**). These data therefore indicate a possible correlation between the role of O-acetyl groups in epitopes targeted by specific mAbs and their functional activity.

3.4.5 Measurement of the functional mAbs binding affinity towards short oligosaccharides by SPR experiments

The next objective was to map at the atomic level the antigenic epitope recognized by the functional mAbs. For this purpose, CP5 and CP8 PSs were hydrolyzed to obtain smaller oligosaccharides to be used in complex with the mAbs in STD-NMR experiments. The hydrolyzed sample was separated into different length pools by anionic chromatography and NMR/MS analyzes were used to measure the average length and percentage of O-Acetylation after hydrolysis. Oligosaccharides of an average length of 3 repeating units (av3RU – avDP3) were selected for both serotypes and details are given in the **Table 14**. Before proceeding with STD-NMR investigation, affinity binding of functional mAbs toward the av3RU OSs were measured in competitive SPR experiments using the OS as competitors of the immobilized PS. CP5 and CP8 PSs were used as reference in both experiments. The functional mAbs show high binding to the OS fragments for both serotypes (**Figure 36**).

Table 14. Characterization of CP5 and CP8 oligosaccharide pools avDP3

	NMR		MS
Oligosaccharides pools	**O-Acetylation %**	**DP estimation**	**DP estimation**
CP5 avDP3	95,7	3,2	2,9
CP8 avDP3	82,6	3,9	2,9

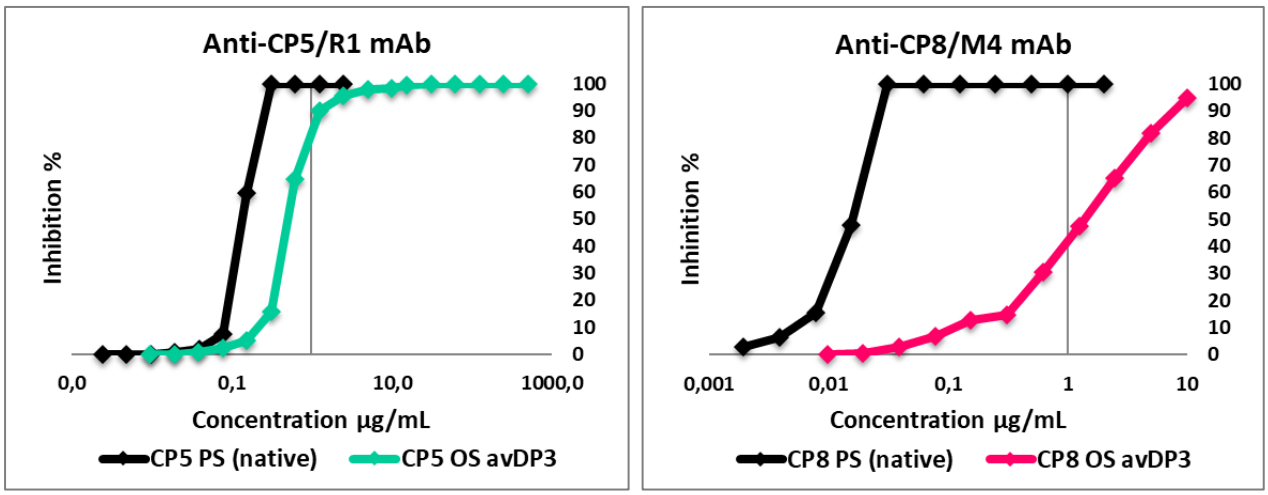

Figure 36. Recognition of CP5 and CP8 oligosaccharides avDP3 by monoclonal antibodies.

3.4.6 Elucidating the molecular interaction between functional anti-CP5 and anti-CP8 mAbs and short oligosaccharides pools from CP5 and CP8 PS

CP5 av3RU-mAb complex

The interaction between the Rat anti-CP5/R1 mAb and the CP5 oligosaccharide was investigated by titration NMR experiments. Ligand line broadening in the presence of the protein is an indicator of protein–ligand interactions. In the regime of fast exchange, K_d in the µM to mM, the degree of line broadening depends on many factors, including the fraction of the ligand in the free and bound state, among others. By varying the ligand:protein ratio, the fraction of free over bound ligand changes, which is translated into a difference in the ligand NMR signals width at half height. We performed ^{1}H NMR titration experiments at the protein:ligand ratio of 1:0 (apo antibody), 1:25, 1:50, 1:75, 1:100. The titration was carried out by adding increasing amounts of CP5 av3RU ligand (100 µM, 200 µM, 300 µM, 400 µM) to a sample containing the anti-CP5/R1 mAb (4µM in deuterated buffer). At each point of the titration, a standard 1D ^{1}H NMR spectrum was recorded (**Figure 37**). Ligand NMR signals line broadening was observed and, thus, considered as first proof of binding.

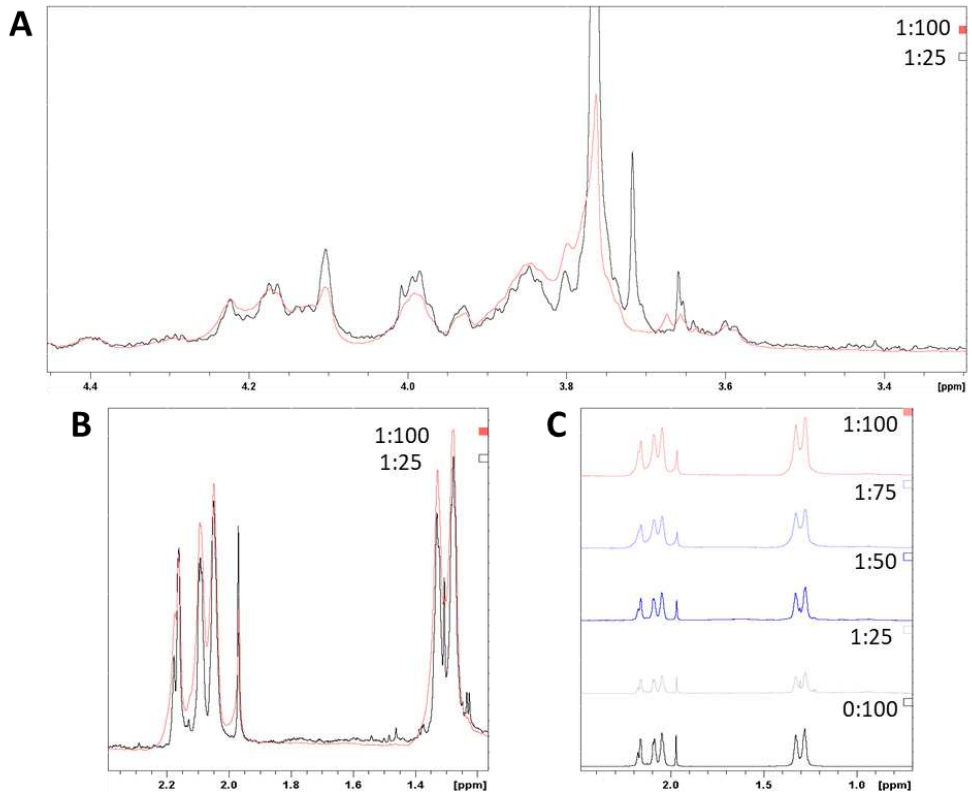

Figure 37. **A)** Stacked ^{1}H-NMR spectra of functional anti-CP5/R1 mAb (4 µM in deuterated buffer) with 25 equivalents (in black) and 100 (in pink) of CP5 ligand; **B)** Expansion of the Acetyl and methyl ^{1}H-NMR signals; **C)** Stacked ^{1}H-NMR spectra acquired during the titration of ligand CP5 to a sample containing functional anti-

CP5/R1 mAb (4 μM in deuterated buffer). The relative mAb:ligand ratios are reported above each spectrum. The black spectrum (0:100) is the spectrum of the ligand CP5 alone reported as reference.

Next, we performed proton Saturation Transfer Difference NMR (^{1}H STD-NMR) to get atomic details of the intermolecular interaction. ^{1}H-STD NMR experiment performed on the free antibody as control did not detect STD signals (data not shown). Next, ^{1}H STD-NMR experiments of the CP5-mAb complex was performed and different experimental conditions were tested changing the protein:ligand molar ratio, protein irradiation frequency and temperature. The best results were obtained at 310K with a 1:100 of protein:ligand molar ratio and aliphatic irradiation of the protons of the protein, which resulted to be much more efficient than that at the aromatic protons (data not shown). This observation suggests that the antibody binding site is mainly rich in aliphatic residues. The ^{1}H STD NMR spectrum and the corresponding off resonance spectrum (spectrum acquired without direct irradiation of the protein) as well as the derived ligand epitope mapping are reported in **Figure 38**. The strongest STD signals arise from the acetyl groups along the oligosaccharide. Further, the H2-H4 and H5 of the central residue, the FucNAcα ring, provide medium to strong STD signals. Weak signals come from the methyl groups of the fucose rings. No STD signals were detected from the ring protons of the manno configurated sugar nor from the beta fucose. On the basis of this evidence, it can be deduced that the CP5 mAb binding site establishes the majority of contacts with the central O-Acetylated FucNAcα ring of the polysaccharide, while the flanking sugars contribute exclusively through their acetyl moieties.

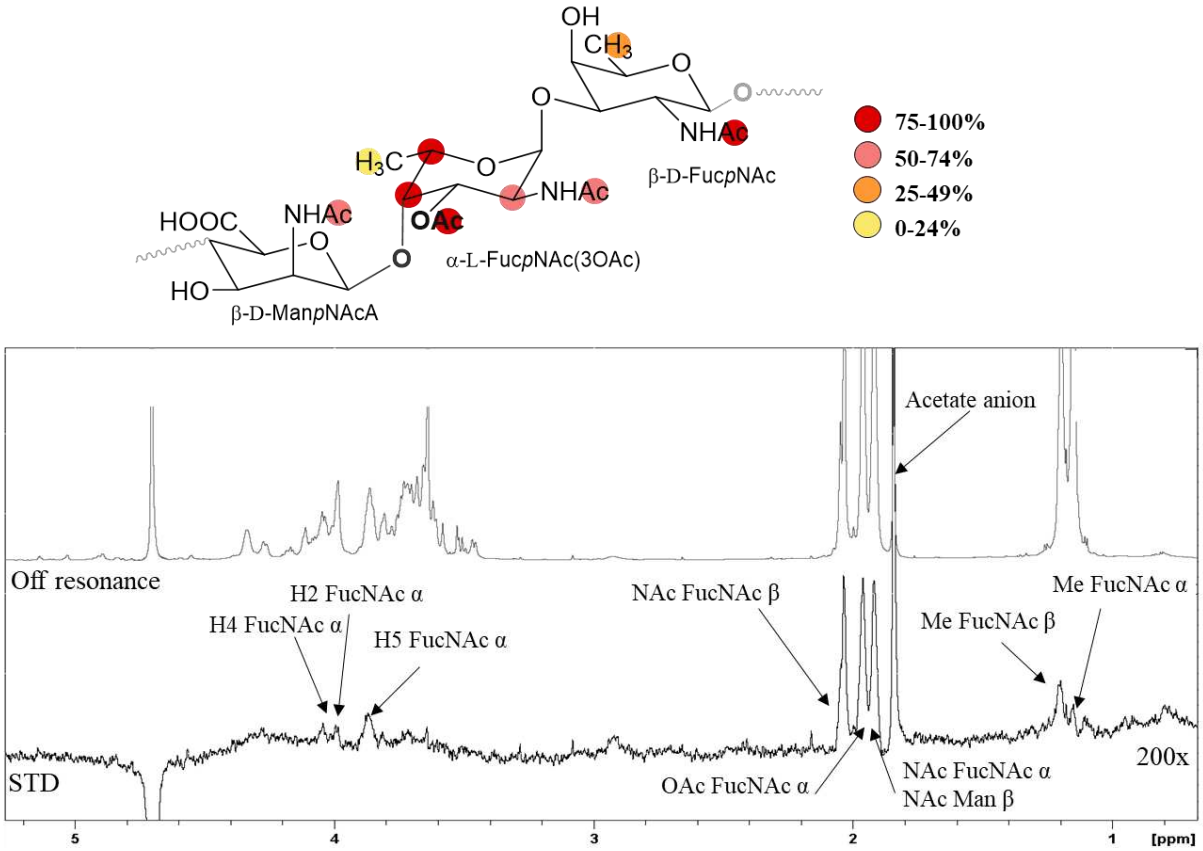

Figure 38. STD CP5 ligand and CP5/R1 mAb. Lower panel: off-resonance spectrum and STD spectrum with annotations of the main ^{1}H signals reported. The irradiation of the STD spectrum was set at δ 0.00 ppm and mAb:ligand molar ratio employed was 1:100 (being the protein at a concentration of 4 μM). The STD experiments were acquired with 2 seconds of saturation time, 3 seconds of relaxation time and at 310K. Upper panel: representation of the binding epitope obtained from the analysis of the STD spectrum with the relative color legend.

CP8 av3RU-mAb complex

Subsequently, anti-CP8/M4 complexed with CP8 av3RU was analyzed following the same experimental procedure. The titration of the ligand monitored with ^{1}H NMR experiments was performed by adding increasing CP8 av3RU ligand (100 μM, 200 μM, 300 μM, 400 μM) to a sample containing anti-CP8/M4 mAb (4μM in deuterated buffer), thus obtaining a protein:ligand ratio of 1:0 (apo lectin), 1:25, 1:50, 1:75 and 1:100 respectively. The stacked spectra of the titration are reported in **Figure 39**. Also in this case, perturbations on the ligand's signals were detected in terms of line broadening, suggesting that the binding is occurring.

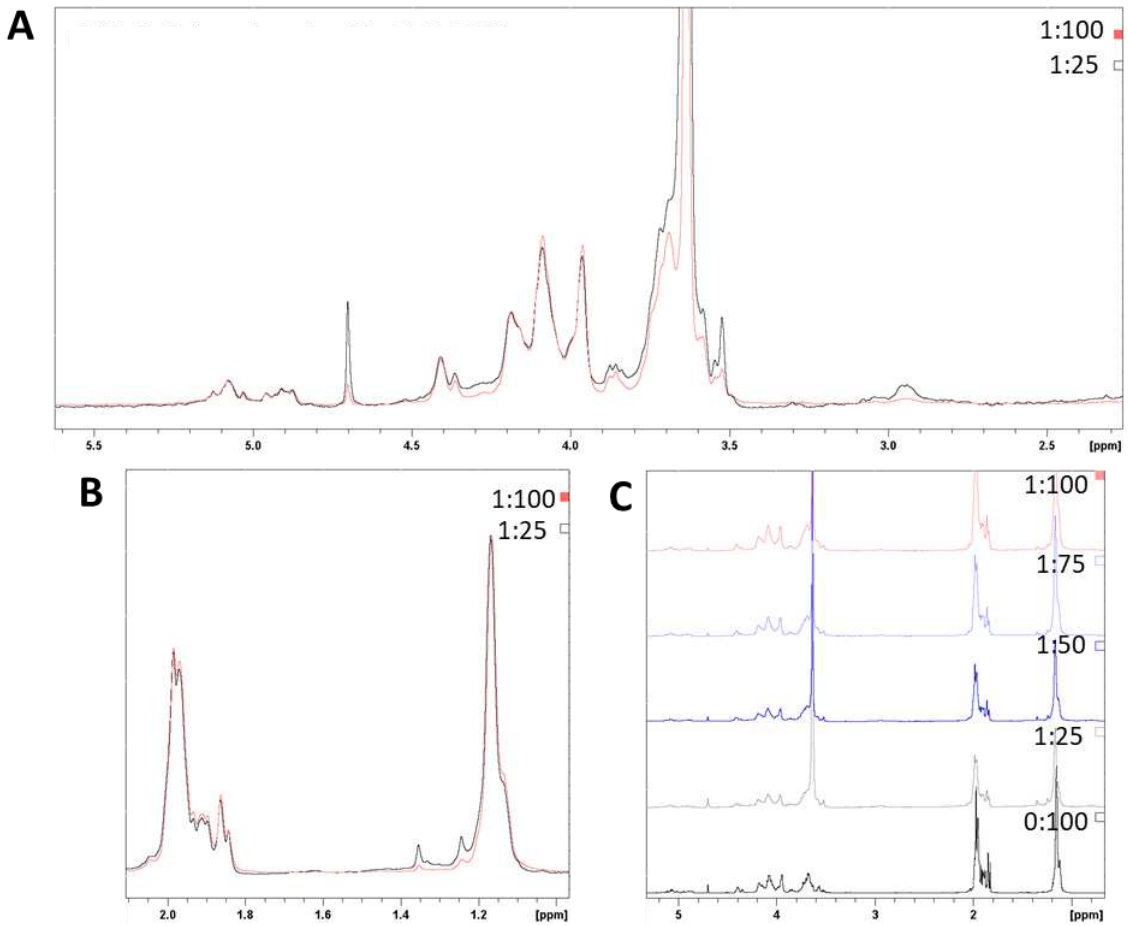

Figure 39. A) Stacked ^{1}H-NMR spectra of functional mouse anti-CP8/M4 mAb (4 µM in deuterated buffer) with 25 equivalents (in black) and 100 (in pink) of CP8 ligand; **B)** Expansion of the Acetyl and methyl ^{1}H-NMR signals; **C)** Stacked ^{1}H-NMR spectra acquired during the titration of ligand CP8 to a sample containing functional mouse anti-CP8/M4 mAb (4 µM in deuterated buffer). The relative mAb:ligand ratios are reported above each spectrum. The black spectrum (0:100) is the spectrum of the ligand CP8 alone reported as reference.

Again, STD-NMR experiments were employed in order to obtain ligand binding epitope and also in this case no STD signals of the free antibody were detected (data not shown).

The optimization of the experiment for the mAb:oligosaccharide complex, leads to the setting of the temperature at 310K, 1:100 of protein:ligand molar ratio and aliphatic irradiation of the antibody. **Figure 40** shows the STD-NMR spectrum obtained for the CP8-mAb complex using aliphatic irradiation; the same experiments acquired with aromatic irradiation (not shown) displayed lower STD signals, suggesting that, as well as for CP5 mAb, also in the case of CP8 mAb the binding site is rich in aliphatic residues and void of aromatics moieties.

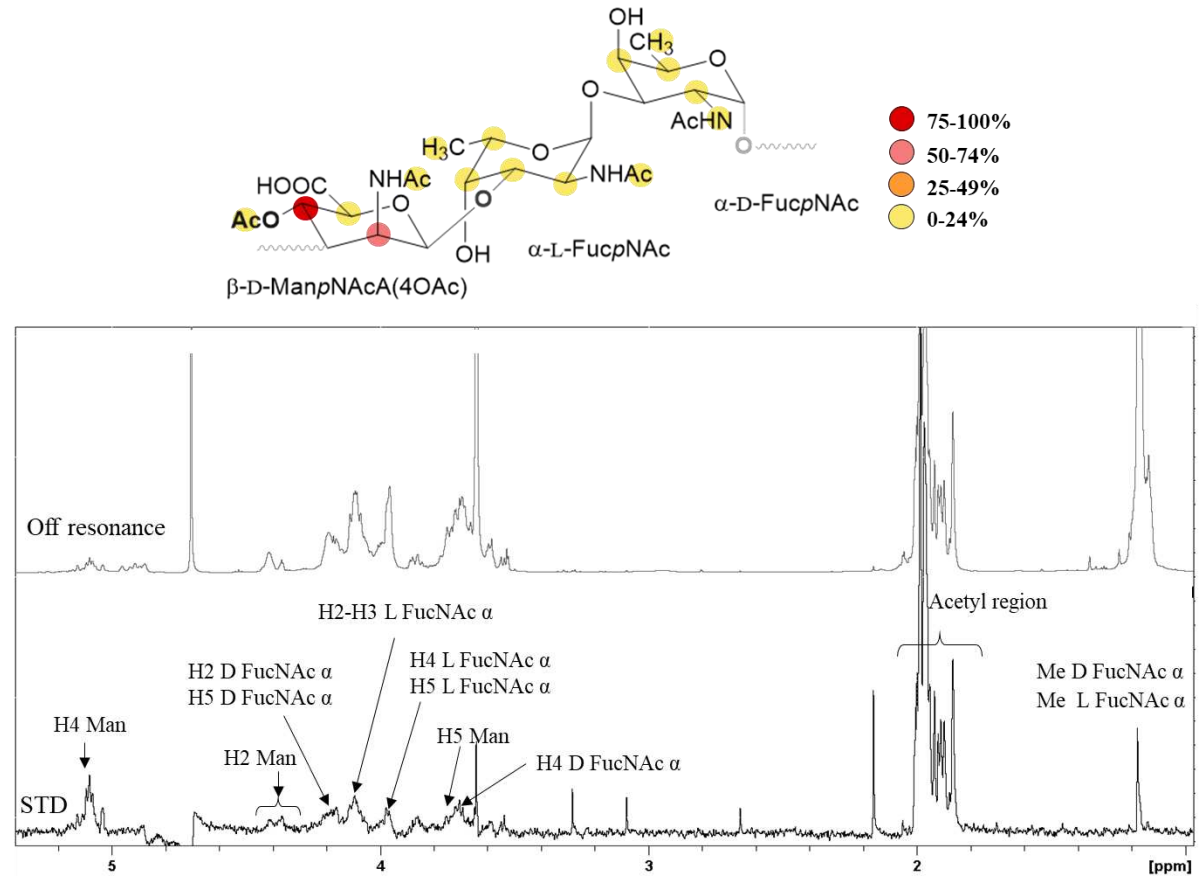

Figure 40. STD CP8 ligand and anti-CP8/M4 mAb. Lower panel: off-resonance spectrum and STD spectrum with annotations of the main ^{1}H signals reported. The irradiation of the STD spectrum was set at δ 0.00 ppm and mAb:ligand molar ratio employed was 1:100 (being the protein at a concentration of 4 μM). The STD experiments were acquired with 2 seconds of saturation time, 3 seconds of relaxation time and at 310K. Upper panel: representation of the binding epitope obtained from the analysis of the STD spectrum with the relative color legend.

The strongest STD signal arises from the H4 proton of the Man moiety, and a medium-intense signal is also detected for H2. All the other STD signals are scaled on the basis of the extremely high intensity of H4 and therefore result into a relative low-intensity contributions, although their absolute values are significant. Moreover, the ligand spectrum is complex and with high degree of overlapping signals, which makes difficult the NMR signals assignment. For instance, while in the cases of CP5 it was possible to discern the contributions of the different acetyl groups, in this case the region is impossible to resolve. However, as general evidence, the main interaction point with the antibody interests the mannose ring, especially in the neighboring of the N-acetyl and O-acetylation. The fucose residues also participate to mAb binding but with lower contribution with respect to the O-acetylated monosaccharide.

Overall, the NMR results show the existence of specific interactions in both cases of study. In particular, significant STD signals are detected for the moiety bearing the O-Acetylation (FucNAcα for CP5 and Man for CP8), confirming the important role of the O-Acetyl groups in the binding.

3.5 DISCUSSION

The high antibiotic resistance profile of *S. aureus* reinforces the need for an efficient vaccine development. The last two decades have seen considerable effort by the scientific community to develop a protective vaccine and so far no candidates have proven successful during clinical testing [166]. Currently, several new vaccine candidates are being tested in human clinical trials in a variety of target populations. Despite their failure in clinical phases when used alone, CP5 and CP8 conjugate are believed to be important components for a multivalent staphylococcal vaccine [72]. Indeed, it is known that an ideal vaccine against *S. aureus* should be composed of a combination of multiple antigens targeting a multivalent mechanism [166]. As already discussed, several parameters concerning both the saccharide and protein parts can modulate the immunogenicity of a glycoconjugate vaccine [105]. In particular, our work focused on the impact of saccharide size and of saccharide:protein ratio to CP5 glycoconjugate immunogenicity and on the role of PS decorative O-acetyl groups. The first two variables were examined through an *in vivo* comparison of three CP5-Hla conjugates differing in the saccharide length and in the degree of glycosylation. IgG titers both anti-CP5 and anti-Hla were measured through Luminex technology revealing that the tested variables did not show an evident influence on immunogenicity, except for the lowering of the anti-Hla titer caused by the high glycosylated glycoconjugate. Although preliminary, these studies do not seem to highlight a crucial importance of saccharide length and degree of glycosylation on glycoconjugates immunogenicity.

We therefore focused our attention to another parameter reported to be essential for the vaccine immunogenicity of different bacteria [61], the O-acetylation. O-acetyl groups of CP5 and CP8 polysaccharides repeating units has been shown to be fundamental for the generation of functional antibodies against *S. aureus* infections [73]. To evaluate how small differences in O-acetylation could affect antibody recognition, polysaccharides and oligosaccharides at different O-acetylation degrees have been generated and the recognition by different polyclonal and monoclonal antibodies was measured through competitive SPR experiments. Rabbit and human polyclonals sera showed similar behavior. For CP5, the presence of OAc moieties seems to not influence the antibody recognition since fully acetylated and deacetylated PSs and OSs are recognized in the same way. On the other hands, in the case of CP8, O-acetyl group appears to have a more important role as it determine an increased recognition compared to deacetylated epitopes. Trying to explain this different behavior between CP5 and CP8 recognition, MD Simulation experiments were done to predict the conformation of the two different

polysaccharides. Interestingly, studies revealed a different orientation of acetyl groups in the two PSs: in CP5 the N- and O-acetyl groups are randomly oriented towards different directions without a marked preferred orientation, while in CP8 polysaccharide all acetyl groups are facing the same side. This strong difference in the acetyl exposition can be responsible of guiding the recognition in different ways and in part explain the different behavior between the two serotypes observed in polyclonal antibody recognition. Moreover, the fact that in CP8 all acetyl groups face the same side could imply the presence of an O-acetyl-based immunodominant epitope. In CP5, on the other hand, we can speculate that CP5 do not have an immunodominant epitope but a more heterogeneous set of antibodies targeting different epitopes where O-acetyl moieties are less involved. These MD data could also help to better understand the known lack of cross reactivity between CP5 and CP8.

Subsequently, we tested the recognition of different levels of O-acetylation by a panel of anti-CP5 and anti-CP8 monoclonal antibodies through competitive SPR experiments. This allowed to select for both serotypes mAbs specific for the acetylated and de-O-acetylated epitopes. Functional assays performed on the selected antibodies have shown greater functionality for the two anti-CP5 and anti-CP8 mAbs targeting O-acetylated epitopes.

To characterize at the atomic level the epitopes recognized by the two mAbs exhibiting the highest functional activity, STD-NMR experiments were performed using complexes with CP5 and CP8 oligosaccharides (av3RU) respectively. STD-NMR results were able to identify all positions of the sugar important for the interaction and therefore to confirm the involvement of the O-acetyl groups.

These synergic multi-techniques approach proved useful to underline the importance of O-acetylation in *S. aureus* PS as a fundamental critical quality attribute that should be carefully monitored during the development of a glycoconjugate-based vaccine.

DISCUSSION AND CONCLUSIONS

Glycoconjugates vaccine are among the safest and most successful vaccines developed during the last 40 years. Today we have successful vaccines licensed worldwide that have had a huge impact on global infant mortality and morbidity [10]. To open the way to a rational design of efficacious glycoconjugates, different key parameters have to be taken in consideration to understand how they can modulate the immunogenicity of a conjugate vaccine. These variables include the size of saccharide moiety, the O-acetylation degree of the saccharide, the conjugation strategy, the carbohydrate loading on the carrier protein and the nature of both linker and carrier proteins [105]. The aim of my PhD thesis was to initially conduct structural studies in order to characterize the essential antigenic determinants of Hib and Staph polysaccharides, and subsequently correlate them with *in vivo* data in animals. For the Hib project, we centered our attention on the impact of saccharide antigen size. Although most of the conjugated vaccines have been obtained through the conjugation of the natural polysaccharide to the carrier protein, the use of oligosaccharides has also been reported. Indeed, the commercial QuimiHib vaccine is composed of a synthetic oligosaccharide with a length of about 7 repeating units [107]. Over the years, different methods have been developed to obtain Hib oligosaccharides by depolymerization of natural polysaccharide [46, 108-110] and by chemical synthesis [111-113] which allowed to investigate on the minimal length needed for antibody recognition. We evaluated which is the minimal saccharide portion recognized by a functional human monoclonal antibody by using a multidisciplinary approach involving SPR, STD-NMR and X-ray crystallography. The synergism of these powerful tools allowed to conduct structural studies aimed at characterizing at atomic level the Hib polysaccharide minimal epitope, comprise within two repeating units. A subsequent *in vivo* comparison of different TT-conjugates confirmed that two repeating units are sufficient to elicit specific IgG anti Hib-PS.

The studies performed on *S. aureus* project for CP5 and CP8 PS have instead focused on other variables important for a glycoconjugate immunogenicity: in addition to the length of the antigen, we focused our attention on the glycosylation degree and on the role of O-acetyl moieties. The latter turned out to be the most impactful in antibody binding, as well as in glycoconjugates immunogenicity, as reported in previous papers [73, 171]. SPR and STD-NMR experiments allowed to elucidate the important role of the acetyl groups in specific binding to antibodies, both polyclonal and monoclonal. The MD results offered us a key to understanding

the different behaviors between CP5 and CP8, and the functional data allowed us to hypothesize that mAbs targeting O-acetylated epitopes led to increased functional activity.

An improved understanding of structural features that determine antigenicity is crucial for a rational vaccine design. Multidisciplinary approaches involving advanced screening of glycan oligosaccharide arrays, structural and computational methods have been utilized so far to guide the identification of key epitopes of different pathogens. Highlighting the details of antigen-antibody interaction may help the design of more specific next-generation epitope-based glycoconjugate vaccines that can be obtained by synthetic or enzymatic approaches.

TRANSPARENCY STATEMENT

This work was sponsored by GlaxoSmithKline Biologicals SA.

Francesca Nonne is a PhD student at the University of Siena and participates in a post graduate studentship program at GSK, Siena, Italy.

QuimiHib is a trademark of CIGB.

REFERENCES

1. Marchetti, R., et al., *Solving the structural puzzle of bacterial glycome.* Curr Opin Struct Biol, 2021. **68**: p. 74-83.
2. Filloux, A. and C. Whitfield, *Editorial: The many wonders of the bacterial cell surface.* FEMS Microbiol Rev, 2016. **40**(2): p. 161-3.
3. Silhavy, T.J., D. Kahne, and S. Walker, *The bacterial cell envelope.* Cold Spring Harb Perspect Biol, 2010. **2**(5): p. a000414.
4. Costantino, P., R. Rappuoli, and F. Berti, *The design of semi-synthetic and synthetic glycoconjugate vaccines.* Expert Opin. Drug Discov., 2011. **6**(10): p. 1045-1066.
5. Y COLIN M. MAcLEOD, R.G.H., MICHAEL HEIDELBERGER, WILLIAM G. BERNHARD, *PREVENTION OF PNEUMOCOCCAL PNEUMONIA BY IMMUNIZATION WITH SPECIFIC CAPSULAR POLYSACCHARIDES.* J. Exp. Med., 1945. **82**: p. 445-465.
6. Artenstein, M.S., Gold, R., Zimmerly, J.G., *Prevention of meningococcal disease by group C polysaccharide vaccine.* N. Engl. J. Med., 1970. **282**: p. 417-420.
7. Gold, R., Artenstein, M.S., *Meningococcal infections. 2. Field Trial of group C meningococcal polysaccharide vaccine in 1969-1970.* Bull World Health Organ, 1971. **45**: p. 279-282.
8. Peltola, H.M., H.; Kayhty, H. , *Clinical efficacy of meningococus group A capsular polysaccharide vaccine in children three months to five years of age.* N. Engl. J. Med., 1977. **297**: p. 686-691.
9. Peltola, H.S., A. ; Kayhty, H.; Makela, H., *Haemophilus influenzae type B capsular polysaccharide vaccine in children: a double blind field study of 100000 vaccinees 3 months to 5 years of age in Finland.* Pediatrics, 1977. **60**: p. 730-737.
10. Rappuoli, R., *Glycoconjugate vaccines: Principles and mechanisms.* SCIENCE TRANSLATIONAL MEDICINE, 2018. **10**: p. 456-461.
11. Jackson, L.A., et al., *Influence of initial vaccination with 13-valent pneumococcal conjugate vaccine or 23-valent pneumococcal polysaccharide vaccine on anti-pneumococcal responses following subsequent pneumococcal vaccination in adults 50 years and older.* Vaccine, 2013. **31**(35): p. 3594-602.
12. Greenberg, R.N., et al., *Sequential administration of 13-valent pneumococcal conjugate vaccine and 23-valent pneumococcal polysaccharide vaccine in pneumococcal vaccine–naïve adults 60–64 years of age.* Vaccine, 2014. **32**(20): p. 2364-2374.
13. Ramsay, M.E., et al., *Herd immunity from meningococcal serogroup C conjugate vaccination in England: database analysis.* BMJ, 2003. **326**: p. 365-366.
14. Avery, O.T. and W.F. Goebel, *Chemo-Immunological Studies on Conjugated Carbohydrate-Proteins : V. The Immunological Specifity of an Antigen Prepared by Combining the Capsular Polysaccharide of Type Iii Pneumococcus with Foreign Protein.* J Exp Med, 1931. **54**(3): p. 437-47.
15. Schneerson, R., et al., *Preparation, characterization, and immunogenicity of Haemophilus influenzae type b polysaccharide-protein conjugates.* J. Exp. Med. , 1980. **152**: p. 361-376.
16. Geno, K.A., et al., *Pneumococcal Capsules and Their Types: Past, Present, and Future.* Clin Microbiol Rev, 2015. **28**(3): p. 871-99.
17. Pace, D. and A.J. Pollard, *Meningococcal A, C, Y and W-135 polysaccharide-protein conjugate vaccines.* Arch Dis Child, 2007. **92**(10): p. 909-15.
18. Acharya I.L., L.C.U., Thapa R., Gurubachaya V.L., Shrestha M.B., Cadoz M., Schulz D., Armand J., Bryla D.A., Trollfors B. et al., *Prevention of typhoid fever in Nepal with the Vi capsular polysaccharide of Salmonella typhi.* New Engl. J. Med., 1987. **317**(18): p. 1101-1104.

19. Klugman K.P., G.I.T., Koornhof H.J., Robbins J.B., Schneerson R., Schultz D., Cadoz M., Armand J., *Protective activity of Vi capsular polysaccharide vaccine against typhoid fever.* Lancet 1987. **2**(8569): p. 1165-1169.
20. Tacket C.O., L.M.M., Robbins J.B., *Persistence of antibody titres three years after vaccination with Vi polysaccharide vaccine against typhoid fever.* Vaccine, 1988. **6**(4): p. 307-308.
21. Francesca Micoli, P.C., Roberto Adamo, *Potential targets for next generation antimicrobial glycoconjugate vaccines.* FEMS Microbiology Reviews, 2018. **42**: p. 388–423.
22. Broker, M., et al., *Polysaccharide conjugate vaccine protein carriers as a "neglected valency" - Potential and limitations.* Vaccine, 2017. **35**(25): p. 3286-3294.
23. Broker, M., et al., *Biochemical and biological characteristics of cross-reacting material 197 CRM197, a non-toxic mutant of diphtheria toxin: use as a conjugation protein in vaccines and other potential clinical applications.* Biologicals, 2011. **39**(4): p. 195-204.
24. Biemans, R., F. Micoli, and M.R. Romano, *Glycoconjugate vaccines, production and characterization*, in *Recent Trends in Carbohydrate Chemistry*. 2020. p. 285-313.
25. Micoli, F., R. Adamo, and P. Costantino, *Protein Carriers for Glycoconjugate Vaccines: History, Selection Criteria, Characterization and New Trends.* Molecules, 2018. **23**(6).
26. Marburg, S., et al., *Bimolecular Chemistry of Macromolecules: Synthesis of Bacterial Polysaccharide Conjugates with Neisseria meningitidis Membrane Protein.* J. Am. Chem. SOC. 1986, 108, , 1986. **108**: p. 5282-5287.
27. Zou, W. and H.J. Jennings, *Preparation of glycoconjugate vaccines. In Carbohydrate-Based Vaccines and Immunotherapies 2009, Eds Zhongwu Guo and Geert-Jan Boons. John Wiley & Sons, Inc; Hoboken, New Jersey* 2009: p. p. 55-88.
28. Anderson, P.W., et al., *Vaccines consisting of periodate-cleaved oligosaccharides from the capsule of Haemophilus influenzae type b coupled to protein carrier: structural and temporal a requirements for priming in the human infant.* J. Immunol. , 1986. **137**(4): p. 1181-1186.
29. CDC, *Food and Drug Administration Approval for Use of Hiberix as a 3-Dose Primary Haemophilus influenzae Type b (Hib) Vaccination Series.* MMWR Morb Mortal Wkly Rep, 2016. **65**(16): p. 418-419.
30. Lees , A., B.L. Nelson, and J.J. Mond, *Activation of soluble polysaccharides with 1 cyano-4-dimethylaminopyridinium tetrafluoroborate for use in protein-polysaccharide conjugate vaccines and immunological reagents.* Vaccine, 1996. **14**(3): p. 190-198.
31. Turner, A.E.B., et al., *Novel polysaccharide-protein conjugates provide an immunogenic 13-valent pneumococcal conjugate vaccine for S. pneumoniae.* Synth Syst Biotechnol, 2017. **2**(1): p. 49-58.
32. Broker, M., et al., *Chemistry of a new investigational quadrivalent meningococcal conjugate vaccine that is immunogenic at all ages.* Vaccine, 2009. **27**(41): p. 5574-80.
33. Bardotti, A., et al., *Physicochemical characterisation of glycoconjugate vaccines for prevention of meningococcal diseases.* Vaccine, 2008. **26**(18): p. 2284-96.
34. Costantino, P., et al., *Size fractionation of bacterial capsular polysaccharides for their use in conjugate vaccines.* Vaccine, 1999. **17**: p. 1251±1263.
35. Arcuri, M., et al., *The influence of conjugation variables on the design and immunogenicity of a glycoconjugate vaccine against Salmonella Typhi.* Plos One, 2017. **12**(12): p. e0189100.
36. Broker, M., F. Berti, and P. Costantino, *Factors contributing to the immunogenicity of meningococcal conjugate vaccines.* Hum Vaccin Immunother, 2016. **12**(7): p. 1808-24.
37. Anish, C., et al., *Chemical Biology Approaches to Designing Defined Carbohydrate Vaccines.* Chemistry & Biology, 2014. **21**(1): p. 38-50.
38. Adamo, R., *Advancing Homogeneous Antimicrobial Glycoconjugate Vaccines.* Acc Chem Res, 2017. **50**(5): p. 1270-1279.
39. Verez-Bencomo, V., et al., *A synthetic conjugate polysaccharide vaccine against Haemophilus influenzae type b.* Science, 2004. **305**(5683): p. 522-5.
40. Ihssen, J., et al., *Production of glycoprotein vaccines in Escherichia coli.* Microb Cell Fact, 2010. **9**: p. 61.

41. Feldman, M.F., et al., *Engineering N-linked protein glycosylation with diverse O antigen lipopolysaccharide structures in Escherichia coli.* Proc Natl Acad Sci U S A, 2005. **102**(8): p. 3016-21.
42. Kabat, E.A., *The Upper Limit for the Size of the Human Antidextran Combining Site.* The Journal of Immunology, 1960. **84**(1): p. 82.
43. Seppala, I. and O. Makela, *Antigenicity of dextran-protein conjugates in mice. Effect of molecular weight of the carbohydrate and comparison of two modes of coupling.* J Immunol, 1989. **143**(4): p. 1259-64.
44. Laferrière, C.A., et al., *The synthesis of Streptococcus pneumoniae polysaccharide-tetanus toxoid conjugates and the effect of chain length on immunogenicity.* Vaccine, 1997. **15**(2): p. 179-186.
45. Pozsgay, V., et al., *Protein conjugates of synthetic saccharides elicit higher levels of serum IgG lipopolysaccharide antibodies in mice than do those of the O-specific polysaccharide from Shigella dysenteriae type 1.* Proc Natl Acad Sci U S A, 1999. **96**(9): p. 5194-7.
46. P W Anderson, M.E.P., E C Stein, S Porcelli, R F Betts, D M Connuck, D Korones, R A Insel, J M Zahradnik, R Eby, *Effect of oligosaccharide chain length, exposed terminal group, and hapten loading on the antibody response of human adults and infants to vaccines consisting of Haemophilus influenzae type b capsular antigen unterminally coupled to the diphtheria protein CRM_{197}.* The Journal of Immunology, 1989. **142**: p. 2464-2468.
47. Peeters, J.M., et al., *Comparison of four bifunctional reagents for coupling peptides to proteins and the effect of the three moieties on the immunogenicity of the conjugates.* Journal of Immunological Methods, 1989. **120**(1): p. 133-143.
48. Buskas, T., Y. Li, and G.J. Boons, *The immunogenicity of the tumor-associated antigen Lewis(y) may be suppressed by a bifunctional cross-linker required for coupling to a carrier protein.* Chemistry, 2004. **10**(14): p. 3517-24.
49. Phalipon, A., et al., *A synthetic carbohydrate-protein conjugate vaccine candidate against Shigella flexneri 2a infection.* J Immunol, 2009. **182**(4): p. 2241-7.
50. Giannini, G., R. Rappuoli, and G. Ratti, *The amino-acid sequence of two non-toxic mutants of diphtheria toxin: CRM45 and CRM197.* Nucleic Acids Res, 1984. **12**(10): p. 4063-9.
51. Donnelly, J.J., R.R. Deck, and M.A. Liu, *Immunogenicity of a Haemophilus influenzae polysaccharide-Neisseria meningitidis outer membrane protein complex conjugate vaccine.* J Immunol, 1990. **145**(9): p. 3071-9.
52. Prymula, R. and L. Schuerman, *10-valent pneumococcal nontypeable Haemophilus influenzae PD conjugate vaccine: Synflorix.* Expert Rev Vaccines, 2009. **8**(11): p. 1479-500.
53. Forsgren, A., K. Riesbeck, and H. Janson, *Protein D of Haemophilus influenzae: a protective nontypeable H. influenzae antigen and a carrier for pneumococcal conjugate vaccines.* Clin Infect Dis, 2008. **46**(5): p. 726-31.
54. Fattom, A., et al., *Laboratory and clinical evaluation of conjugate vaccines composed of Staphylococcus aureus type 5 and type 8 capsular polysaccharides bound to Pseudomonas aeruginosa recombinant exoprotein A.* Infect Immun, 1993. **61**(3): p. 1023-32.
55. Szu, S.C., et al., *Vi capsular polysaccharide-protein conjugates for prevention of typhoid fever. Preparation, characterization, and immunogenicity in laboratory animals.* J Exp Med, 1987. **166**(5): p. 1510-24.
56. Decker, M.D., et al., *Comparative trial in infants of four conjugate Haemophilus influenzae type b vaccines.* The Journal of Pediatrics, 1992. **120**(2): p. 184-189.
57. Granoff, D.M., et al., *Differences in the immunogenicity of three Haemophilus influenzae type b conjugate vaccines in infants.* The Journal of Pediatrics, 1992. **121**(2): p. 187-194.
58. Halperin, S.A., et al., *Comparison of the safety and immunogenicity of an investigational and a licensed quadrivalent meningococcal conjugate vaccine in children 2-10 years of age.* Vaccine, 2010. **28**(50): p. 7865-72.

59. Southern, J., et al., *Immunogenicity of a reduced schedule of meningococcal group C conjugate vaccine given concomitantly with the Prevenar and Pediacel vaccines in healthy infants in the United Kingdom.* Clin Vaccine Immunol, 2009. **16**(2): p. 194-9.
60. Jackson, L.A., et al., *Phase III comparison of an investigational quadrivalent meningococcal conjugate vaccine with the licensed meningococcal ACWY conjugate vaccine in adolescents.* Clin Infect Dis, 2009. **49**(1): p. 1-10.
61. Berti, F., R. De Ricco, and R. Rappuoli, *Role of O-Acetylation in the Immunogenicity of Bacterial Polysaccharide Vaccines.* Molecules, 2018. **23**(6).
62. Berry, D.S., et al., *Effect of O acetylation of Neisseria meningitidis serogroup A capsular polysaccharide on development of functional immune responses.* Infect Immun, 2002. **70**(7): p. 3707-13.
63. Borrow, R. and J. Findlow, *Prevention of meningococcal serogroup C disease by NeisVac-C.* Expert Rev Vaccines, 2009. **8**(3): p. 265-79.
64. Michon, F., et al., *Structure activity studies on group C meningococcal polysaccharide-protein conjugate vaccines: effect of O-acetylation on the nature of the protective epitope.* Dev Biol (Basel), 2000. **103**: p. 151-60.
65. Lewis, A.L., V. Nizet, and A. Varki, *Discovery and characterization of sialic acid O-acetylation in group B Streptococcus.* Proc Natl Acad Sci U S A, 2004. **101**(30): p. 11123-8.
66. Pannaraj, P.S., et al., *Group B streptococcal conjugate vaccines elicit functional antibodies independent of strain O-acetylation.* Vaccine, 2009. **27**(33): p. 4452-6.
67. McNeely, T.B., et al., *Antibody responses to capsular polysaccharide backbone and O-acetate side groups of Streptococcus pneumoniae type 9V in humans and rhesus macaques.* Infect Immun, 1998. **66**(8): p. 3705-10.
68. Chang, J., et al., *Relevance of O-acetyl and phosphoglycerol groups for the antigenicity of Streptococcus pneumoniae serotype 18C capsular polysaccharide.* Vaccine, 2012. **30**(49): p. 7090-6.
69. Szu, S.C., *Development of Vi conjugate - a new generation of typhoid vaccine.* Expert Rev Vaccines, 2013. **12**(11): p. 1273-86.
70. Bazhenova, A., et al., *Glycoconjugate vaccines against Salmonella enterica serovars and Shigella species: existing and emerging methods for their analysis.* Biophys Rev, 2021: p. 1-26.
71. Szu, S.C., et al., *Relation between structure and immunologic properties of the Vi capsular polysaccharide.* Infect Immun, 1991. **59**(12): p. 4555-61.
72. Weidenmaier, C. and J.C. Lee, *Structure and Function of Surface Polysaccharides of Staphylococcus aureus.* Curr Top Microbiol Immunol, 2017. **409**: p. 57-93.
73. Scully, I.L., et al., *O-Acetylation is essential for functional antibody generation against Staphylococcus aureus capsular polysaccharide.* Hum Vaccin Immunother, 2018. **14**(1): p. 81-84.
74. Valente, A.P. and M. Manzano-Rendeiro, *Mapping conformational epitopes by NMR spectroscopy.* Curr Opin Virol, 2021. **49**: p. 1-6.
75. Arnon, R. and M.H. Van Regenmortel, *Structural basis of antigenic specificity and design of new vaccines.* FASEB J, 1992. **6**(14): p. 3265-74.
76. Anish, C., et al., *Chemical biology approaches to designing defined carbohydrate vaccines.* Chem Biol, 2014. **21**(1): p. 38-50.
77. Oberli, M.A., et al., *Molecular analysis of carbohydrate-antibody interactions: case study using a Bacillus anthracis tetrasaccharide.* J Am Chem Soc, 2010. **132**(30): p. 10239-41.
78. C. E. Martin, F.B., M. A. Oberli, J. Komor, J. Mattner, C. Anish, and P. H. Seeberger, *Immunological Evaluation of a Synthetic Clostridium difficile Oligosaccharide Conjugate Vaccine Candidate and Identification of a Minimal Epitope.* Journal of the American Chemical Society, 2013. **26**: p. 9713-9722.
79. Broecker, F., Hanske, J., Martin, C. et al., *Multivalent display of minimal Clostridium difficile glycan epitopes mimics antigenic properties of larger glycans.* Nature Communications, 2016. **7**.

80. D. R. Bundle, C.N., C. Costello, R. Rennie, and T. Lipinski, *Design of a Candida albicans Disaccharide Conjugate Vaccine by Reverse Engineering a Protective Monoclonal Antibody.* ACS Chemical Biology, 2012. **10**: p. 1754-1763.
81. Phalipon, A., et al., *Characterization of functional oligosaccharide mimics of the Shigella flexneri serotype 2a O-antigen: implications for the development of a chemically defined glycoconjugate vaccine.* J Immunol, 2006. **176**(3): p. 1686-94.
82. F. Carboni, R.A., M. Fabbrini, R. De Ricco, V. Cattaneo, B. Brogioni, D. Veggi, V. Pinto, I. Passalacqua, D. Oldrini, R. Rappuoli, E. Malito, I. Margarit, F. Berti, *Structure of a protective epitope of group B Streptococcus type III capsular polysaccharide.* PNAS, 2017. **19**: p. 5017-5022.
83. P. Henriques, L.D.I., A. Gimeno, A. Biolchi, M.R. Romano, A. Arda, G. J. L. Bernardes, J. Jimenez-Barbero, F. Berti, R. Rappuoli, R. Adamo, *Structure of a protective epitope reveals the importance of acetylation of Neisseria meningitidis serogroup A capsular polysaccharide.* PNAS, 2020. **47**: p. 29795-29802.
84. Sikora, M., et al., *Computational epitope map of SARS-CoV-2 spike protein.* PLoS Comput Biol, 2021. **17**(4): p. e1008790.
85. Casalino, L., et al., *Beyond Shielding: The Roles of Glycans in the SARS-CoV-2 Spike Protein.* ACS Cent Sci, 2020. **6**(10): p. 1722-1734.
86. Pinto, D., et al., *Cross-neutralization of SARS-CoV-2 by a human monoclonal SARS-CoV antibody.* Nature, 2020. **583**(7815): p. 290-295.
87. Berti, B.B.a.F., *Surface plasmon resonance for the characterization of bacterial polysaccharide antigens: a review.* Med. Chem. Commun. , 2014. **5**: p. 1058-1066.
88. Davidoff, S.N., et al., *Surface Plasmon Resonance for Therapeutic Antibody Characterization*, in *Label-Free Biosensor Methods in Drug Discovery*. 2015. p. 35-76.
89. Meyer, B. and T. Peters, *NMR spectroscopy techniques for screening and identifying ligand binding to protein receptors.* Angew Chem Int Ed Engl, 2003. **42**(8): p. 864-90.
90. Mayer, M. and B. Meyer, *Characterization of Ligand Binding by Saturation Transfer Difference NMR Spectroscopy.* Angewandte Chemie International Edition, 1999. **38**(12): p. 1784-1788.
91. Di Carluccio, C., et al., *Investigation of protein-ligand complexes by ligand-based NMR methods.* Carbohydr Res, 2021. **503**: p. 108313.
92. Sumner, J.B., *The Isolation and Crystallization of the Enzyme Urease.* Journal of Biological Chemistry, 1926. **69**(2): p. 435-441.
93. Kendrew, J.C., et al., *A three-dimensional model of the myoglobin molecule obtained by x-ray analysis.* Nature, 1958. **181**(4610): p. 662-6.
94. Kendrew, J.C., et al., *Structure of myoglobin: A three-dimensional Fourier synthesis at 2 A. resolution.* Nature, 1960. **185**(4711): p. 422-7.
95. Mariuzza, R.A., S.E. Phillips, and R.J. Poljak, *The structural basis of antigen-antibody recognition.* Annu Rev Biophys Biophys Chem, 1987. **16**: p. 139-59.
96. Gawas, U.B., V.K. Mandrekar, and M.S. Majik, *Chapter 5 - Structural analysis of proteins using X-ray diffraction technique*, in *Advances in Biological Science Research*, S.N. Meena and M.M. Naik, Editors. 2019, Academic Press. p. 69-84.
97. Shuchismita Dutta, R.K.G., and Catherine L. Lawson. *Educational portal of PDB*. Available from: https://pdb101.rcsb.org/learn/guide-to-understanding-pdb-data/biological-assemblies.
98. C. Soliman, G.B.P.a.P.A.R., *Antibody recognition of bacterial surfaces and extracellular polysaccharides.* Curr Opin Struct Biol, 2020. **62**: p. 48-55.
99. Slack, M.P.E., *Long Term Impact of Conjugate Vaccines on Haemophilus influenzae Meningitis: Narrative Review.* Microorganisms, 2021. **9**(5).
100. Wen, S., et al., *Molecular epidemiology and evolution of Haemophilus influenzae.* Infect Genet Evol, 2020. **80**: p. 104205.

101. J. Y. Baek, A.G., D. C. K. Rathwell, D. Meierhofer, C. L. Pereira and P. H. Seeberger, *A modular synthetic route to size-defined immunogenic Haemophilus influenzae b antigens is key to the identification of an octasaccharide lead vaccine candidate.* Chemical Science, 2018. **9**: p. 1279-1288.
102. Khatuntseva, E.A. and N.E. Nifantiev, *Glycoconjugate Vaccines for Prevention of Haemophilus influenzae Type b Diseases.* Russ J Bioorg Chem, 2021. **47**(1): p. 26-52.
103. Smith, D.H., et al., *Responses of children immunized with the capsular polysaccharide of Hemophilus influenzae, type b.* Pediatrics, 1973. **52**(5): p. 637-44.
104. Käyhty H, K.V., Peltola H, Mäkelä PH, *Serum antibodies after vaccination with Haemophilus influenzae type b capsular polysaccharide and responses to reimmunization: no evidence of immunologic tolerance or memory.* Pediatrics, 1984. **74**: p. 857-865.
105. P. Costantino, R.R.F.B., *The design of semi-synthetic and synthetic glycoconjugate vaccines.* Expert Opinion, 2011. **6**: p. 1045-1066.
106. Heath, P.T., *Haemophilus influenzae type b conjugate vaccines: a review of efficacy data.* Pediatr Infect Dis J, 1998. **17**(9 Suppl): p. S117-22.
107. Verez-Bencomo V, F.-S.V., Hardy E, Toledo ME, Rodríguez MC, Heynngnezz L, Rodriguez A, Baly A, Herrera L, Izquierdo M, Villar A, Valdés Y, Cosme K, Deler ML, Montane M, Garcia E, Ramos A, Aguilar A, Medina E, Toraño G, Sosa I, Hernandez I, Martínez R, Muzachio A, Carmenates A, Costa L, Cardoso F, Campa C, Diaz M, Roy R, *A synthetic conjugate polysaccharide vaccine against Haemophilus influenzae type b.* Science, 2004. **305**(5683): p. 522-525.
108. Anderson, P., *Antibody Responses to Haemophilus influenzae Type b and Diphtheria Toxin Induced by Conjugates of Oligosaccharides of the Type b Capsule with the Nontoxic Protein CRM_{197}.* Infection and Immunity, 1983. **39**: p. 233-238.
109. P. W. Anderson, M.E.P., R. A. Insel, R. Betts, R. Eby and D. H. Smith, *Vaccines consisting of periodate-cleaved oligosaccharides from the capsule of Haemophilus influenzae type b coupled to a protein carrier: structural and temporal requirements for priming in the human infant.* The Journal of Immunology, 1986. **137**: p. 1181-1186.
110. R. Rana, J.D., D. Singh, N. Kumar, S. Hanif, N. Joshi, M.K. Chhikara, *Development and characterization of Haemophilus influenzae type bconjugate vaccine prepared using different polysaccharide chainlengths.* Vaccine, 2015. **33**: p. 2646–2654.
111. Evenberg, D., et al., *Preparation, antigenicity, and immunogenicity of synthetic ribosylribitol phosphate oligomer-protein conjugates and their potential use for vaccination against Haemophilus influenzae type b disease.* J Infect Dis, 1992. **165 Suppl 1**: p. S152-5.
112. Peeters, C.C., et al., *Synthetic trimer and tetramer of 3-beta-D-ribose-(1-1)-D-ribitol-5-phosphate conjugated to protein induce antibody responses to Haemophilus influenzae type b capsular polysaccharide in mice and monkeys.* Infect Immun, 1992. **60**(5): p. 1826-33.
113. Chong, P., et al., *A strategy for rational design of fully synthetic glycopeptide conjugate vaccines.* Infect Immun, 1997. **65**(12): p. 4918-25.
114. S. Pillai, S.C., M. Koster, R. Eby, *Distinct Pattern of Antibody Reactivity with Oligomeric or Polymeric Forms of the Capsular Polysaccharide of Haemophilus influenzae Type b.* Infection and Immunity, 1991. **59**: p. 4371 - 4376.
115. Smith, D.H., et al., *Haemophilus b oligosaccharide-CRM197 and other Haemophilus b conjugate vaccines: a status report.* Adv Exp Med Biol, 1989. **251**: p. 65-82.
116. Porter Anderson, M.P., Kathryn Edwards, Carol Ray Porch and Richard Insel, *Priming and induction of Haemophilus influenzae type b capsular antibodies early infancy by Dpo20, an oligosaccharide-protein conjugate vaccine.* The Journal of Pediatrics, 1987. **111**: p. 644-650.
117. Carboni, F., et al., *Evaluation of Immune Responses to Group B Streptococcus Type III Oligosaccharides Containing a Minimal Protective Epitope.* J Infect Dis, 2020. **221**(6): p. 943-947.
118. Pietri, G.P., et al., *Elucidating the Structural and Minimal Protective Epitope of the Serogroup X Meningococcal Capsular Polysaccharide.* Front Mol Biosci, 2021. **8**: p. 745360.

119. N Ravenscroft, G.A., A Bartoloni, S Berti, M Bigio, V Carinci, P Costantino, S D'Ascenzi, A Giannozzi, F Norelli, C Pennatini, D Proietti, C Ceccarini, P Cescutti, *Size determination of bacterial capsular oligosaccharides used to prepare conjugate vaccines.* Vaccine, 1999. **17**: p. 2802-2816.
120. A. H. Lucas, j.W.L., and d. C. Reason, *Variable Region Sequences of a Protective Human Monoclonal Antibody Specific for the Haemophilus influenzae Type b Capsular Polysaccharide.* Infection and immunity, 1994. **62**: p. 3873-3880.
121. Beilsten-Edmands, J., et al., *Scaling diffraction data in the DIALS software package: algorithms and new approaches for multi-crystal scaling.* Acta Crystallogr D Struct Biol, 2020. **76**(Pt 4): p. 385-399.
122. Evans, P.R. and G.N. Murshudov, *How good are my data and what is the resolution?* Acta Crystallogr D Biol Crystallogr, 2013. **69**(Pt 7): p. 1204-14.
123. Collaborative Computational Project, N., *The CCP4 suite: programs for protein crystallography.* Acta Crystallogr D Biol Crystallogr, 1994. **50**(Pt 5): p. 760-3.
124. McCoy, A.J., et al., *Phaser crystallographic software.* J Appl Crystallogr, 2007. **40**(Pt 4): p. 658-674.
125. Adams, P.D., et al., *PHENIX: a comprehensive Python-based system for macromolecular structure solution.* Acta Crystallogr D Biol Crystallogr, 2010. **66**(Pt 2): p. 213-21.
126. Emsley, P., et al., *Features and development of Coot.* Acta Crystallogr D Biol Crystallogr, 2010. **66**(Pt 4): p. 486-501.
127. Chen, V.B., et al., *MolProbity: all-atom structure validation for macromolecular crystallography.* Acta Crystallographica Section D Biological Crystallography, 2009. **66**(1): p. 12-21.
128. Krissinel, E. and K. Henrick, *Inference of macromolecular assemblies from crystalline state.* J Mol Biol, 2007. **372**(3): p. 774-97.
129. Rappuoli, R., *Glycoconjugate vaccines: Principles and mechanisms.* Sci Transl Med, 2018. **10**(456).
130. Safari, D., et al., *Identification of the smallest structure capable of evoking opsonophagocytic antibodies against Streptococcus pneumoniae type 14.* Infect Immun, 2008. **76**(10): p. 4615-23.
131. Johnson, M.A. and D.R. Bundle, *Designing a new antifungal glycoconjugate vaccine.* Chem Soc Rev, 2013. **42**(10): p. 4327-44.
132. Adamo, R., et al., *Synthetically defined glycoprotein vaccines: current status and future directions.* Chem Sci, 2013. **4**(8): p. 2995-3008.
133. Insel, R.A., E.E. Adderson, and W.L. Carroll, *The repertoire of human antibody to the Haemophilus influenzae type b capsular polysaccharide.* Int Rev Immunol, 1992. **9**(1): p. 25-43.
134. Ozdilek, A., et al., *A Structural Model for the Ligand Binding of Pneumococcal Serotype 3 Capsular Polysaccharide-Specific Protective Antibodies.* mBio, 2021. **12**(3): p. e0080021.
135. Villeneuve, S., et al., *Crystal structure of an anti-carbohydrate antibody directed against Vibrio cholerae O1 in complex with antigen: molecular basis for serotype specificity.* Proc Natl Acad Sci U S A, 2000. **97**(15): p. 8433-8.
136. Vulliez-Le Normand, B., et al., *Structures of synthetic O-antigen fragments from serotype 2a Shigella flexneri in complex with a protective monoclonal antibody.* Proc Natl Acad Sci U S A, 2008. **105**(29): p. 9976-81.
137. Evans, S.V., et al., *Evidence for the extended helical nature of polysaccharide epitopes. The 2.8 A resolution structure and thermodynamics of ligand binding of an antigen binding fragment specific for alpha-(2-->8)-polysialic acid.* Biochemistry, 1995. **34**(20): p. 6737-44.
138. Nagae, M., et al., *Crystal structure of anti-polysialic acid antibody single chain Fv fragment complexed with octasialic acid: insight into the binding preference for polysialic acid.* J Biol Chem, 2013. **288**(47): p. 33784-33796.

139. Hougs, L., et al., *Structural requirements of the major protective antibody to Haemophilus influenzae type b.* Infect Immun, 1999. **67**(5): p. 2503-14.
140. Haji-Ghassemi, O., et al., *Antibody recognition of carbohydrate epitopesdagger.* Glycobiology, 2015. **25**(9): p. 920-52.
141. Haji-Ghassemi, O., et al., *Groove-type recognition of chlamydiaceae-specific lipopolysaccharide antigen by a family of antibodies possessing an unusual variable heavy chain N-linked glycan.* J Biol Chem, 2014. **289**(24): p. 16644-61.
142. S. Pillai, S.C., M. Koster, R. Eby, *Distinct Pattern of Antibody Reactivity with Oligomeric or Polymeric Forms of the Capsular Polysaccharide of Haemophilus influenzae Type b.* Infection and Immunity, 1991. **59**: p. 4371-4376.
143. Ryan, K.J. and C.G. Ray, *Sherris Medical Microbiology*. 2003: Mcgraw-hill.
144. Ford, C.A., I.M. Hurford, and J.E. Cassat, *Antivirulence Strategies for the Treatment of Staphylococcus aureus Infections: A Mini Review.* Front Microbiol, 2020. **11**: p. 632706.
145. Lowy, F.D., *Staphylococcus aureus infections.* N Engl J Med, 1998. **339**(8): p. 520-32.
146. Fabio Bagnoli, R.R., Guido Grandi, *Staphylococcus aureus.* Springer, 2017. **409**: p. XII, 540.
147. Aryee, A. and J.D. Edgeworth, *Carriage, Clinical Microbiology and Transmission of Staphylococcus aureus.* Curr Top Microbiol Immunol, 2017. **409**: p. 1-19.
148. Morata, L., J. Mensa, and A. Soriano, *New antibiotics against gram-positives: present and future indications.* Curr Opin Pharmacol, 2015. **24**: p. 45-51.
149. Thakker, M., et al., *Staphylococcus aureus serotype 5 capsular polysaccharide is antiphagocytic and enhances bacterial virulence in a murine bacteremia model.* Infect Immun, 1998. **66**(11): p. 5183-9.
150. Watts, A., et al., *Staphylococcus aureus strains that express serotype 5 or serotype 8 capsular polysaccharides differ in virulence.* Infect Immun, 2005. **73**(6): p. 3502-11.
151. Armentrout, E.I., G.Y. Liu, and G.A. Martins, *T Cell Immunity and the Quest for Protective Vaccines against Staphylococcus aureus Infection.* Microorganisms, 2020. **8**(12).
152. Berube, B.J. and J. Bubeck Wardenburg, *Staphylococcus aureus alpha-toxin: nearly a century of intrigue.* Toxins (Basel), 2013. **5**(6): p. 1140-66.
153. Fiaschi, L., et al., *Auto-Assembling Detoxified Staphylococcus aureus Alpha-Hemolysin Mimicking the Wild-Type Cytolytic Toxin.* Clin Vaccine Immunol, 2016. **23**(6): p. 442-50.
154. Fattom, A., et al., *Synthesis and immunologic properties in mice of vaccines composed of Staphylococcus aureus type 5 and type 8 capsular polysaccharides conjugated to Pseudomonas aeruginosa exotoxin A.* Infect Immun, 1990. **58**(7): p. 2367-74.
155. Fattom, A., et al., *Efficacy profile of a bivalent Staphylococcus aureus glycoconjugated vaccine in adults on hemodialysis: Phase III randomized study.* Hum Vaccin Immunother, 2015. **11**(3): p. 632-41.
156. Anderson, A.S., et al., *Development of a multicomponent Staphylococcus aureus vaccine designed to counter multiple bacterial virulence factors.* Hum Vaccin Immunother, 2012. **8**(11): p. 1585-94.
157. Dayan, G.H., et al., *Staphylococcus aureus: the current state of disease, pathophysiology and strategies for prevention.* Expert Rev Vaccines, 2016. **15**(11): p. 1373-1392.
158. Gurtman, A., et al., *The development of a staphylococcus aureus four antigen vaccine for use prior to elective orthopedic surgery.* Hum Vaccin Immunother, 2019. **15**(2): p. 358-370.
159. Scully, I.L., et al., *Performance of a Four-Antigen Staphylococcus aureus Vaccine in Preclinical Models of Invasive S. aureus Disease.* Microorganisms, 2021. **9**(1).
160. Levy, J., et al., *Safety and immunogenicity of an investigational 4-component Staphylococcus aureus vaccine with or without AS03B adjuvant: Results of a randomized phase I trial.* Hum Vaccin Immunother, 2015. **11**(3): p. 620-31.
161. Zeng, H., et al., *Rapid and Broad Immune Efficacy of a Recombinant Five-Antigen Vaccine against Staphylococcus Aureus Infection in Animal Models.* Vaccines (Basel), 2020. **8**(1).
162. *Safety, Immunogenicity and Efficacy of GSK S. Aureus Candidate Vaccine (GSK3878858A) When Administered to Healthy Adults (Dose-escalation) and to Adults 18 to 50 Years of Age*

With a Recent S. Aureus Skin and Soft Tissue Infection (SSTI). Available from: https://clinicaltrials.gov/ct2/show/NCT04420221?cond=NCT04420221&draw=2&rank=1.
163. Schmidt, C.S., et al., *NDV-3, a recombinant alum-adjuvanted vaccine for Candida and Staphylococcus aureus, is safe and immunogenic in healthy adults.* Vaccine, 2012. **30**(52): p. 7594-600.
164. Chen, W.H., et al., *Safety and Immunogenicity of a Parenterally Administered, Structure-Based Rationally Modified Recombinant Staphylococcal Enterotoxin B Protein Vaccine, STEBVax.* Clin Vaccine Immunol, 2016. **23**(12): p. 918-925.
165. Karauzum, H., et al., *IBT-V02: A Multicomponent Toxoid Vaccine Protects Against Primary and Secondary Skin Infections Caused by Staphylococcus aureus.* Front Immunol, 2021. **12**: p. 624310.
166. Clegg, J., et al., *Staphylococcus aureus Vaccine Research and Development: The Past, Present and Future, Including Novel Therapeutic Strategies.* Front Immunol, 2021. **12**: p. 705360.
167. Francois, B., et al., *Safety and tolerability of a single administration of AR-301, a human monoclonal antibody, in ICU patients with severe pneumonia caused by Staphylococcus aureus: first-in-human trial.* Intensive Care Med, 2018. **44**(11): p. 1787-1796.
168. O'Riordan, K. and J.C. Lee, *Staphylococcus aureus capsular polysaccharides.* Clin Microbiol Rev, 2004. **17**(1): p. 218-34.
169. Wacker, M., et al., *Prevention of Staphylococcus aureus infections by glycoprotein vaccines synthesized in Escherichia coli.* J Infect Dis, 2014. **209**(10): p. 1551-61.
170. Coccia, M., et al., *Cellular and molecular synergy in AS01-adjuvanted vaccines results in an early IFNgamma response promoting vaccine immunogenicity.* NPJ Vaccines, 2017. **2**: p. 25.
171. Bhasin, N., et al., *Identification of a gene essential for O-acetylation of the Staphylococcus aureus type 5 capsular polysaccharide.* Mol Microbiol, 1998. **27**(1): p. 9-21.

RINGRAZIAMENTI

Ringrazio il Dipartimento di Biotecnologie, Chimica e Farmacia dell'Università di Siena e GSK Vaccines per avermi dato la possibilità di intraprendere questo percorso di Dottorato.

Un ringraziamento sincero ai miei relatori, il Professor Maurizio Taddei e la Dottoressa Maria Rosaria Romano, per avermi guidato e supportato nella realizzazione del progetto.

Ringrazio il Professor Jesús Jiménez Barbero del CIC bioGUNE di Bilbao per il suo contributo negli studi di Molecular Dynamic e spettroscopia NMR.

Infine, un ringraziamento speciale a tutte le persone che negli anni sono state coinvolte nel progetto dando il proprio contributo alla realizzazione dello stesso.

Francesca